Iridium-PCP- Pincer Complexes – C-H Oxidative addition Reactions and Functionalisation

***

Iridium-PCP-Pincer-Komplexe - Oxidative C-H-Additionsreaktionen und Funktionalisierung

DISSERTATION

der Fakultät für Chemie und Pharmazie

der Eberhard-Karls-Universität Tübingen

zur Erlangung des Grades eines Doktors

der Naturwissenschaften

2002

vorgelegt von

Hani Ali Yasin Mohammad

Tag der mündlichen Prüfung:	26 August 2002

Dekan:	Prof. Dr. H. Probst
1. Berichterstatter:	Prof. Dr. H. A. Mayer
2. Berichterstatter:	Prof. Dr. E. Lindner

Im Namen Allahs, des Sich Erbarmenden, des Barmherzigen

In the Name of Allah, the Most Beneficent, the Most Merciful

To my Family

Die vorliegende Arbeit wurde am
Institüt für Anorganische Chemie der
Eberhard-Karls- Universität Tübingen
unter der Leitung von
Herren Prof. Dr. H. A. Mayer
angefertigt

Meinem Doktorvater,
Herren Prof. Dr. H. A. Mayer
danke ich herzlich für die interessante Themenstellung,
für die Bereitstellung ausgezeichneter Arbeitsbedingungen,
die wertvollen Anregungen und Diskussionen
sowie sein stetes Interesse an dieser Arbeit.

Acknowledgement

First of all **Thanks** to our creator (**ALLAH**) who donates us our lifes and the will for achievement, success, and who enabled me to do this work. Thanks to all persons who participated in giving me the chance to continue my study or in accomplishing this work.

Many thanks ***specially*** to my supervisor: **Prof. Herman A. Mayer** who gave me all assistance he can either scientific or financial. I had very interesting discussions and practically enjoyed my work with him. I can say truely that he is a highly recognised scientist and a kind man. **I wish also to thank**

Prof. Ekkehard Lindner for all his assistance and distinguished guidance for such a scientific center.

Prof. Bernd Speiser for his cooperation in doing the electrochemical study.

Prof. Hans-Georg Mack for doing quantum mechanical calculations.

Dr. Klaus Eichele for aesthetic X-ray structures and analysis.

Prof. William C. Kaska for his helpful discussions.

Angelika Ehman for her kindness, patience and her effort in doing NMR spectra.

DFG, Fonds der chemischen Industrie, DEGUSSA AG for financial Support.

All kind colleagues and staff who were specially friendly and helpful.

Abbreviations and Symbols

CV	cyclovoltammetry
Cp*	pentamethylcyclopentadienyl anion
d	doublet
dd/ddd	doublet of doublet/ doublet of doublet of doublet
DEPT	Distortionless Enhancement by Polarization Transfer
DFT	Density Functional Theory
DMF	Dimethylformamide
δ	Chemical shift (ppm)
FAB	Fast atomic bombardement
FD	Field Desorption
$^{n}J_{ij}$	coupling constant for a pair of nuclei i,j over n bonds
IR	Infrared
mp	melting point
m	multiplet
Me	Methyl
MHz	Megahertz
MS	Mass Spectrometry
m/z	mass to charge ratio
NBA	Nitrobenzyl alcohol
NMR	Nuclear Magnetic Resonance
ν	wave number(cm^{-1})
ppm	parts per million
rt	room temperature
s	singlet
t	triplet

^{t}Bu	t-Butyl
TBAHFP	Tetrabutylammoniumhexaflourophosphate
THF	Tetrahydrofuran
TMS	Tetramethylsilane
TLC	Thin Layer Chromatography

Contents

Introduction

The selective functionalization of aliphatic groups is one of the great unsolved problems of chemistry. One of the most commercially important possibilities is the production of major organic feedstocks such as terminal alkenes (α–olefins) through regioselective aliphatic dehydrogenation reactions. Terminal alkenes (α-olefins) are a major feedstock for the production of plastics, detergents and lubricants. The dehydrogenation of alkanes to produce alkenes, in addition to being highly endothermic (experimentally about 33 Kcal/mol), is a symmetry-forbidden reaction and has an extremely high barrier without a catalyst.[1] Thus, the reaction usually proceeds only under UV irradiation or in the presence of a hydrogen acceptor. Even with a catalyst, the reaction still requires energy and typically occurs only at higher temperatures.[2] Several studies of alkane activation by rhodium and iridium complexes have shown that oxidative addition of C-H bonds is kinetically preferred despite their greater bond strength. During the past decade, there has been steady progress in the development of soluble transition metal complexes as catalysts for the dehydrogenation of alkanes to alkenes at moderate conditions based on C-H bond activation of the alkane.[3-6]

Homogeneous catalytic dehydrogenation of saturated hydrocarbons is just one part of a concerted effort to develop and broaden the scope of transition metal catalyzed carbon-hydrogen bond reactivity.[7]. The chemistry of iridium[8,9] has played a central role in the expansion of this challenging field.[10] The multifaceted complex Cp*(PMe_3)IrMeOTf can activate alkanes by a "σ-bond metathesis" pathway, by an oxidative addition-reductive elimination pathway or by electrophilic activation.[13-16] Similar pathways can be expected for the interaction of (PCP)IrH_2 pincer complexes with alkanes.[17] Consequently, there is considerable interest in determining which of these mechanistic pathways are important in catalytic dehydrogenation and other C-H interactions so that more efficient complexes can be designed to facilitate the reaction. Experimental observations in some instances seem to support reductive elimination of H_2 from $Ir^{III}H_2$ to generate a reactive 14e Ir^{I} species. This coordinatively unsaturated fragment oxidatively adds RH to give an $Ir^{III}R(H)$ complex, which results in an olefin complex by β-H transfer. Release of the olefin is the last step to re-form the starting material.[18-21]

Recent calculations suggest a more prominent role for an oxidative addition pathway from Ir^{III} to Ir^{V} in catalytic C-H activation reactions.[21-23] Experimental observations appear to

support this pathway including the reactions of novel high temperature systems.[26] Examples which involve catalytic systems are sparse.The PCP dihydrido pincer complexes [C_6H_3-2,6-(CH_2PR_2)$_2$]IrH_2 (R = ^{t}Bu, ^{i}Pr) are extraordinary active and robust catalysts for aliphatic dehydrogenation reactions. Their application to alkane dehydrogenation has resulted in the first efficient catalytic systems for homogeneous thermochemical alkane dehydrogenation. The pincer catalysts also affect other aliphatic dehydrogenations which had not previously been accomplished via homogeneous catalysis. These processes include the conversion of cycloalkanes to arenes, ethylbenzene to styrene, and THF to furan .[11,12]

The PCP pincer complexes of iridium may have presented the opportunity of a breakthrough in this area because they can interact with alkanes via dehydrogenation pathways to give olefins at 200°C and above.[18,26-28] The key to the effectivness of the PCP – based catalysts appears to be their long –term stability at very high temperatures (e.g 200°C) . Such temperatures are sufficiently high, in principle, to overcome the large positive enthalpy of dehydrogenation without the use of a sacrificial acceptor.[13,14]

However, these systems suffer from poor conversions and low selectivity. At higher product concentrations, the alkene inhibits the catalyst and tends to isomerise to the more substituted alkenes. Only approximately 10% of the alkane can be dehydrogenated. Overcoming the problem of product inhibition and to improve selectivity of the reaction is one of the major challenges to be met in the development of synthetically usefull methods based on complex catalysed dehydrogenation reactions.

The broad temperature range of stability and interaction suggests that functionalisation of the PCP pincer complexes for immobilisation to enable easy separation of the catalyst from the products is promising.[29] Very often the incorporation of a functional group into the ligand backbone is accompanied with changes in reactivity of the corresponding metal complex. Therefore, investigations of model compounds which are closely related, electronically and structurally, to the supported catalysts need to be performed. In this thesis the synthesis and characterisation of functionalised PCP iridium complexes is reported. In contrast to the non-functionalised congener, it was found that some complexes are kinetically unstable and undergo a second intramolecular C-H activation. Interestingly this is a low temperature C-H activation by a 16e Ir^{III} species.

1. General Section

1.1 Aspects of Pincer Ligands[15]

The control of the properties of metal centers by a well defined ligand system is an ultimate goal of inorganic and organometallic chemistry. Chelation, that is the binding of a ligand to a metal through two or more bonds, is a versatile method to realise this. In organometallic complexes containing a direct (transition) metal-carbon bond, chelation leads to the formation of metallacycles, which provide additional stabilisation of M-C bonds. Pincer complexes are the first organometallic complexes containing terdentate monoanionic ligands which were reported in the late 1970s. These `` pincer `` ligands have the general formula $[2,6\text{-}(ECH_2)_2C_6H_3]^-$ (ECE) and comprise a potentially ECE terdentate coordinating, monoanionic array, where E is a neutral two-electron donor such as NR_2, PR_2, AsR_2, OR, or SR, while C represents the anionic aryl carbon atom of the 2,6-disubstituted phenyl ring. Metal complexation with pincer ligands usually occurs with formation of two five-membered metallacycles to afford complexes $[MX_n(ECE)L_m]$ (Scheme 1).

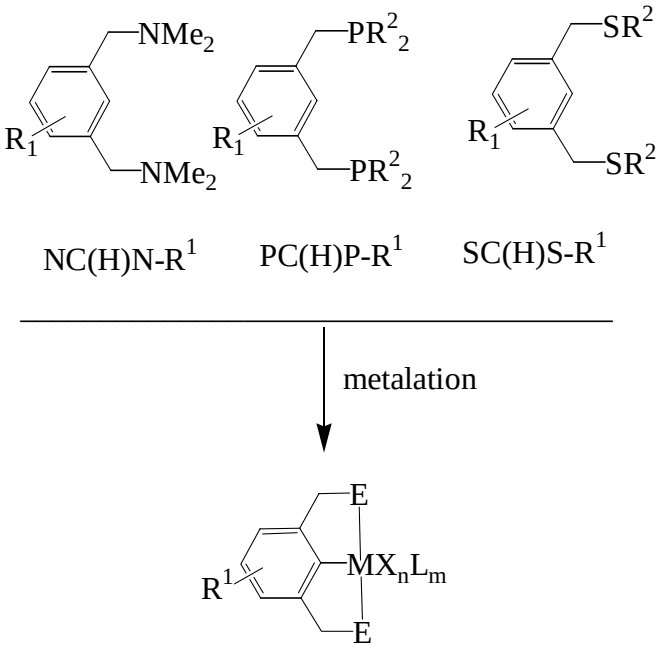

Scheme 1

By far the most frequently observed is the meridional η^3-ECE-coordination mode, in which the ligand bonds to the metal center in a terdentate manner as a six-electron donor with

trans-positioned neutral donors E. This bonding mode forces the aryl ring of the pincer ligand into a conformation which is approximately coplanar with the coordination plane of d^8 square-planar centers (Rh^I, Ir^I, Ni^{II}, Pd^{II}, Pt^{II}) or with the basal plane of d^6 square-pyramidal metal geometries (Ru^{II}, Rh^{III}, Ir^{III}). Modification of various ligand parameters allows for a refined adjustment of the steric and electronic properties of the complexed metal center without changing its bonding pattern significantly. In such pincer systems, the correlation of modifications in the ligand with the properties of the metal center is exceptionally high. For example, steric influences may be varied by alternating the size of the donor substituents or by introducing functional groups in the benzylic positions. Clearly, some of these modifications will also have electronic consequences. Strong electronic effects are attributed to the type of donor atoms E and the electron-withdrawing or –releasing character of the substituents. Fine-tuning of the electronic properties can also be achieved by further substitution of the aromatic ring. Sites which do not exhibit significant or undesirable influences on the metal center may be used for other purposes, for example, for the introduction of molecular recognition sites or for the anchoring of the ECE-metal group to a support. Thus far the majority of investigations have been carried out with pincer ligands containing nitrogen, phosphorous, or sulfur donor groups.

Direct cyclometalation [eq. 1, R^3=H, CR_3, SiR_3] is a particularly attractive method for the formation of a new M-C bond, since it does not require prefunctionalisation of the pincer ligand in order to achieve regioselective metalation. PCP iridium complexes can be prepared by direct cyclometalation through C-H or C-C bond activation.

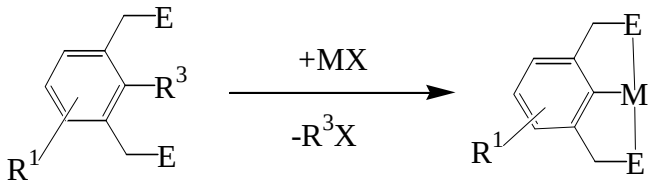

(eq 1)

One aspect common to all pincer metal complexes is the high electron density on the metal center, which provides the metal with Lewis base properties. The pronounced nucleophilic character is a direct consequence of the monoanionic ECE donor motif of the pincer ligand. Complexes containing bicyclometalated pincer ligands offer particularly attractive possibilities for catalytic applications. First, the terdentate binding mode and the covalent M-C σ–bond stabilise the catalytically active (metal) site. This stabilisation is

assumed to effeciently prevent metal leaching, and hence circumvents a problem common to most catalysts containing exclusively heteroatom-coordinated metals. Second, the electronic properties of the metal center are highly sensitive towards modifications in the donor array (substitution patterns and hybridisation of the donor atom E, element alteration). Electronic fine-tuning through variation of the aromatic substituent R^1 represents an additional option in some cases. The steric requirements around the catalytic site may be modified to discriminate against some substrates or to create a chiral pocket for asymmetric catalysis.

1.2 Synthesis of the pincer ligands 1-4

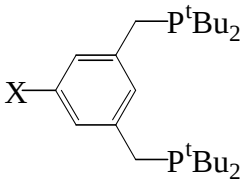

1-4

X = OMe	(**1**)
OH	(**2**)
O^-	(**3**)
$NHCOCH_3$	(**4**)

Chart 1

Pincer ligands **1-4** have been synthesised through multistep synthetic routes according to literature procedures.[16-20] 3,5-Di(t-butylphosphinomethyl)anisole (**1**) was prepared starting with 5-hydroxyisophthalic acid **5** as shown in Scheme 2. Two alternative methods are available to prepare **2**; either by treatment of **8** with BBr_3 and then according to the procedures for the phosphine synthesis (Scheme 3a), or starting from **5** and following the reactions in Scheme 3b. Treatment of ligand **2** with NaH/THF affords **3** (Scheme 3a). The pincer ligand **4** has been prepared starting with 5-aminoisophthalic acid dimethylester **13** following Scheme 4.

All functional groups at position 1 in the PCP pincer ligands **1-4** are electron-donating, increasing the electron density on the aromatic ring. The phosphines **1-4** are all sensitive to air and are soluble in acetone, chloroform and dichloromethane. Methoxyfunctionalised **1** was isolated as gel-like material, while **2** and **4** represent colourless solids. The ionic ligand **3** was only synthesized in THF solutions.

The ligands have been characterised by their $^{31}P\{^1H\}$ NMR as well as ^1H NMR spectra and in the case of **1** by its $^{13}C\{^1H\}$ NMR spectrum (Table 1). Hydroxy functionalised **2** was identified by comparison of its NMR spectra with the reported data.[21] For ligands **1-4**, characteristic features are singlets in the $^{31}P\{^1H\}$ NMR spectra which are in accordance with the ligands strength toward electron donation such that an increase in electron donation causes an upfield shift. O^- has the strongest electron donation ability and therefore **3** has the lowest chemical shift of 30.6 ppm. The functional groups OH and OMe are less powerfull than O^- but stronger than $NHCOCH_3$, and therefore **4** has the highest chemical shift value of 34.4 ppm, whereas **1** and **2** resonate in between, 33.9 and 33.8 ppm, respectively.

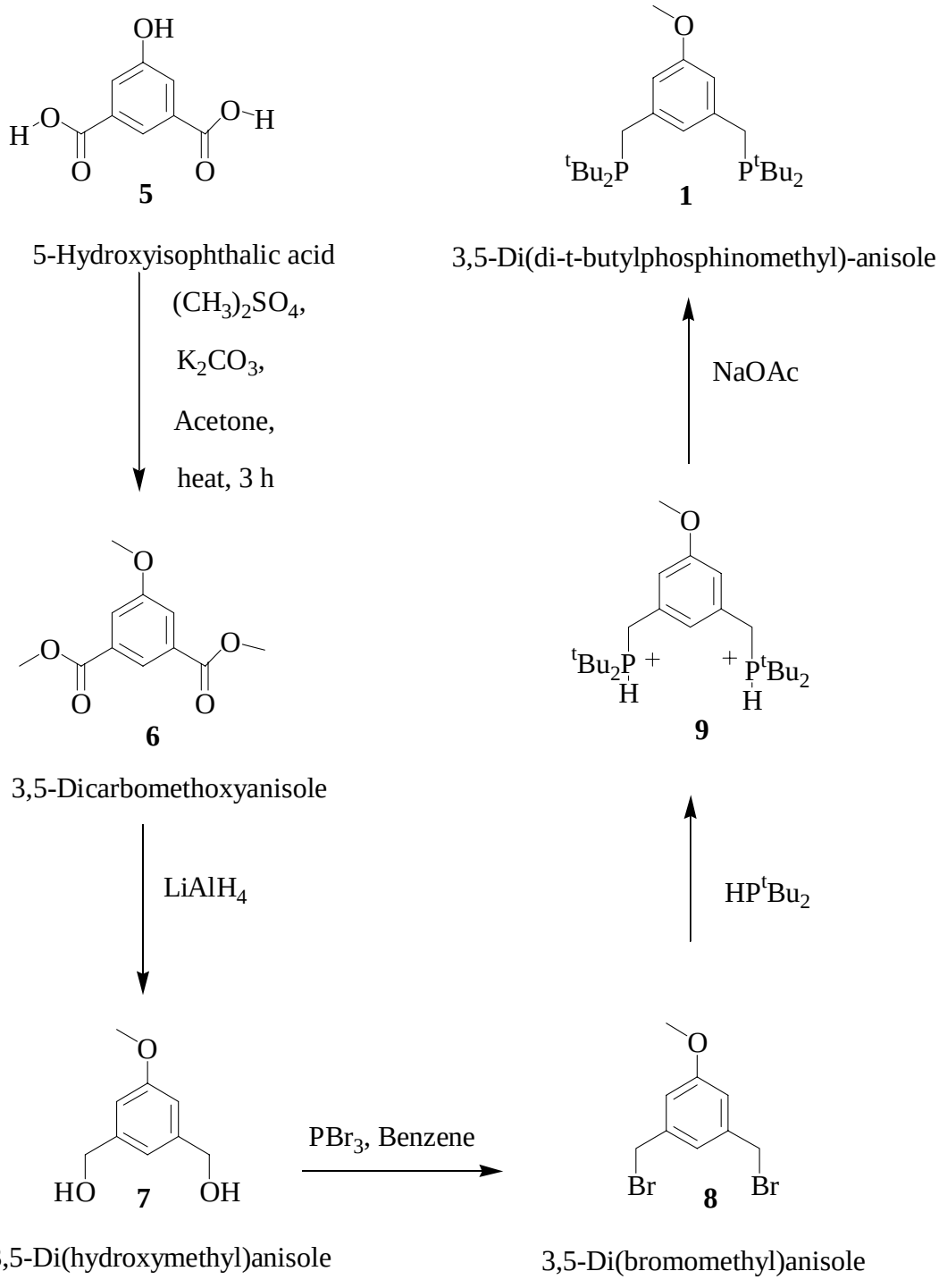
OH
H
O
O
O
O
H
5
5-Hydroxyisophthalic acid
(CH3)2SO4,
K2CO3,
Acetone,
heat, 3 h
O
O
O
O
O
6
3,5-Dicarbomethoxyanisole
LiAlH4
O
HO
7
OH
3,5-Di(hydroxymethyl)anisole
PBr3, Benzene
O
Br
8
Br
3,5-Di(bromomethyl)anisole
HPtBu2
O
tBu2P +
H
+ PtBu2
H
9
NaOAc
O
tBu2P
PtBu2
1
3,5-Di(di-t-butylphosphinomethyl)-anisole

Scheme 2

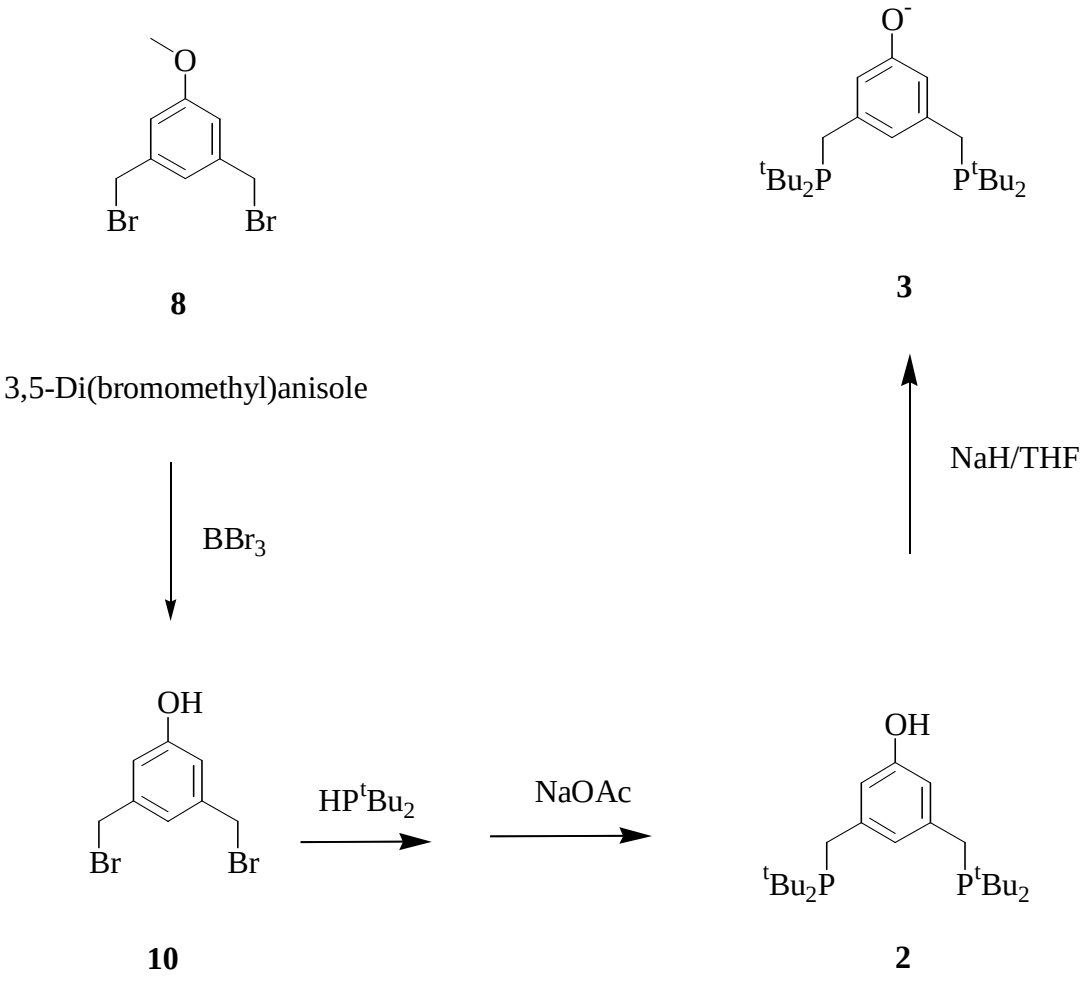

Scheme 3a

In the ^{1}H NMR spectra of **1** and **4** the t-butyl groups appeared as doublets at 1.04 and 1.11 ppm, respectively, due to splitting by the phosphorous atoms, while the methylene protons gave one broad peak at 2.69 ppm for **1** and a doublet at δ 2.80 in the case of **4**. Aromatic protons appeared as two sets in the ratio of 2:1. The methoxy group of **1** showed a singlet at δ 3.65. In **4** the amide NH proton appeared as a broad hump at δ 9.04, while the methyl function of the amide group showed a singlet at δ 2.13. There is a clear downfield shift in δ values of the aliphatic and aromatic protons in **4** due to less electron donation by the amide group which makes the system less shielded compared to **1**.

In the $^{13}C\{^1H\}$ NMR spectrum of **1** the t-butyl groups, the quaternary aliphatic carbons, and the methylene carbons, each appeared as one resonance at δ 28.7, 30.6, 27.5, respectively which is splitted into a doublet by the phosphorous nuclei. The two aromatic carbon atoms CH_3OCCH appeared as a doublet at δ 111.2, the carbon $CHCCH_2P$ displayed a triplet at δ 122.3, while the quaternary carbon atoms CCH_2P gave a doublet at δ 141.4. All splittings took place by the phosphorous atoms. The methoxy group and the quaternary carbon attached to it, resonate as singlets at δ 54.1 and 158.4 respectively.

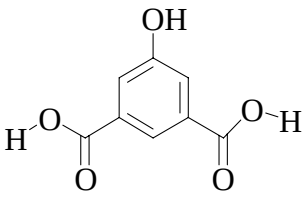

5

5-Hydroxyisophthalic acid

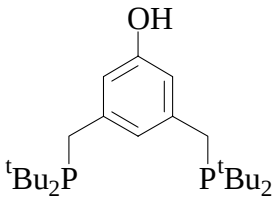

2

3,5-Di(di-t-butylphosphinomethyl)phenol

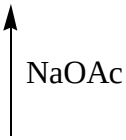

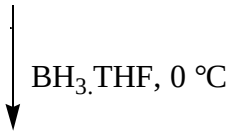

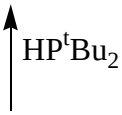

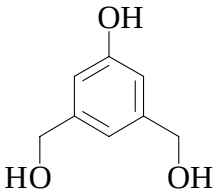

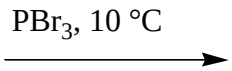

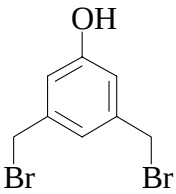

11

3,5-Di(hydroxymethyl)phenol.

12

3,5-Di(bromomethyl)phenol

Scheme 3b

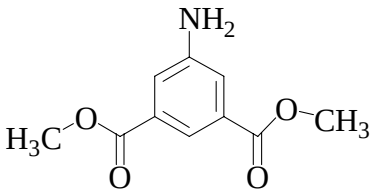

13

5-Aminoisophthalic acid dimethylester

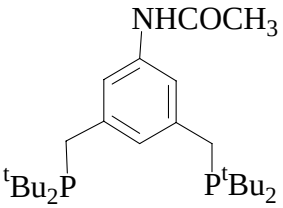

4

N-acetyl-3,5-di(di-t-butylphosphinomethyl)aniline

$LiAlH_4$,

THF

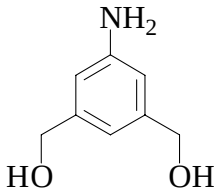

14

3,5-Di(hydroxymethyl)aniline

HP^tBu_2, K_2CO_3,

70°C, 16 h, DMF

Et_3N,

Ac_2O, rt,

stirr 3 h

1) pyridine,

$SOCl_2/CH_2Cl_2$,

0 °C

2) rt, 18 h

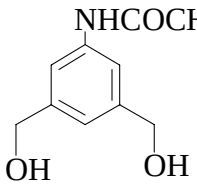

15

N-acetyl- 3,5-di(hydroxymethyl)aniline

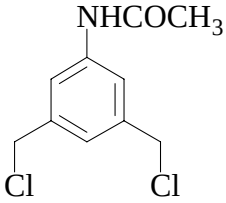

16

N-acetyl- 3,5-di(chloromethyl)aniline

Scheme 4

1.3 Functionalisation with hydrolysable groups

To synthesize stationary phases with the aid of sol-gel process, hydrolysable end groups need to be introduced in the periphery of the complexes that can be used for the conversion of alkanes to alkenes in the interphase. In general the reaction of an alcohol or a phenol with phenylisocyanate gives products known as urethanes, or carbamates, (eq 2).

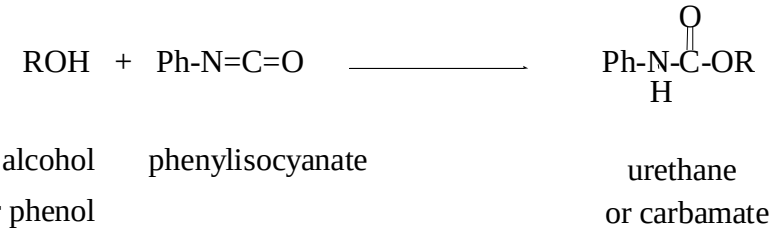

(eq 2)

The commercially available 3-(triethoxysilyl)propylisocyanate can be coupled with both alcohols and amines at different reaction conditions, (eq 3 and 4).

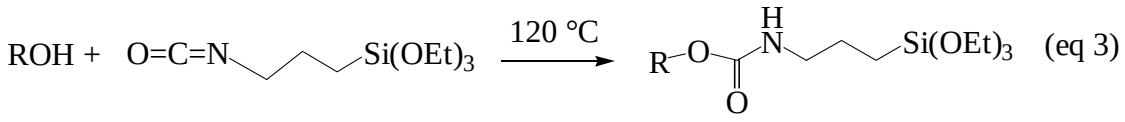

(eq 3)

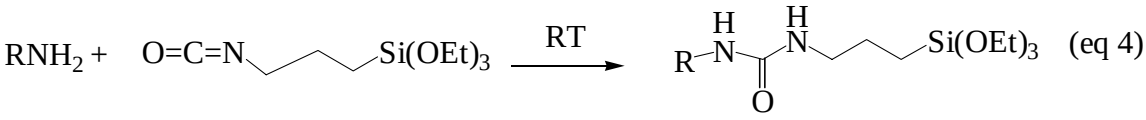

(eq 4)

The reaction of isocyanate with an amine is highly exothermic and takes place at room temperature to form N-substituted amide derivatives, whereas with alcohols the reaction is endothermic and needs heating to form urethanes.[21,22] The progress of the conversion can be followed by recording the change in the IR absorption band of the isocyanate group at 2273 cm^{-1} and the appearance of the carbonyl group absorption band at about 1715 cm^{-1} as well as the N-H bands at about 3336 and 1598 cm^{-1}. The ^{1}H NMR spectrum of 3-(triethoxysilyl)propylisocyanate has well defined splittings which can be used for comparison with the spectrum of the product.

In principle there are three stages where the hydrolysable end group can be introduced to the ligand system. First at the level of the dibromophenol **10**, second at the level of the phosphine ligand **2**, and finally at the transition metal complex.

1.3.1 Reaction of 3,5-dibromophenol (10) with 3-(triethoxysilyl)propylisocyanate

In a first attempt to convert the OH group into a hydrolysable function 3,5-dibromophenol was treated with 3-(triethoxysilyl)propylisocyanate before being coupled with the phosphine to obtain **17**, Scheme 5.The reaction goes through a nucleophilic addition by the phenol OH to the carbonyl of the isocyanate group. The reaction was followed by IR spectroscopy and the products characterised by NMR and mass spectroscopy.

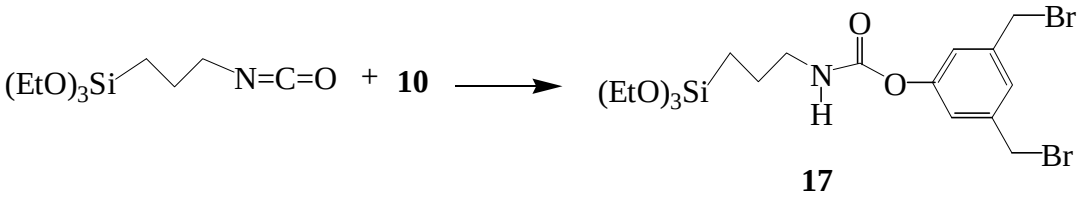

17

Scheme 5

The reaction was done on different stages. The changes in the prominent IR peaks are as follows: Heating the isocyanate and **10** at 65 °C for 90 minutes lead to the appearence of a N-H streching peak (broad) at 3336 cm^{-1}, a N-H bending peak (sharp) at 1599 cm^{-1}, and the carbonyl group absorption (weak) at 1715 cm^{-1}, while the -N=C=O peak (strong) is still observed at 2273 cm^{-1}. Extending the reaction time to 19 h resulted in stronger N-H as well as CO peaks, and a reduced -N=C=O absorption. Increasing the temperature and reaction time to 85°C and 7 h and finally to 95°C and 16 h, according to IR spectra, the -N=C=O function was completely consumed on the cost of the characteristic peaks for the –NHCOO function. Thus mixing the neat reactants stoichiometrically, and increasing the temperature and reaction time gradually indicated a clear reaction, as was recorded by IR spectroscopy.

In the mass spectrum of **17** a peak is observed at 528.1 (100%) for the expected product cation $(M+1)^+$. Another peak at 806.9 (30%) also had appeared which can be identified as a condensation product formed by combination between the main reaction product **17** with the parent phenol **10** (Scheme 6). Loss of H_2O from this intermediate gives a peak at 789.3 (90%) for **19**.

Thin layer chromatography (TLC) analysis of the reaction mixture indicated the presence of the phenol **10** in addition to two more compounds. Trying to seperate these

compounds on silica plates gave complicated spectra, which indicates the decomposition of these products. The seperation and isolation of **17** or **19** was not successful.

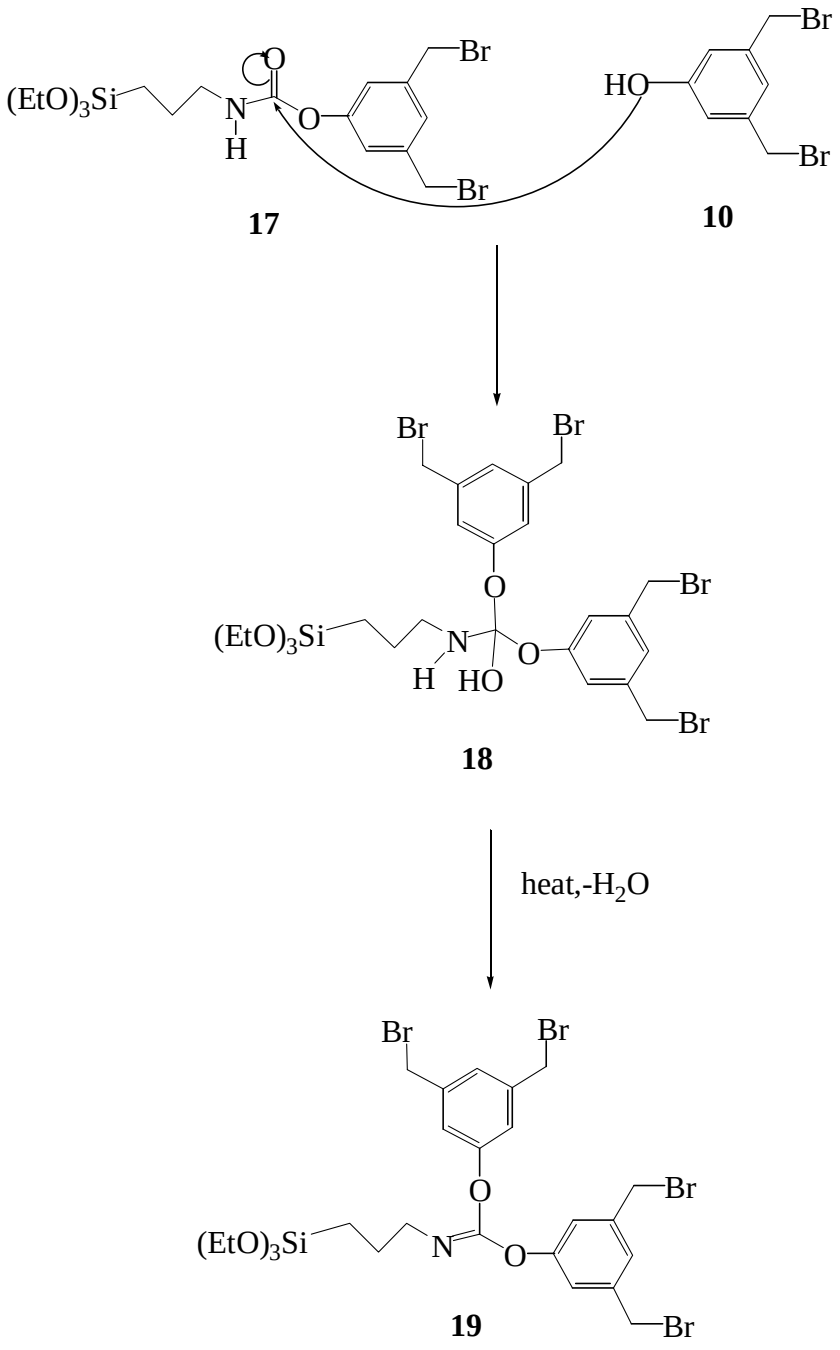

Scheme 6

1.3.2 Reaction of 2 with 3-(triethoxysilyl)propylisocyanate

To avoid side reactions as observed in the case of the dibromophenol the condensation reaction of **2** with 3-(triethoxysilyl)propylisocyanate was performed at low temperatures in solution (Scheme 7). The ligand **2** might be more vulnerable to high temperatures and the acidity of the phenolic group should allow easy transfer of the proton to isocyanate nitrogen already at lower temperatures. Though the results of the reaction were not promising.

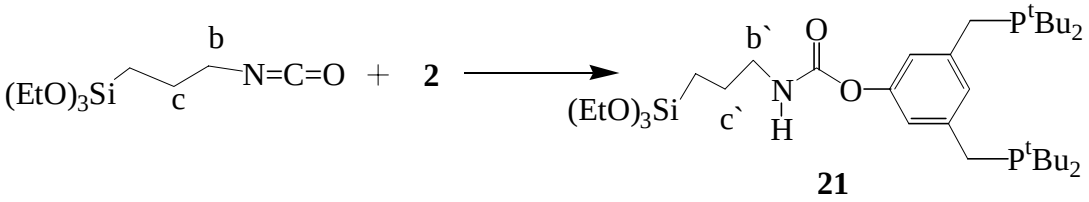

Scheme 7

The reaction was done twice; once by stirring stoichiometric amounts of reactants at room temperature for 18 h in CH_2Cl_2, and a second time by heating the components at 35 °C for 4 h and then stirring at room temperature for about 5 h in CH_2Cl_2. In the ^1H NMR spectrum of the reaction product the resonance of the nitrgen bound CH_2 group changed position from 3.16 to 2.71 at b´in the product **21** which is an indication that a reaction took place. The $^{31}P\{^1H\}$ NMR spectrum of the product displays almost the same chemical shift (δ 33.03) as the starting phosphine (δ 33.83) which is expected as there is no appreciable change in the environment of the phosphorous atoms. A more detailed analysis of the ^1H NMR spectrum revealed that several reactions had occured. Especially the integration ratio of the t-butyl protons and the ethoxy protons suggest that a nucleophilic attack of the phenol at the Si atom has replaced some of the ethoxy groups.

1.3.3 Reaction of 3 with 3-(triethoxysilyl)chloropropane

In a further alternative to generate **22** the sodium salt of the phenol ligand **3** has been treated with 3-(triethoxysilyl)chloropropane to affect an S_N^2 reaction which is known in this case as Williamson synthesis of ethers (Scheme 8).

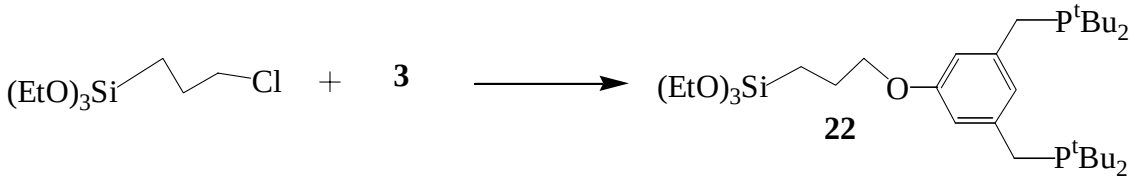

Scheme 8

The reaction was carried out stoichiometrically in THF by heating the miyture at 60 °C for 10h. The results indicated that the reaction was not successful, since there was no clear comparison between ^{1}H NMR spectra of the product and starting $(EtO)_3Si(CH_2)_3Cl$. ^{31}P NMR spectroscopy is not so indicative since it changed from 30.6 ppm for the phenoxide **3** to 32.9 ppm of the product. It seems that the phenoxide acts as a strong base and attacks at silicon center.

1.3.4 Reaction of 3 with 3-(triisopropoxysilyl)chloropropane

To avoid attack at the silicon atom the ligand **3** has been reacted with 3-(triisopropoxysilyl)chloropropane since the isopropyl group is larger than the ethyl group. The reaction was done by heating stoichiometric amounts of the reactants at 60 °C for 12 h in THF (Scheme 9). Results indicated a clear change in the chemical shift of the CH_2Cl protons (position b) at δ 3.53 in the reactant $(^{i}PrO)_3Si(CH_2)_3Cl$ compared to δ 3.23 at b` in the product **23**. This is a clear indication that the reaction has occured. (^{1}H NMR spectra of $(iPrO)_3Si(CH_2)Cl$ and **23** could be compared).^{31}P NMR spectroscopy is not indicative in this case also, and there is no detectable change in δ of ^{31}P NMR.

The product **23** has been reacted then with stoichiometric ratio of $[IrCl(COE)_2]_2$ in C_6D_6 at 60 °C for 12 h (Scheme 9). The ^{31}P and ^{1}H NMR spectra of the product **23a** has been recorded. The CH_2Cl protons at b`` in **23a** appeared at 3.24 ppm the same as in **23** since there is no appreciable change in their environment. A hydride peak appeared at –43.3(t) which is a strong evidence for the formation of a hydride complexed to the metal, but it is very small due to low concentration of the product. The ^{31}P NMR spectrum gave a peak at 69.2 among other peaks.These results are a positive indication for the formation of **23a**.

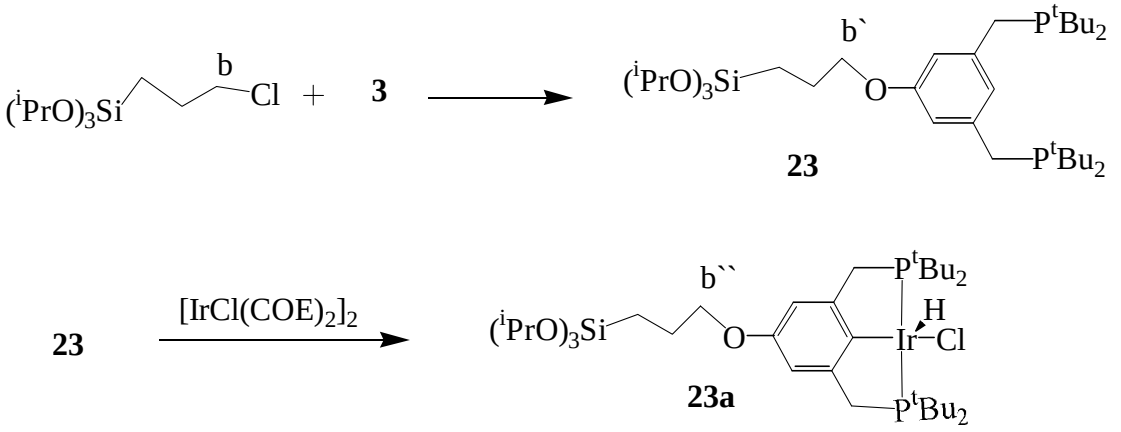

Scheme 9

1.3.5 Summary

Reaction of phenols with isocyanates is well known as mentioned above, but in presence of the triethoxy group on silicon it seems that there are some difficulties. At high temperatures the reaction was proceeding well, and the reqiured product was clearly formed as was indicated by IR and mass spectroscopy but a side product was formed by condensation of the expected product with the parent phenol. Trying to purify the final product on silica plates resulted in decomposition to unidentified species. Phenol group reacts with isocyanate through a nucleophilic addition reaction. Phenol is not a strong nucleophile due to high electronegativity of the oxygen atom, thats why the reaction needs a high temperature. Doing the reaction at low temperaturs in a solvent did not give the aimed product although a reaction took place, but it seems that the phenol attacks the silicon center in the $(EtO)_3Si$- moeity.

Replacing the phenol group with the phenoxide did not give better results since the phenoxide is considered to be a strong base and it was clear that it attacks the silicon center. It was found that using the isopropyl group instead of the ethoxy group and using the phenoxide as a nucleophile gives a positive reaction signs. It is well known also that the reaction of amines with isocyanates is more feasible for the N atom being less electronegative and can be more nucleophilic than oxygen to react with the isocyanate group. Therefore if one can introduce the NH_2 group in the pincer ligands instead of the OH group that would give better

results towards functionalisation of these ligands. We tried to do that for some time, and we've been able to prepare just traces of the amide ligand **4**, but it was not straight forward to get the amine ligand. It is needed to optimise the solvent medium as one major factor to be able to get good yields of **4** or to get the amine ligand. This could be the subject of a new effort needed by another candidate.

1.4 Complex Chemistry of the Pincer Ligands

1.4.1 Intramolecular C-H oxidative addition to Ir^{III}

Over the years many research groups have exploited the synthesis and chemistry of various (PCP)[M] pincer metal complexes ([M] = Rh, Ir, Ru, Pt fragments)[15] first described by Shaw.[23-25] The complexation of C_6H_4-1,3-$(CH_2P^tBu_2)_2$ to a metal fragment generates two five-membered metalacycles and in the case of a d^6 Ir^{III} metal center a square-pyramidal coordination geometry.

However, the treatment of the methoxy functionalized ligand **1** with $IrCl_3 \cdot nH_2O$ in *iso*-propanol/water gave a reaction mixture from which deep red crystals were isolated and identified as the doubly cyclometalated Ir^{III} complex **1b** (Scheme 10). In addition, **1a** was also present in the reaction mixture. Changing to a non-polar reaction medium by treating **1** with stoichiometric amounts of $[Ir(COE)_2Cl]_2$ in toluene also leads to reaction mixtures which contain both **1a** and **1b**. The ratio of **1a** : **1b** varies with reaction time and temperature and the amount of hydrogen present in the system. Thus, if hydrogen is allowed to escape from the reaction mixture, **1b** is observed. On the other hand, if **1b** is treated with hydrogen, **1a** is formed exclusively. (Figure 1) displays a series of $^{31}P\{^1H\}$ NMR spectra recorded for a typical reaction of **1** with $[Ir(COE)_2Cl]_2$ in toluene. The chlorohydrido complex **1a** already arises when the solution is stirred at room temperature for 4 h. The $^{31}P\{^1H\}$ NMR spectrum taken after stirring of the reaction mixture for 3 d shows appreciable amounts of **1b**. Additional heating of the solution at 80 °C for another day leads to the consumption of **1** to form **1a**, which is gradually converted into **1b**. The spectra demonstrate that the cyclometalated chlorohydrido complex **1a** is generated first. In a second step a *t*-butyl C-H bond is intramolecularly oxidatively added to the Ir^{III} complex followed by the reductive elimination of H_2 to give **1b**. C-H oxidative addition, that proceeds from Ir^{III} to Ir^V, has been observed once[26] and was predicted by DFT calculations of $(PCP)IrH_2$ complexes.[27] The deep red complex **1b** can be handled and stored under air for weeks and melts at 200 °C without decomposition.

The NMR spectra of **1a** are comparable with those of previously reported square-pyramidal pincer ligand chlorohydrido complexes where the hydride occupies the apical site.[20,23] Thus, the plane of symmetry perpendicular to the aromatic ring and the metal carbon bond is responsible for the equivalence of the aromatic CH, the ring-CH_2 and two of the *t*-butyl groups. The two $[A_9X]_2$ patterns in the ^1H and the two AXX' multiplets in the $^{13}C\{^1H\}$

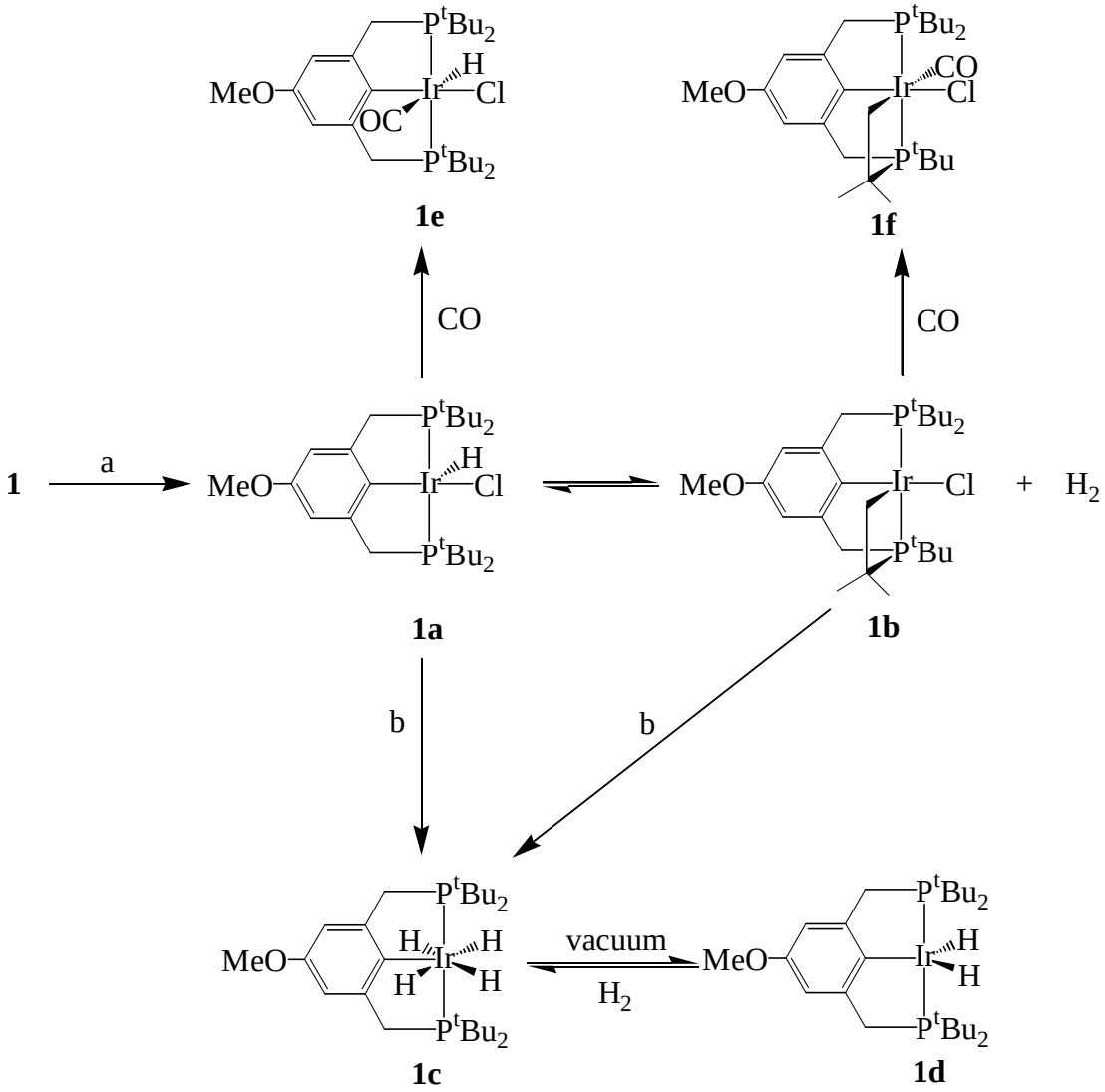

a) $IrCl_3(H_2O)_3$, 2-propanol/water or 1/2 $Ir(COE)_2Cl]_2$, benzene
b) NaH, H_2,THF, sonication 6 h

Scheme 10

NMR spectra as well as the singlet in the $^{31}P\{^1H\}$ NMR spectrum (δ 69.1) are consistent with the $^tBu_2P$-Ir(H,Cl)-P^tBu_2 fragment in the molecule of **1a**. This is also supported by the triplet observed in the ^1H NMR spectrum at –43.21 ppm ($^2J(P,H)$ = 12.8 Hz). The spectroscopic data reveal a square-pyramidal arrangement around iridium with the hydride ligand positioned at the apical site which is in agreement with the X-ray structure analysis of the analogous nitro compound {4-NO_2-C_6H_3-2,6-$(CH_2P^tBu_2)_2$}Ir(H)Cl.[20]

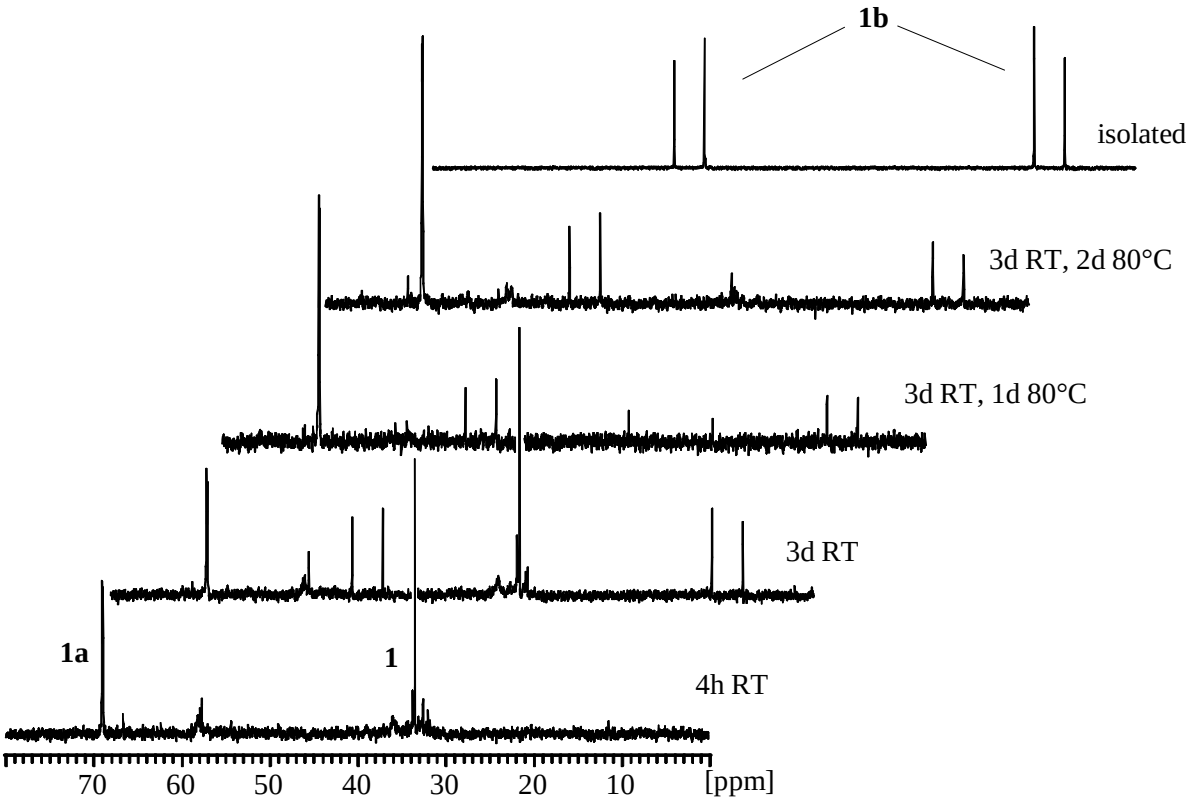

Figure 1 $^{31}P\{^1H\}$ NMR spectra of the reaction of **1** with $[Ir(COE)_2Cl]_2$

On the other hand, the oxidative addition of one *t*-butyl C-H bond to iridium causes the formation of an additional four-membered ring and the loss of any symmetry in the molecule. This is reflected by an increased number of resonances in the NMR spectra of **1b**. Thus the $^{31}P\{^1H\}$ NMR spectrum of **1b** displays two doublets at δ 50.8 and 9.8 which are assigned to P^tBu_2 or (P1) and P^tBu or (P2), respectively (Figure 1, top trace).[28] The large phosphorus-phosphorus coupling of 351.1 Hz agrees with the mutual *trans* position of the two

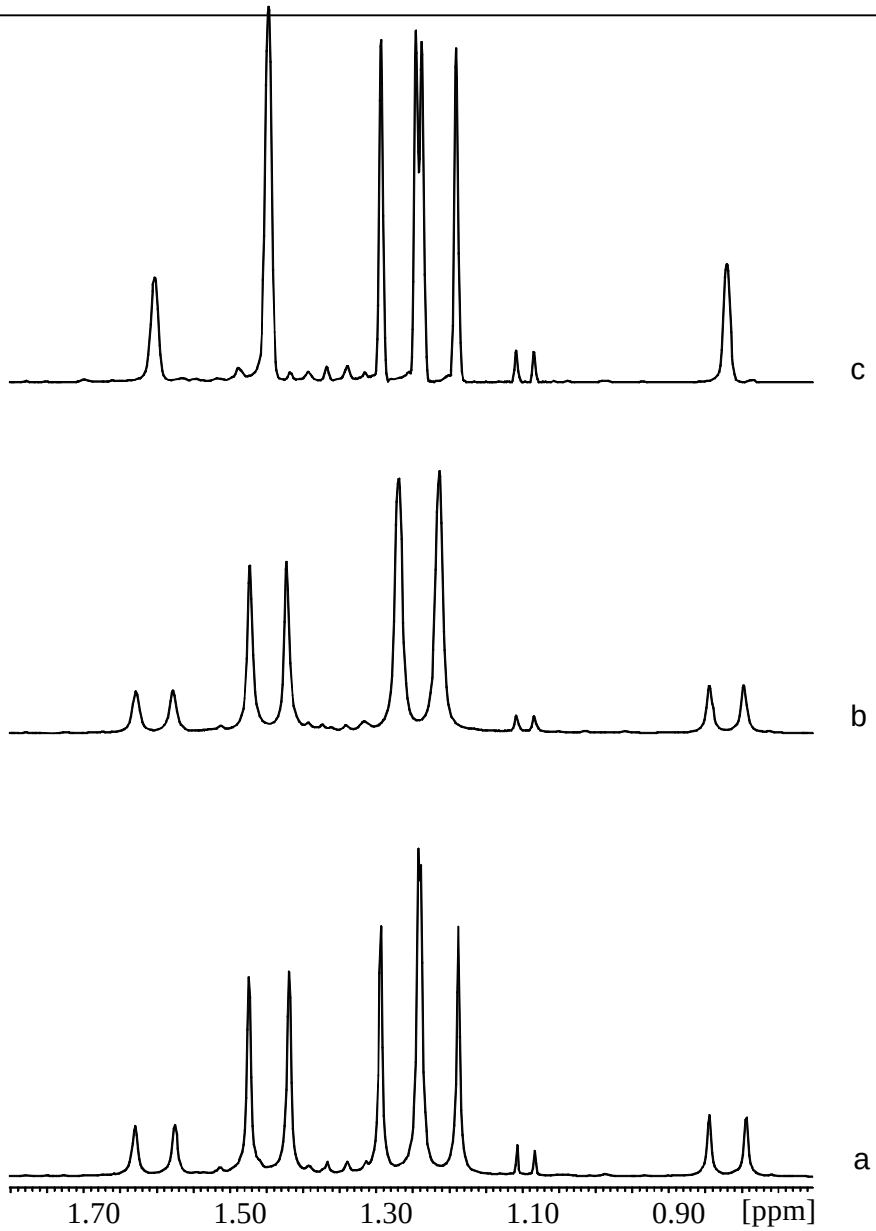

Figure 2a ^{1}H NMR spectra of the t-butyl and methyl groups of **1b** a) regular, b) decoupling of P_1, c) decoupling of P_2

phosphine groups. Three resonances, which are split by the interaction with the corresponding adjacent phosphorus nucleus, are observed for the intact *t*-butyl groups in the ^{1}H (Figure 2a) and $^{13}C\{^{1}H\}$ NMR spectra (Figure 3a, 3b) and (Table 4). Special features are generated by the nuclei of the four-membered ring. Thus, in the ^{1}H NMR spectrum the two diastereotopic protons of the ring methylene group give rise to doublets of doublets of doublets due to coupling to each other and to the two inequivalent phosphorus nuclei (Figure 2b). The resonance of the metal bound CH_2 group is shifted to δ –6.7 in the $^{13}C\{^{1}H\}$ NMR spectrum

and is split into a doublet of doublets by a large and a small phosphorus carbon interaction (Figure 3b). The two geminal methyl groups are observed as doublets each. There is no indication of either hydridic or weakly bound hydrogen to iridium in the ^{1}H NMR spectra at different temperatures.

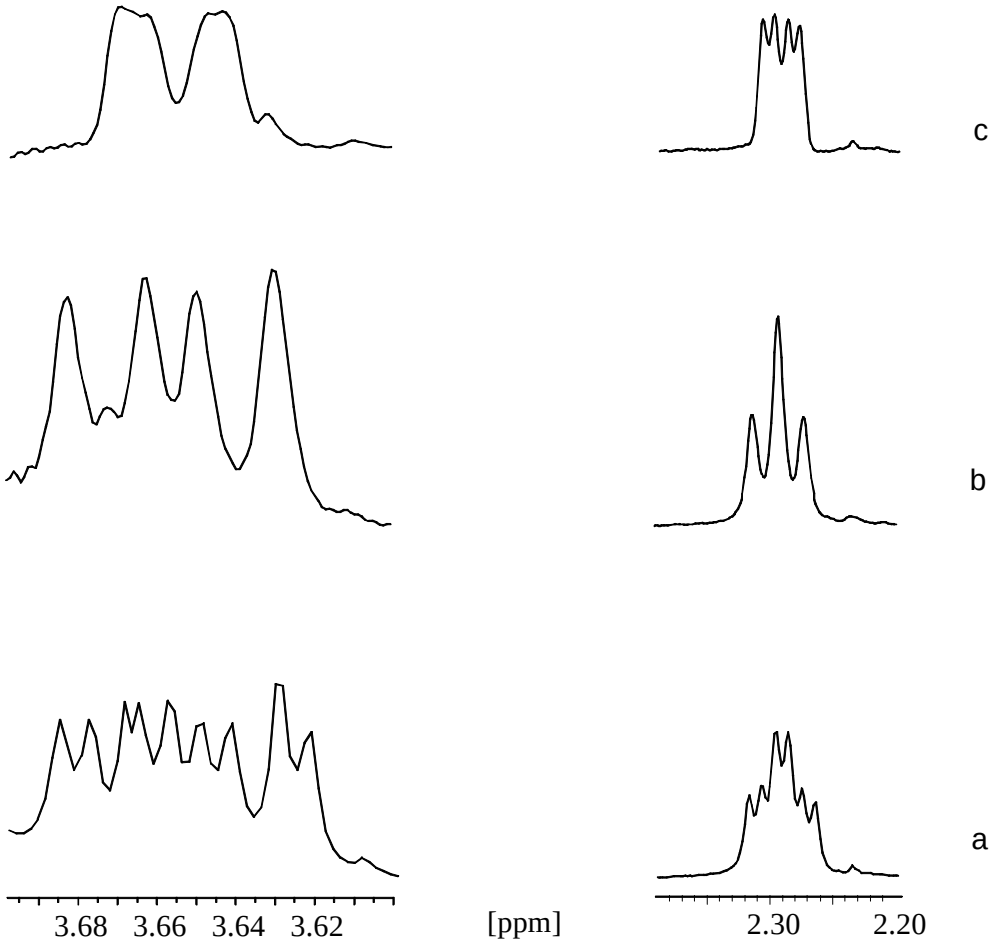

Figure 2b ^{1}H NMR spectra of the bridging CH_2 group of **1b** a) regular, b) decoupling of P_1, c) decoupling of P_2

Table 1. NMR data of compounds **1**, **1a** and **1e** (chemical shifts in ppm, coupling constants in Hz)

	1	**1a**	**1e**
$^{31}P\{^{1}H\}$ NMR			
	33.9; s	69.1; s	57.0; s
^{1}H NMR			
^{t}Bu	1.02; d, ^{3}J(P,H) = 11.06	1.23; m*, N = 12.80	1.27; m*, N = 13.50
		1.28; m*, N = 12.80	1.38; m*, N = 13.81
PCH_2	2.69; s	2.99; m	2.88; m
		3.03; m	
$CHCCH_2P$	6.80; s		
$CHCOCH_3$	6.62; s	6.70; s	6.61; s
OCH_3	3.65; s	3.56; s	3.51; s
Ir-H		-43.21; t, ^{2}J(P,H) = 12.8	-7.59; t, ^{2}J(P,H) = 15.38
$^{13}C\{^{1}H\}$ NMR			
CCH_3	29.6; d, ^{2}J(P,C) = 18.87	29.21; m*, N = 4.7	29.1; m*, N = 4.1
		29.97; m*, N = 4.7	29.9; m*, N = 4.1
CCH_3	31.4; d, ^{1}J(P,C) = 25.16	34.74; m*, N = 22.20	36.47; m*, N = 20.2
		37.54 ; m*, N = 19.60	36.81; m*, N = 26.27
CH_2P	28.3; d, ^{1}J(P,C) = 25.16	35.93; m*, N = 27.80	38.30; m*, N = 28.29
CCH_2P	142.2; d, ^{2}J(P,C) = 12.58	152.18; m, N = 16.8	147.02; m*, N = 12.13
$OCCH$	112.0; d, ^{3}J(P,C) = 12.58	107.83; m, N = 16.17	108.30; m*, N = 15.49
CH_2CCH	123.1; t, ^{3}J(P,C) = 9.43		
OCH_3	54.8; s	54.65; s	54.77; s
$COCH_3$	159.2; s	135.33; s	127.0; s
C-Ir		157.34; t, ^{2}J(P,C) = 2.0	157.70; t, ^{2}J (P,C)= 1.4
CO			182.40; t, ^{2}J (P,C) = 5.0

m* see experimental part

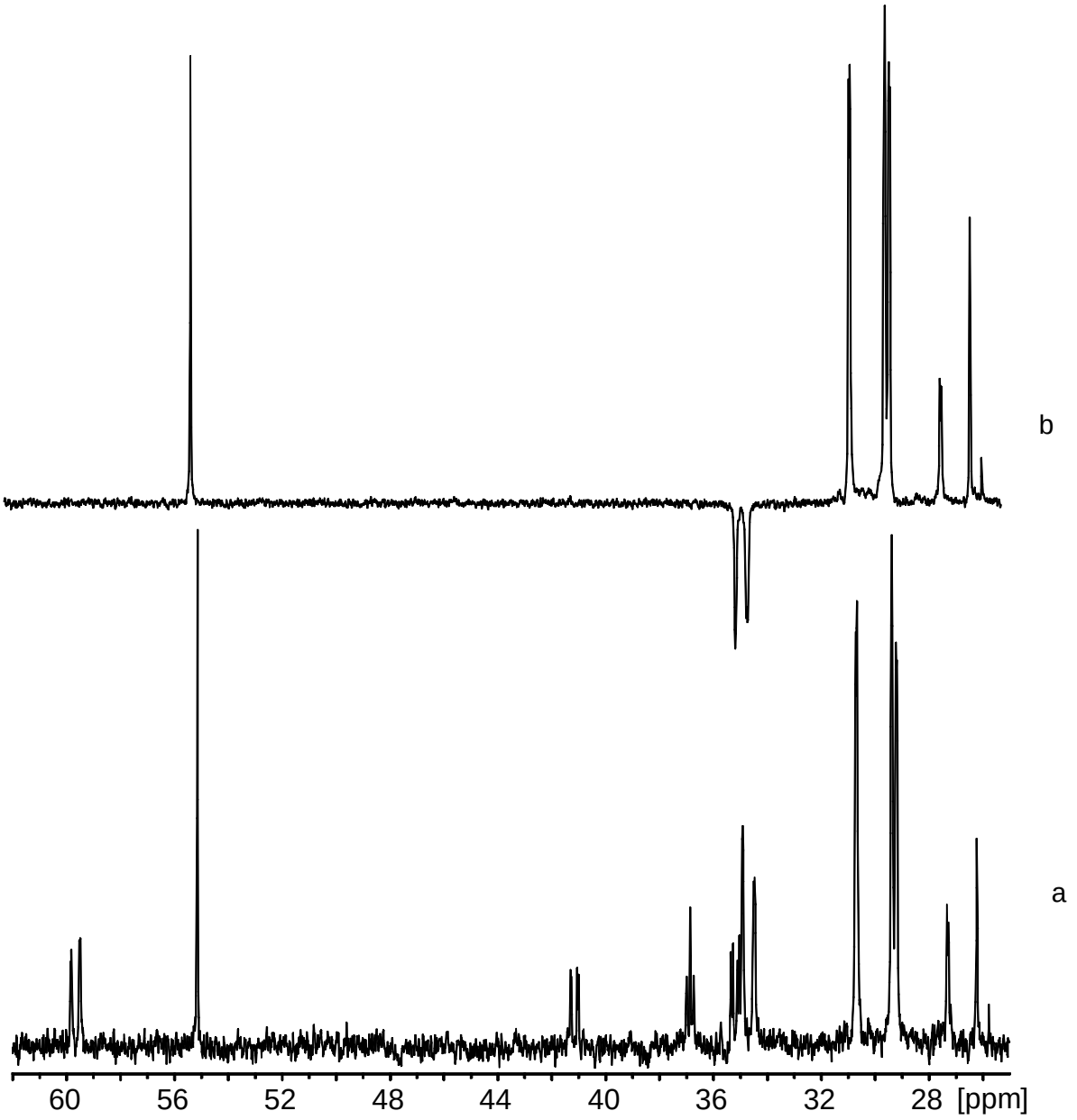

Figure 3a $^{13}C\{^{1}H\}$ NMR spectra of **1b** a) alkane region b) DEPT135

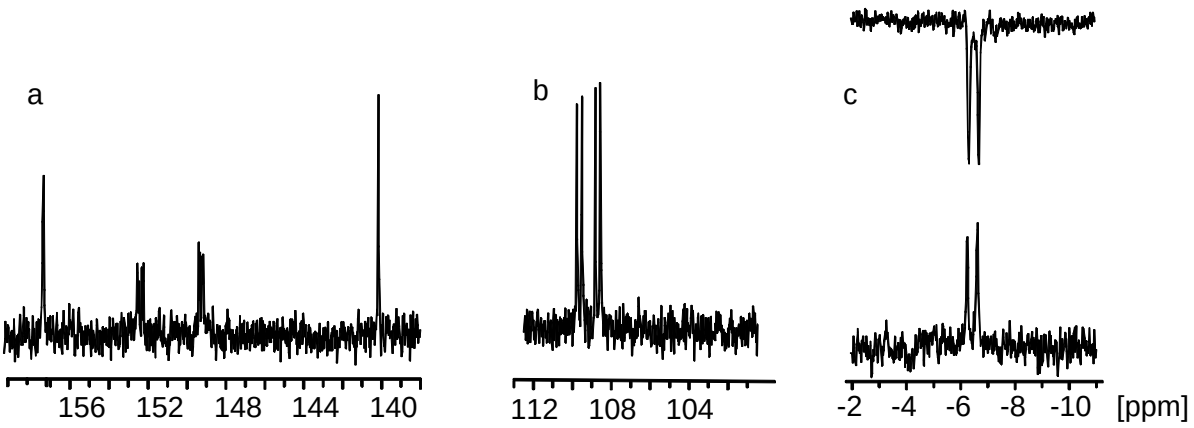

Figure 3b $^{13}C\{^{1}H\}$ NMR spectra of **1b** a) aromatic region b) aromatic CH c) CH_2Ir

1.4.2 X-ray structure analysis of 1b

The stereochemistry of **1b**, which was deduced by NMR spectroscopy in solution, is compatible with the geometry found by an X-ray structure analysis in the solid state. (Figure 4) presents the molecular structure of **1b** in the solid state, bond lengths and angles are collected in (Table 2). Single crystals were obtained by slowly precipitating **1b** from a solution of *iso*-propanol/water. Complex **1b** crystallizes in the monoclinic space group $P2_1/\underline{n}$. The coordination geometry around iridium is best described as distorted square pyramidal. The iridium atom deviates only by 0.016 Å from the basal plane composed of the two phosphorus atoms P(1) and P(2), the carbon atom C(19), and the chlorine. Interestingly, the bond lengths and angles involving the atoms in this plane are comparable to those found for the dihydrido complex $\{C_6H_3\text{-}2,6\text{-}(CH_2P^tBu_2)_2\}IrH_2$,[11] the dinitrogen compound $[\{C_6H_3\text{-}2,6\text{-}(CH_2P^tBu_2)_2\}Ir]_2(\mu\text{-}N_2)$,[29] the hydrido hydroxy complex $\{C_6H_3\text{-}2,6\text{-}(CH_2P^tBu_2)_2\}IrH(OH)$,[30] and the nitro functionalized hydrochloro compound $\{4\text{-}NO_2\text{-}C_6H_2\text{-}2,6\text{-}(CH_2P^tBu_2)_2\}Ir(H)Cl$.[20] Variations are observed for the two Ir-P distances in **1b**, the Ir-P(2) bond being shorter by 0.052 Å than the Ir-P(1) bond. Thus, the formation of the four-membered ring pulls P(2) closer to the metal. In spite of that the Ir-C(10) bond is longer (2.064(4) Å) than the Ir-C(19) distance (2.042(4) Å). The metalated CH_2 group in the apical position is shifted towards the four-membered ring as indicated by the small C(10)-Ir-P(2), 70.85°, and large C(10)-Ir-P(1), 104.23°, angles. A nearly perpendicular arrangement is obvious by the dihedral angle (89.46°) between the planes consisting of the atoms Ir, P(2),

C(9), C(10) and Cl, P(2), C(19), P(1), Ir. From the positions of the Ir and C(8) it is concluded that there is an agostic interaction[31] between the metal and the C(8)-H(8B) bond. The Ir-C(8) distance amounts to 3.021(9) Å, from which the Ir-H(8B) bond length of 2.335(1) Å is obtained.[32,33] An asymmetric cavity at the free coordination site of iridium is generated as the C(13)-P(2)-Ir and C(5)-P(1)-Ir angles differ by 28.6°. Crystal data and collection parameters of **1b** as obtained by x-ray diffraction are collected in appendix A1. Atomic coordinates and equivalent isotopic displacement parameters are in appendix A2.

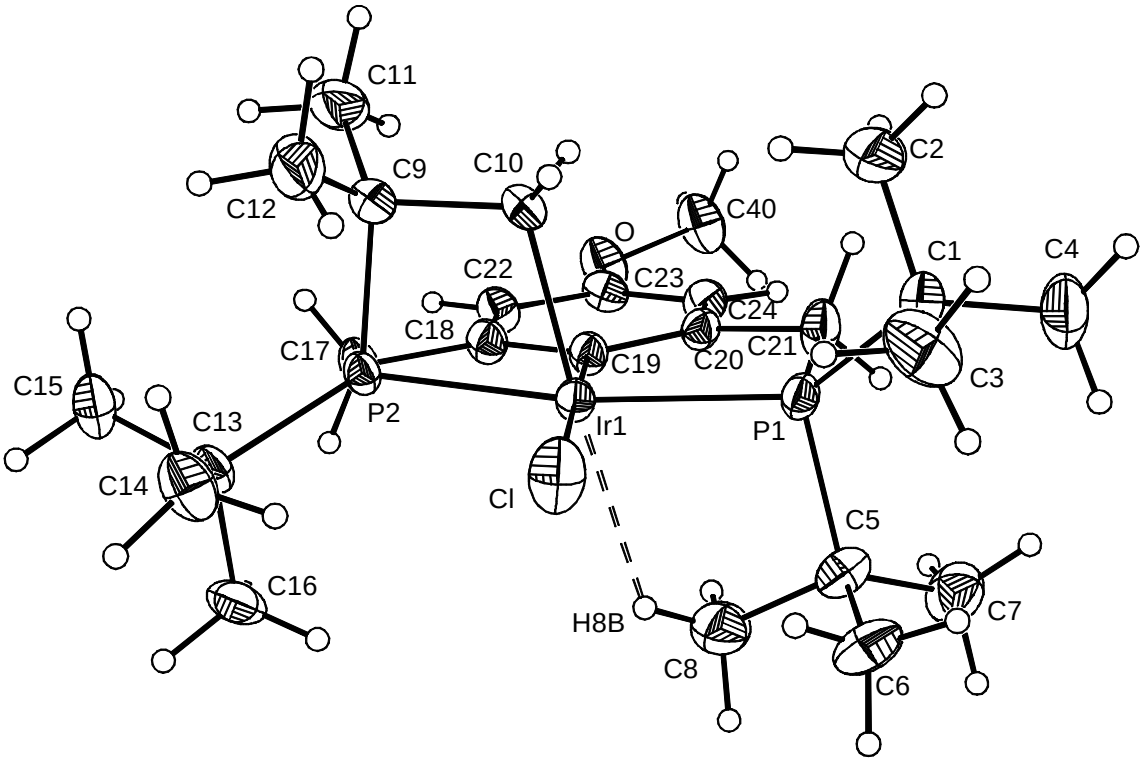

Figure 4 ORTEP representation of complex **1b**

Table 2 Relevant structural parameters of **1b** as obtained by X-ray diffraction and density functional calculations(bond lengths in [Å], angles in [°])

	X-ray	B3LYP/LACVP*	SVWN/LACVP*
Ir(1)-C(19)	2.042(4)	2.053	2.025
Ir(1)-C(10)	2.064(4)	2.086	2.057
Ir(1)-P(2)	2.2702(11)	2.304	2.267
Ir(1)-P(1)	2.3217(11)	2.365	2.275
Ir(1)-Cl	2.4643(11)	2.505	2.430
Ir(1)…C(8)	3.021	3.260	3.462
Ir(1)…(H8B)	2.325	2.827	2.699
P(2)-C(9)	1.872(5)	1.915	1.881
C(9)-C(10)	1.559(6)	1.558	1.538
C(19)-Ir(1)-C(10)	88.37(18)	88.0	83.8
C(19)-Ir(1)-P(2)	82.49(11)	83.0	82.6
C(10)-Ir(1)-P(2)	70.85(12)	71.2	71.1
C(19)-Ir(1)-P(1)	83.29(11)	83.2	82.1
C(10)-Ir(1)-P(1)	104.23(12)	103.3	103.9
P(2)-Ir(1)-P(1)	165.06(4)	165.2	164.2
C(19)-Ir(1)-Cl	177.38(12)	171.2	177.2
C(10)-Ir(1)-Cl	94.16(14)	100.7	93.5
P(2)-Ir(1)-Cl	97.70(4)	98.0	97.0
P(1)-Ir(1)-Cl	96.72(4)	96.4	98.4
C(9)-P(2)-Ir(1)	88.71(15)	87.6	87.8
C(10)-C(9)-P(2)	94.0(3)	94.6	94.4
C(9)-C(10)-Ir(1)	106.0(3)	106.4	106.1

1.4.3 Reactivity of complexes 1a and 1b towards NaH and CO

Reactions of complexes **1a** and **1b** are presented in Scheme 10. Treatment of solutions of either **1a** or **1b** in THF with NaH under a hydrogen atmosphere gives iridium tetrahydride **1c** in nearly quantitative yield. If the solvent is removed under vacuum or by a stream of argon the iridium dihydride **1d** is obtained exclusively. Reaction of **1b** with NaH in THF under an argon atmosphere gives mixtures of **1c** and **1d**, and according to $^{31}P\{^{1}H\}$ NMR spectroscopy, one additional product which has not yet been identified. The hydrides **1c** and

Table 3 NMR data of the tetrahydride **1c** and and the dihydride **1d** (chemical shifts in ppm, coupling constants in Hz)

	tetrahydride **1c**	dihydride **1d**
$^{31}P\{^{1}H\}$ NMR		
	74.50, s	87.4; s
^{1}H NMR		
^{t}Bu	1.19; m*, N = 12.8	1.35; m*, N = 13.24
CH_2	3.25; m*, N = 7.46	3.24; m
CH	6.82; s	7.02; s
OCH_3	3.59; s	3.58; s
Ir-H	-9.12; t, ^{2}J(P,H) = 9.66	-19.75; t, ^{2}J(P,H) = 9.14
$^{13}C\ \{^{1}H\}$ NMR		
$C(CH_3)_3$	25.7; s	
CP	29.7; d, ^{1}J(P,C) = 2.5	
	30.3; s	
CH_2	41.9; m*, N = 30.3	
CH	107.3; m*, N = 15.2	
OCH_3	55.1; s	
C-Ir	141.5; s	
$CHCCH_2$	149.3; dd, N = 15.3 ?	
$COCH_3$	Not detected	

m* see experimental part

1d were characterized by their NMR spectra (Table 3) which are fully compatible with those of analogous PCP pincer complexes.[11,34] In the ^{1}H NMR spectra of **1c** and **1d** the equivalence of all four *t*-butyl groups indicates a higher symmetry (C_{2V}) of the molecules as compared to **1a** and **1b**.

The triplets observed at –9.12 (^{2}J(P,H) = 9.66 Hz) or –19.75 (^{2}J(P,H) = 9.14 Hz) agree well with the tetrahydride **1c** and the dihydride **1d**, respectively. This is supported by the singlets in the $^{31}P\{^{1}H\}$ NMR spectra at δ 74.5 (**1c**) and 87.4 (**1d**), which split into a quintet and a triplet upon decoupling of the protons with exception of the hydride region (Figure 5).

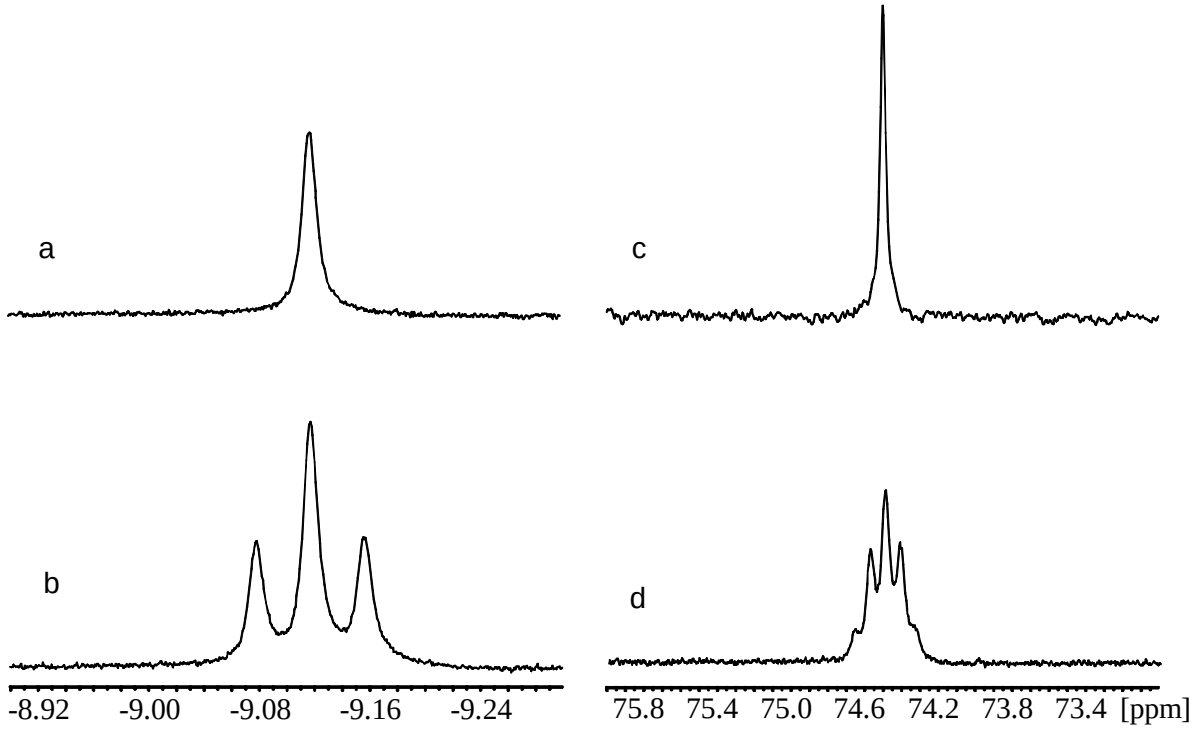

Figure 5 NMR spectra of **1c** a) $^{1}H\{^{31}P\}$ decoupled, hydride region, b) ^{1}H, hydride region, c) $^{31}P\{^{1}H\}$ decoupled, d) $^{31}P\{^{1}H\}$ selectively decoupled

Different products are observed when the deep red solutions of **1a** and **1b** in benzene are treated with carbon monoxide (Scheme 10). In both cases colorless solutions are formed immediately. The spectroscopic data of the carbonyl complex **1e** (Table 1) agree with the

structure displayed in Scheme 10 and are compatible with those reported for {C_6H_3-2,6-($CH_2P^tBu_2$)$_2$}Ir(CO)(H)Cl.[23]

The AB pattern in the $^{31}P\{^1H\}$ NMR spectrum, the number of resonances and their multiplicities in the ^1H and $^{13}C\{^1H\}$ NMR spectra of the carbonyl complex **1f** (Table 4) are comparable with those of the educt **1b** and demonstrate that the four-membered ring is maintained. The reduced electron density at the metal center of **1f** as compared to **1b** has a pronounced effect on the nuclei of the four-membered ring. For this reason, P(2) experiences a high field shift by 32.6 ppm. A high field shift of 1.36 and 1.44 ppm, respectively, is also observed for the protons of the $IrCH_2$ group. In contrast to this, the carbon resonance of the $IrCH_2$ group is shifted down field by 20.96 ppm. Characteristic absorptions in the infrared spectra are observed at 1987 cm^{-1} (**1e**) and 1990 cm^{-1} (**1f**) for the CO stretching vibration.

Table 4 NMR data of compounds **1b** and **1f** (chemical shifts in ppm, coupling constants in Hz)

	1b	**1f**
$^{31}P\{^1H\}$ NMR		
	50.8; d, ^2J(P,P) = 351.1 P_1	-22.8; d, ^2J(P,P)= 314.5
	9.8; d, ^2J(P,P) = 351.1 P_2	42.1; d, ^2J(P,P) = 314.5
^1H NMR		
^{t}Bu	1.11; d, $^3J(P_1,H)$ = 12.79	1.22; d, ^3J(P,H) = 12.87; ($C(CH_3)_3P_1$)
	1.27; d, $^3J(P_1,H)$ = 12.79	1.29; d, ^3J(P,H) = 13.5, ($C(CH_3)_3P_2$)
	1.35; d, $^3J(P_2,H)$ = 13.71	1.32; d, ^3J(P,H) = 12.56, ($C(CH_3)_3P_1$)
$C(CH_3)_2$	1.50; d, $^3J(P_2,H)$ = 13.71	0.94; d, ^3J(P,H) = 15.38
	0.72; d, $^3J(P_2,H)$ = 12.79	1.77; d, ^2J(P,H) = 16.01
PCH_2	3.08; m, 4H	2.85; ddd, ^2J(H,H) = 34.3, ^2J(P,H) = 16.6, ^4J(P,H) = 9.4 (CH_2P_1)
		3.23; m, (CH_2P_2)
$IrCH_2$	3.55; ddd, ^2J(H,H) = 4.68, $^3J(P_2,H)$ = 9.25, $^3J(P_1,H)$ = 2.17	0.75; ddd, ^2J(H,H) = 8.54, $^3J(P_2,H)$ = 7.69, $^3J(P_1,H)$ = 4.08
	2.19; ddd, ^2J(H,H) = 4.68 ,$^3J(P_2,H)$ = 5.37 , $^3J(P_1,H)$ = 2.40	2.29; ddd, ^2J(H,H) = 8.54, $^3J(P_2,H)$ = 13.58, $^3J(P_1,H)$ = 2.43
CH	6.94; d, ^4J(H,H) = 2.28	6.80; s
	6.88; d, ^4J(H,H) = 2.28	

OCH_3	3.61; s	3.63; s
^{13}C {^1H} NMR		
CH_2-Ir	-6.71; dd, ^2J(P,C) = 23.9, ^2J(P,C) = 1.0	14.25; dd, ^2J(P,C) = 30.65, ^2J(P,C) = 3.03
^{t}Bu	29.23; dd, ^2J(P,C) = ^4J(P,C) = 1.3	30.28; d, ^2J(P,C) = 2.69
	29.38; dd, ^2J(P,C) = ^4J(P,C) = 1.3	30.40; s
	30.70; dd, ^2J(P,C) = ^4J(P,C) = 1.3	33.66; dd, ^2J(P,C) = 3.37, ^4J(P,C) = 0.67
CP	35.19; dd, ^1J(P,C) = 14.5, ^3J(P,C) = 5.1	37.27; dd, ^1J(P,C) = 16.17, ^3J(P,C) = 2.02
	36.86; dd, ^1J(P,C) = ^3J(P,C) = 8.1	38.27; dd, ^1J(P,C) = 15.16, ^3J(P,C) = 6.40
	41.16; dd, ^1J(P,C) = 16.5, ^3J(P,C) = 3.0	55.55; dd, ^1J(P,C) = 27.96, ^3J(P,C) = 5.05
	59.67; dd, ^1J(P,C) = 20.6, ^3J(P,C) = 2.4	34.35; dd, ^1J(P,C) = 8.42, ^3J(P,C) = 8.42
CH_3CP_2	26.23; s	28.35; s
	27.34; d, ^2J(P,C) = 4.0	30.00; s
CH_2P	34.52; d, ^1J(P,C) = 3.4	35.84; d, ^1J(P,C) = 28.97
	34.92; s	36.95; d, ^1J(P,C) = 26.95
CCH_2P	150.00; dd, ^2J(P,C) = 11.1, ^3J(P,C) = 3.7	146.14; dd, ^2J(P,C) = 8.08, ^3J(P,C) = 2.69
	153.16; dd, ^2J(P,C) = 14.1, ^3J(P,C) = 5.4	148.0; dd , ^2J(P,C) = 11.45, ^3J(P,C) = 3.37
CH	108.37; d, ^3J(P,C) = 16.8	108.76; d, ^3J(P,C) = 14.82
	109.33; d, ^3J(P,C) = 16.8	109.72; d, ^3J(P,C) = 15.50
OCH_3	55.14; s	55.22; s
CH_3O*C*	140.76; s	132.1; s
CO		177.53; d, ^2J(P,C) = 6.06
C-Ir	158.0; dd, ^2J(P,C) = 1.7	158.1; dd, ^2J(P,C) = 1.01, ^2J(P,C) = 1.01

m* see experimental part

1.4.3.1 X-ray structure analysis of 1e

The stereochemistry of **1e** which was deduced by NMR spectroscopy in solution, is compatible with the geometry found by an X-ray structure analysis in the solid state. Figure 6 presents the molecular structure of **1e** in the solid state, bond lengths and angles are collected in Table (5). Single crystals were obtained by slowly evaporating the solvent (dichloromethane/ether) under low pressure in a Schlenk tube sealed by a rubber stopper. Complex **1e** crystallises in the monoclinic space group $P2_1/\underline{n}$. The coordination geometry around iridium is best described as a distorted square pyramidal. The angles P(1)-Ir(1)-P(2) = 161.23° and C(15)-Ir(1)-Cl(1) = 175.1° indicates that the iridium atom resides at an apical position relative to the plane which is defined by the atoms C(15), P(1), P(2) and Cl(1). The angles C(26)-Ir(1)-C(15) = 89.9°, C(26)-Ir(1)-Cl(1) = 95.0° shows that the carbonyl group is almost perpendicular to the plane which is defined by the atoms C(15), P(1), P(2) and Cl(1). Interestingly, the bond lengths and angles involving the atoms in this plane are comparable to those found for the dihydrido complex $\{C_6H_3\text{-}2,6\text{-}(CH_2P^tBu_2)_2\}IrH_2$,[11] the dinitrogen compound $[\{C_6H_3\text{-}2,6\text{-}(CH_2P^tBu_2)_2\}Ir]_2(\mu\text{-}N_2)$,[29] the hydrido hydroxy complex $\{C_6H_3\text{-}2,6\text{-}(CH_2P^tBu_2)_2\}IrH(OH)$,[30] and the nitro functionalised hydrochloro compound $\{4\text{-}NO_2\text{-}C_6H_2\text{-}2,6\text{-}(CH_2P^tBu_2)_2\}Ir(H)Cl$.[20] The two Ir-P distances in **1e** are almost the same. Other aliphatic and aromatic bonds and angles are within expected values. The hydride which could not be located is positioned *trans* to the carbonyl group and completes the octahedral environment of iridium.

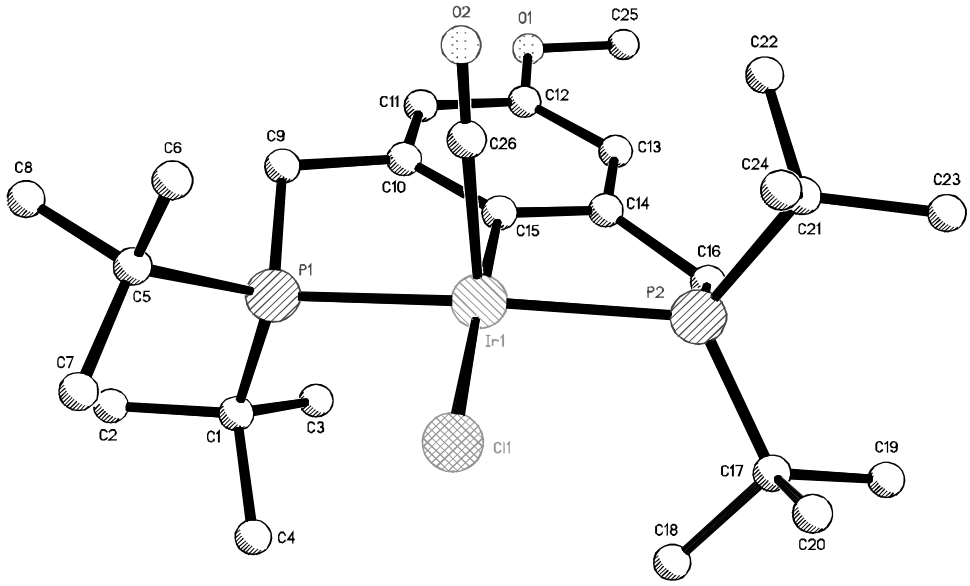

Figure 6 X-ray structure of **1e**

Crystal data and collection parameters of **1e** as obtained by x-ray diffraction are collected in appendix B1. Atomic coordinates and equivalent isotopic displacement parameters are in appendix B2.

Table 5 Selected structural parameters of **1e** as obtained by X-ray diffraction (bond lenghts [Å], angles in [°])

Bond	bond length	angle	angle
Ir(1)- C(26)	2.002	C(26)-Ir(1)-C(15)	89.9
Ir(1)- C(15)	2.048	C(26)-Ir(1)-Cl(1)	95.0
Ir(1)-P(2)	2.352	C(26)-Ir(1)-P(1)	93.0
Ir(1)-P(1)	2.336	C(26)-Ir(1)-P(2)	98.7
Ir(1)-Cl(1)	2.478	C(15)-Ir(1)-P(1)	82.1
P(2)-C(16)	1.824	C(15)-Ir(1)-P(2)	83.2
P(1)-C(9)	1.848	P(1)-Ir(1)-P(2)	161.23
O(1)-C(12)	1.381	C(15)-Ir(1)-Cl(1)	175.1
O(1)-C(25)	1.401	P(1)-Ir(1)-Cl(1)	97.77
O(2)-C(25)	1.056	P(2)-Ir(1)-Cl(1)	95.81
C(9)-C(10)	1.511	C(9)-P(1)-Ir(1)	99.5
C(14)-C(16)	1.519	C(16)-P(2)-Ir(1)	100.1
		C(10)-C(9)-P(1)	108.8
		C(14)-C(16)-P(2)	109.7
		O(2)-C(26)-Ir(1)	174.3

1.4.4 Reactivity of complexes 1a and 1b towards NH_3 and CH_3CN

An aqeous solution of NH_3 reacts instantly with complex **1a** accompanied by a color change from deep red to pale red. Two products are formed **1i**, **1i`**(Scheme 11) according to the $^{31}P\{^1H\}$ NMR spectrum which showed two peaks at δ 49.4 and 50.4 of about the same intensity. In the ^1H NMR spectrum two hydride peaks appeared at δ -20.72 and -21.22 but no discernible splitting was observed. Two methoxy groups at δ 3.62 and 3.64 and the aromatic protons which appeared as two singlets with equal intensity at 6.49 and 6.54 ppm are in agreement with the formation of two products. In contrast when NH_3(g) was used the $^{31}P\{^1H\}$ NMR spectrum changed to give one major peak at δ 50.4, a minor peak at δ 55.1, and small amounts of **1j**. The ^1H NMR spectrum showed two hydrides (triplets) at δ -20.70 (major) (^2J(P,H) = 15.5 Hz) and -23.21 (^2J(P,H) = 15.5 Hz). Two methoxy groups also appeared at 3.62 (major) and 3.67 ppm.

In principle three isomers can be formed by the coordination of ammonia to **1a (1i, 1i`, 1i``** in Scheme 11). The chemical shift range of the observed hydride resonances (-20.70 to -23.21) rule out isomer **1i``**. According to the spectroscopic series of the ligands, the hydride absorption of **1i``** would have been expected between -5 to –13 ppm. This allows to assign the peak of –23.21 to isomer **1i`** and that at –20.70 to **1i**. The differences of the chemical shifts observed for the products in the two reactions is attributed to the water which is only present in the first case.

An aqeous solution of NH_3 reacts with deep red **1b** immediately to give pale red **1j** (Scheme 11). The $^{31}P\{^1H\}$ NMR spectrum displays two doublets of doublets at δ 34.4, -18.8 (^2J(P,P) = 365.2 Hz) and δ 34.2, -17.4 (^2J(P,P) = 334.5 Hz) respectively. In the ^1H NMR spectrum two methoxy groups were recognised at 3.76 and 3.77 ppm. Treatment of the cyclic compound **1b** with NH_3(g) gave the stereoisomer at δ 34.4 and –18.8 (^2J(P,P) = 365.2 Hz) as the major product along with other compounds. The line width of this isomer is larger than in the reaction with NH_3(aq). This indicates a slow exchange process of the coordinated with the gaseous ammonia.

Excess of CH_3CN reacts instantly with **1b** in solution to give **1h** (Scheme 11) and color changes from deep red to pale red. In CD_2Cl_2 the $^{31}P\{^1H\}$ NMR spectrum showed two doublets at δ 36.7 and -19.5 (^2J(P,P) = 366.6 Hz) which are shifted to higher field by 14.1 and 29.3 ppm, respectively compared to the parent complex **1b**. In benzene and in acetone the

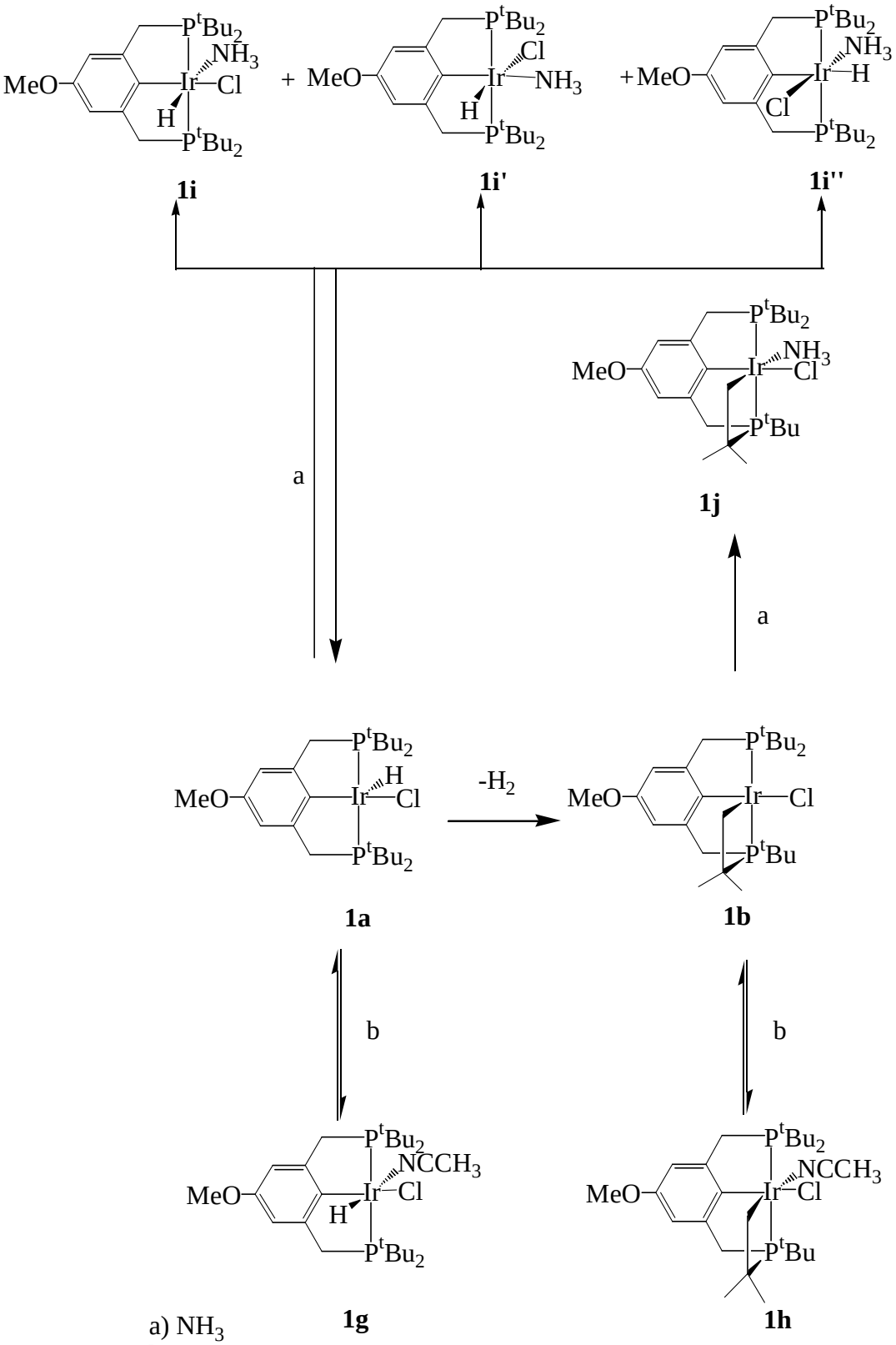

a) NH_3
b) CH_3CN

Scheme 11

position of the resonances was only slightly shifted while in CD_3CN the two doublets appeared at δ 42.37 and -13.54 (^2J(P,P) = 316.4 Hz). Trying to isolate the acetonitrile adduct **1h** by evaporating the solvent and washing the precipitate with pentane, repetitively, the $^{31}P\{^1H\}$ NMR resonances were shifted downfield as the number of washing cycles were increased. All these results indicate that the CH_3CN ligand is labile and an exchange takes place between coordinated and noncoordinated acetonitrile.

Adding CH_3CN to a solution of **1a** in CD_2Cl_2, acetone, or benzene resulted in an immediate color change from deep red to pale red. In each case the $^{31}P\{^1H\}$ NMR spectrum showed a singlet at 55.2 ppm for the major product **1g** (Scheme 11) and a small peak at 51.8 ppm. When the reaction was carried out in CD_3CN exclusively, the major $^{31}P\{^1H\}$ NMR peak appeared at 58.4 (s). In the ^1H NMR of **1g** the hydride resonance is shifted downfield by 20.29 ppm to –22.92 ppm, which is in agreement with the coordination of acetonitrile to the complex. Trying to isolate the acetonitrile adduct resulted in a downfield shift of the $^{31}P\{^1H\}$ NMR resonance which is in agreement with a labile CH_3CN ligand.

When a solution of **1g** in CD_3CN was left at room temperature for 3 days, the ^{31}P NMR spectrum displayed a singlet at 57.8 ppm (major product), and two doublets at δ 56.8 and 34.3 (^2J(P,P) = 367.5 Hz) which indicates that cyclization takes place at room temperature.

1.4.5 Electrochemical studies of 1a and 1b

The redox properties of **1a** and **1b** were investigated by cyclic voltammetric experiments in a dichloromethane/tetra-*n*-butylammonium hexafluorophosphate electrolyte at a Pt electrode. Both compounds are oxidized at potentials only a few hundred mV positive of the ferrocene standard potential (Figure 7). Here, we give a qualitative description of the electron transfer behaviour. A more detailed, quantitative account including simulation studies will be published elsewhere.[35]

Complex **1b** exhibits a peak couple which indicates a simple one-electron oxidation from the starting Ir^{III} form to the Ir^{IV} oxidation state $\mathbf{1b}^+$ (Figure 7, dashed curves, E° ~ +180 mV vs the ferrocene standard[36]). It is important to note that the electrochemical studies of **1b** were performed in the absence of molecular hydrogen. Slow follow up reactions of the oxidized complex may become important only at very slow scan rates. In contrast, complex **1a** shows a more complicated voltammetric signal (Figure 7, full lines). At slow scan rates (see Figure 7a for the example of v = 50 mV/s), the oxidation signal is composed of two waves O_1 ($\mathbf{1b}^+$) and O_2 ($\mathbf{1a}^+$), which are strongly superimposed. Only one reverse peak (R_1) for the first wave at less positive potentials is observed under such conditions. At higher scan rates (see Figure 7b for v = 5 V/s), oxidation wave O_2 becomes dominant. However, at these faster time scales, the reverse (reduction) signal splits into two peaks, R_1 and R_2. The position of R_2 indicates that this peak corresponds to O_2 (E° ~ +270 mV), while R_1 is identical to the reduction peak at slow v (Figure 7a). Furthermore, the superimposition of the cyclic voltammograms of compounds **1a** and **1b** in Figure 7 clearly suggests that the shoulder O_1 and the reduction signal R_1 in voltammograms of **1a** result from the redox couple **1b** $\mathbf{1b}^+ + e^-$. This voltammetric behaviour indicates a "square scheme"[37,38] electrode reaction mechanism with solution equilibria between two redox active complexes on both, the Ir^{III} and the Ir^{IV} oxidation states (Scheme 12). At the beginning of the experiment starting with complex **1a**, the reaction between **1a** and **1b** + H_2 is in equilibrium, with **1b** being formed from **1a**. As the voltammogram at v = 5 V/s shows (Figure 7b), only a small amount of **1b** is present, and the oxidation signal O_1 is almost totally absent under such equilibrium conditions. At v = 50 mV/s, however, **1b** is replenished partially from **1a** by the kinetic process in the Ir^{III} state. Hence, the oxidation signal of **1b** becomes visible. After passage of the oxidation peaks, $\mathbf{1b}^+$ and $\mathbf{1a}^+$ are present and can be observed (by their reduction peaks, R_1 and R_2, respectively) at the fast time scale (v = 5 V/s). If the system is allowed to reach

equilibrium in the Ir^{IV} state (v = 50 mV/s), only R_1 remains. We conclude that the equilibrium between the Ir^{IV} complexes is shifted strongly to the side of **1b**$^+$.

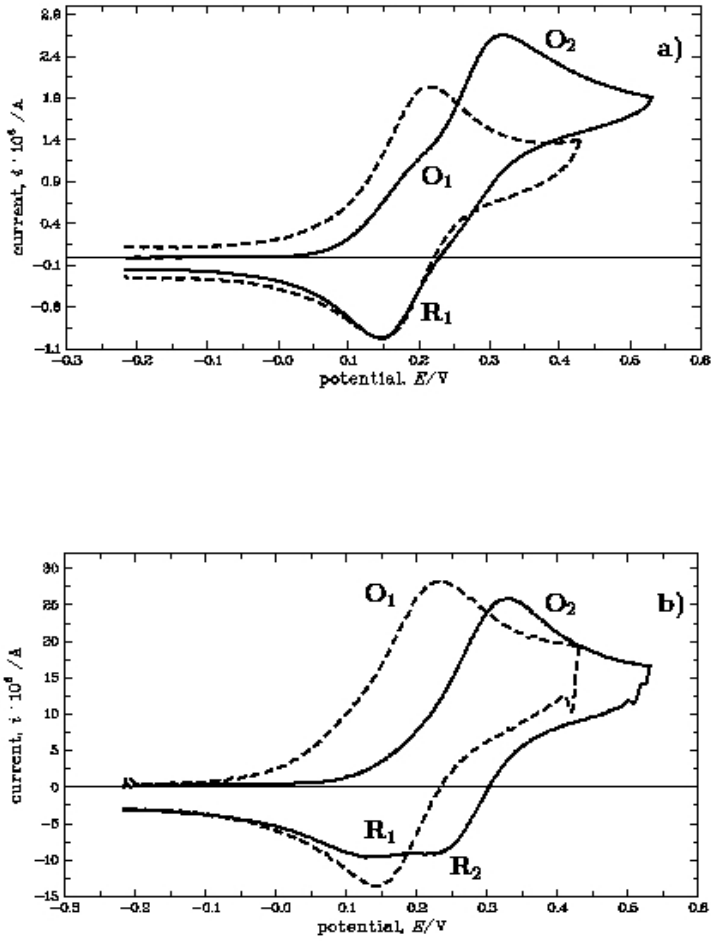

Figure 7 Cyclic voltammograms of complexes **1a** (full lines) and **1b** (dashed lines) in CH_2Cl_2/0.1 M TBAHFP; c(**1a**) = 0.2 mM, c(**1b**) = 0.2 mM; a) v = 50 mV/s, b) v = 5 V/s

A change in the oxidation state of complexes **1a** and **1b** thus reverses the relative stability of the ring open and closed forms: The electrochemical oxidation induces ring formation to generate **1b**. Furthermore, the time scale dependence of signal O_1 clearly indicates the presence of an equilibrium reaction between **1a** and **1b** in the Ir^{III} state.

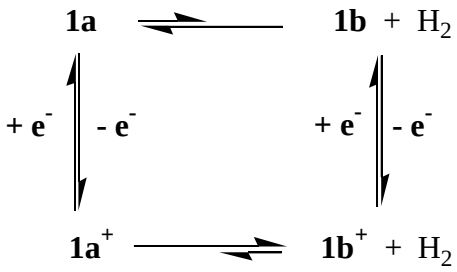

Scheme 12

1.4.6 Quantum Mechanical Calculations

The unusual finding of the stable complex **1b** prompted us to perform density functional calculations at various levels of theory for the model compounds shown in Scheme 13 (X = OCH_3 (prime) and NO_2 (double prime)) as well as for complex **1b** presented in Figure 4. The nitro functionalized complex was taken into consideration, since an X-ray structure of the square-pyramidal {4-NO_2-C_6H_2-2,6-($CH_2P^tBu_2$)$_2$}Ir(H)Cl together with DFT calculations on {4-NO_2-C_6H_2-2,6-(CH_2PH_2)$_2$}Ir(H)Cl was reported.[20] Thus, experimental and theoretical data for the two types of structures represented by **1a** and **1b** can be compared. In the case of the model complexes only one *t*-butyl group was retained during the calculations, the other three groups were replaced by hydrogen atoms in order to reduce the computational effort. The geometric structures of **1a`**, **1a``**, **1b`**, **1k`**, **1l`** and of their nitro functionalized analogues were optimized in the local density approximation (SVWN[39]) as well as with the gradient-corrected B3LYP[40] hybrid functional. For this purpose, the effective core potential SDD[41] (augmented with one set of f-functions on Ir, exponent α_f =

0.938[42]) and LACVP*[43] basis sets were applied using the programs Gaussian 98,[44] Jaguar 3.5[45] and Titan 1.0.5.[46] In the case of **1b**, structure optimizations were performed at the SVWN/LACVP* and B3LYP/LACVP* levels of approximation.

The relative thermodynamical stabilities of the model complexes are presented in appendix C. Almost parallel trends in the theoretical energy differences are obtained for the methoxy and the nitro compounds. All computational procedures predict the square-pyramidal chlorohydrido complexes **1a`**, **1a``** to be most stable. The structures **1m`**, **1m``** are higher in energy by ca. 16 to 30 kcal/mol, depending on whether the SVWN or the B3LYP approach is applied. Therefore, the B3LYP method leads to pronounced larger energy differences (appendix C). The doubly cyclometalated **1b`** and **1b``** (+ $H_2$) are predicted to be highest in energy: they are energetically less stable than **1a`**, **1a``** by about 32 (**1b`**, B3LYP/LACVP*) to 39 kcal/mol (**1b``**, SVWN/SDD(f)). In this case, higher relative energies are obtained in the SVWN approximation. The postulated intermediates **1k`**, **1k``** and **1l`**, **1l``** represent no stable structures on the energy hypersurface. On geometry optimizations they converge to the structures **1a`**, **1a``** at all applied levels of theory.

Bond distances for the model complexes **1a`**, **1a``**, **1m`**, **1m``**, **1b`** and **1b``** as obtained by the various computational procedures are listed in appendix D. In the case of **1m`**, **1m``** the bonding of the two hydrogen atoms to iridium may be best described as η^2-coordinated H_2. The calculated H-H and Ir…$H_{av.}$ distances in these complexes drastically depend on the computational approach. At the SVWN level of theory longer H-H bonds (0.883 to 0.902 Å) and shorter Ir…$H_{av.}$ distances (1.769 to 1.807 Å) are obtained as compared to the B3LYP calculations (H-H: 0.789 to 0.799 Å, Ir…$H_{av.}$: 1.905 to 1.930 Å). In any case, the H-H distances in **1m`**, **1m``** are longer than the theoretical bond length predicted for the $H_2$ molecule (0.743 (B3LYP/LACVP*) and 0.763 Å (SVWN/LACVP*), respectively). Likewise, the Ir…$H_{av.}$ distances in these complexes are much longer than the Ir-H bonds in **1a`**, **1a``** (1.555 (B3LYP/SDD(f), **1a`**) to 1.587 Å (SVWN/LACVP*, **1a``**), see appendix D. These remarkable differences in structural features for **1m`**, **1m``** as obtained by the SVWN and B3LYP methods, respectively, correspond to the trends in the relative energies (see appendix C). The SVWN approximations predict **1m`**, **1m``** to be closer in energy to **1a`**, **1a``** as compared to the B3LYP results. On the other hand, the B3LYP energies are closer to those obtained for complexes **1b`**, **1b``** (+ H_2) than the energies calculated at the SVWN level of theory (appendix C).

Relevant structural parameters of **1b** as obtained by X-ray diffraction and density functional calculations (B3LYP/ LACVP*, SVWN/LACVP*) are collected in Table 2. The same distorted square pyramidal coordination geometry around iridium as observed in the experiment is predicted by the computational procedures. In most cases, the B3LYP bond lengths are too long and the SVWN distances are too short in comparison to the experimental values. Remarkable exceptions are the non-bonded Ir(1)…C(8) and Ir(1)…(H8B) distances, which are predicted to be longer than the experimentally observed ones in both cases. The variation in the two Ir-P bond lengths as well as the difference between the Ir(1)-C(19) and the Ir-C(10) distance are well reproduced by the theoretical approaches. The calculated bond angles are in nearly perfect agreement with the experiment (within the experimental error limits). Exceptions represent the C(19)-Ir(1)-C(10) angle (too small by ca. 4^{o}, SVWN), the C(19)-Ir(1)-Cl angle (too small by ca. 6^{o}, B3LYP) and the C(10)-Ir(1)-Cl angle (too large by ca. 6^{o}, B3LYP). The overall agreement between the experimental crystal structure and the gas-phase structures as predicted for **1b** by both theoretical procedures is very good.

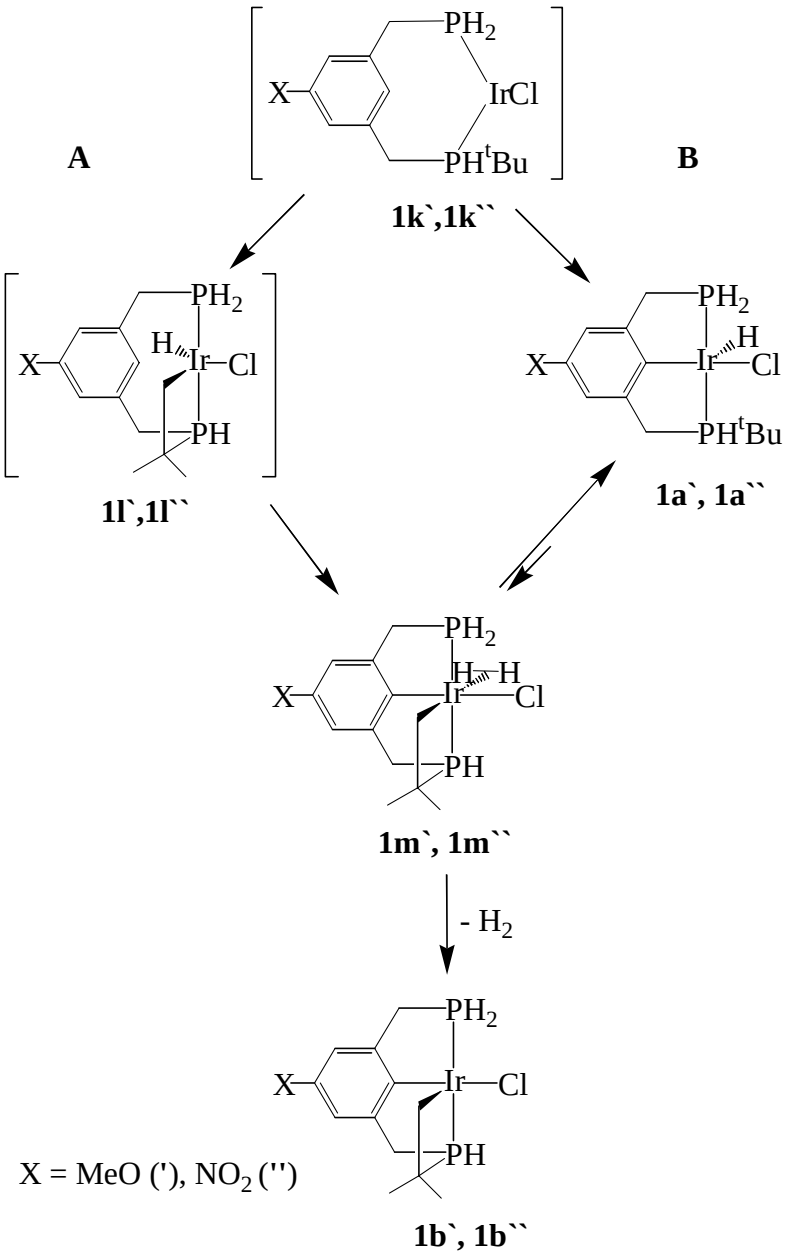

Scheme 13

1.4.7 Reaction of 1a and 1b with Me_3SiOTf

Generation of vacant coordination sites by ligand abstraction is commonplace in inorganic and organometallic chemistry. Me_3SiOT_f is found to be a useful reagent for electrophilic abstraction reactions involving electron-rich complexes RIrLn(R=H,Cl,Me,Ph;L=PMe_3,PEt_3).[21,47] Thus reaction of $Ir(PEt_3)_3Cl$ with trimethylsilyl triflate at room temperature in benzene results in immediate quantitative formation of the novel iridiacycle and Me_3SiCl. It is very likely that the iridiacycle is formed by ligand metallation in the unobserved intermediate $Ir(PEt_3)_3^{+}\ ^{-}OT_f$.

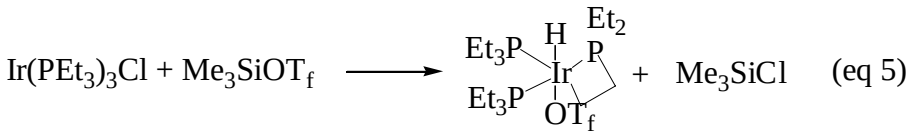

(eq 5)

The complexes $Cp^*(PMe_3)Ir(Me)OT_f$ (Me = CH_3, OT_f = OSO_2CF_3) and $[Cp^*(PMe_3)Ir(Me)(CH_2Cl_2)][BAr_f]$ (BAr_f = $[(3,5\text{-}(CF_3)_2C_6H_3)_4B]^-$ which contain iridium in oxidation state +3 were recently shown to undergo C-H activation reactions with alkanes under mild thermal conditions.[21,48] Two mechanisms are suggested: (a) ‘‘oxidative addition‘‘ path involving Ir(V) intermediate, or (b) a concerted ” σ – bond metathesis ” path (Scheme 14).[21,49]

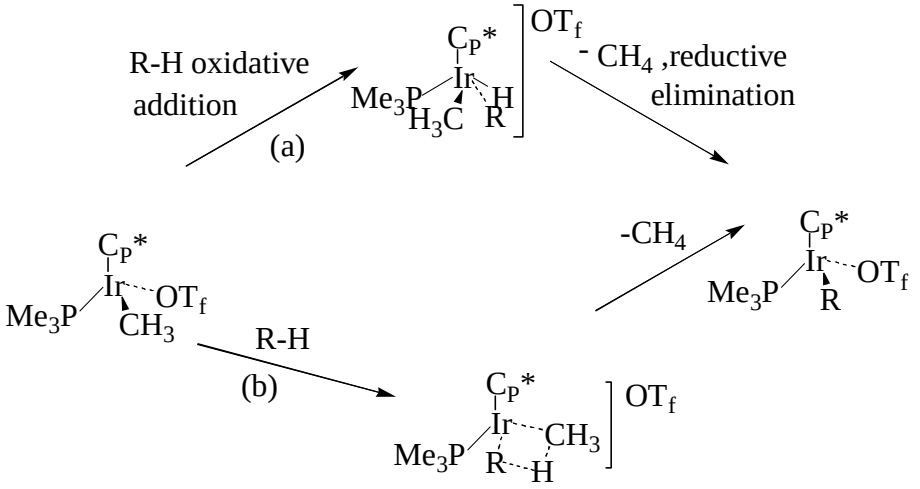

Scheme 14

In order to generate a more reactive species, the cyclic complex **1b** was treated with Me_3SiOT_f in benzene to replace the metal bound chloride by the less coordinating triflate anion. At room temperature the reaction takes place immediately and a blue precipitate is formed which is slightly soluble in benzene and toluene and completely dissolves in acetone. The compound which has been isolated is highly air sensitive and unstable in solution even if kept under argon.

Elucidation of the multinuclear NMR and Mass spectra revealed that a hydrogen is removed from the methylene group in the four membered ring and Me_3SiH is formed instead of the abstraction of the chloride as was expected. The mass spectrum (FD) is governed by three main peaks. The fragment patterns at 648.3 ($[M - CF_3SO_2O]^+$) and 762.5 ($[M - Cl]^+$) demonstrate that both, the triflate and the chloride are constituents of the molecule. Either the triflate or the chloride are able to dissociate from the molecule. This is supported by the appearance of a peak at 613.5 ($[M - CF_3SO_2O - Cl]^+$) where both fragments are lost. The large change of the difference of the chemical shifts of the two non equivalent phosphorous nuclei in **1b** ($\Delta\delta$ = 41 ppm) and **1n** ($\Delta\delta$ = 5.7 ppm) in their $^{31}P\{^1H\}$ NMR spectra speaks about dramatic alterations in the electronic environment of the respective phosphorous nuclei (Figure 8). While the chemical shift of P_2 is hardly affected, P_1 is strongly upfield shifted to give an AB system. The large phosphorous-phosphorous coupling constant of 321.5 Hz proves that the two phosphorous groups remain *trans* to each other. In addition, the number of resonances and their splitting behaviour of the t-butyl and methyl groups in the ^1H NMR spectrum of **1n** (Table 6) state that the structural environment around iridium has not changed compared to **1b**. The strongest evidence for the CH fragment is the doublet of doublet observed at 5.79 ppm in the ^1H NMR spectrum. Upon phosphorous decoupling this multiplet converts into a singlet (Figure 9). This is consistent with the fact that the hydrogen coupling partner is lost in **1n**. The dramatic downfield shift of the carbon atom bound to iridium from –6.7 in **1b** to 50.39 ppm in **1n** is in accordance with a positively charged carbon atom and suggests the structure of **1n** as shown in Scheme 15. Moreover in a ^{13}C DEPT135 experiment the resonance due to this carbon atom phases like the aromatic CH carbons which further supports the hypothesis that a hydrogen from the methylene group in **1b** has been taken off. The connectivity of the proton at δ 5.79 in the ^1H NMR spectrum to the carbon at δ 50.39 in the ^{13}C NMR spectrum was established by a two-domensional C-H correlation experiment. Interestingly the diastereotopic PCH_2 protons of the P_1 group also differ dramatically from those of the P_2 group in **1n**. The ^{19}F chemical shift of δ –78.16 is not indicative, whether the

triflate anion is bound to the carbon or not as no changes of this chemical shift was observed through out all reaction.

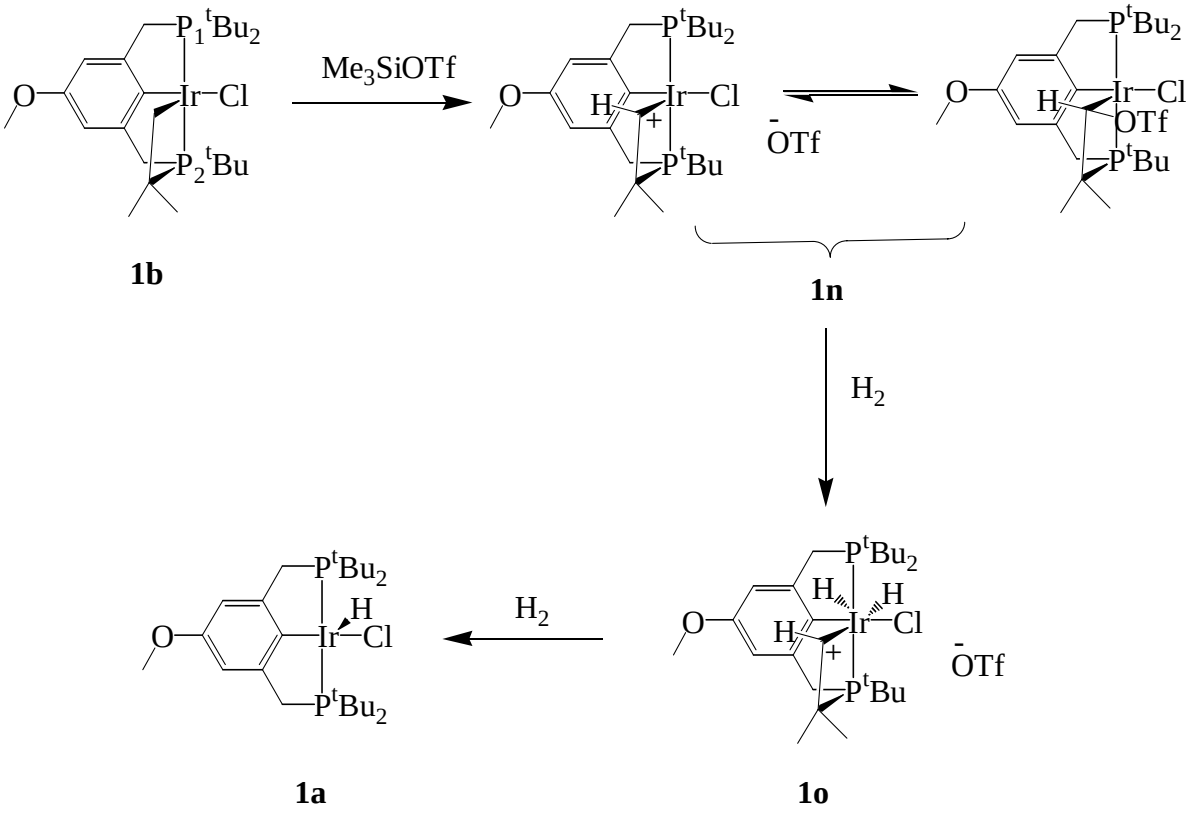

Scheme 15

From a freshly prepared sample of **1n** in toluene-d_8 the argon atmosphere was replaced by a hydrogen atmosphere at –196 °C. In order to allow the hydrogen to diffuse into the mixture the sample was allowed to warm above the melting point of the solution. Immediately after the colour had changed from blue to red the sample was kept at –40 °C. The $^{31}P\{^1H\}$ NMR spectrum of this material showed that a complete conversion of **1n** into a new product had occurred. As the two new doublets at δ 6.2 and –10.7 ($^2J(P,P)$ = 321.5 Hz) do not differ much from those of **1n**, it is assumed that the new complex has a structure which is still similar to that of **1n**. In the ^1H NMR the resonance due to the IrCH proton is shifted further

down field by 0.4 ppm. More importantly two new peaks appear at δ –8.26 and –13.64 which integrate in a 1:1 ratio (Figure 9). This is attributed to two hydrides in different chemical environment bonded to iridium as shown in Scheme 15. Gradually increasing the temperature causes the hydride peaks to disappear. At room temperature a new hydride signal at –42.6 ppm is observed which is split into a triplet by two chemically equivalent phosphorus nuclei. This is confirmed by a singlet at 68.9 ppm in the $^{31}P\{^{1}H\}$ NMR spectrum which upon selectively decoupling the alkane protons gives rise to a doublet. The proton NMR resonances of the t-butyl and the PCH_2 groups are also in agreement with the structure shown in Scheme 15. The presence of triflic acid in the solution is indicated by a broad singlet at δ 12.9 and by the line broadening of the hydride.

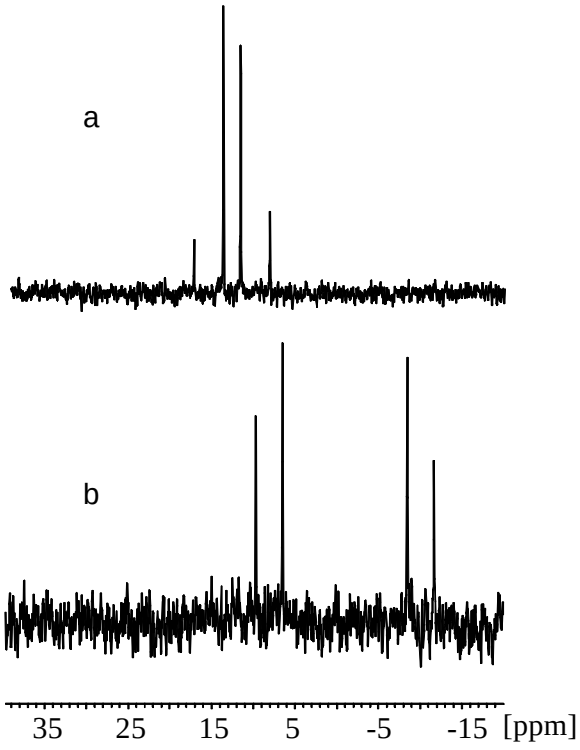

Figure 8 $^{31}P\{^{1}H\}$ NMR spectra of a) **1n** and b) **1o**

Table 6 NMR data for the **1o** and **1n** (chemical shifts in ppm, coupling constants in Hz)

	1o at -40 °C	**1n**
$^{31}P\{^{1}H\}$ NMR		
	-10.7; d, ^{2}J(P,P) = 321.5, P_2	10.4; d, ^{2}J(P,P) = 353.1 P_2
	6.2; d, ^{2}J(P,P) = 321.5 P_1	16.1; d, ^{2}J(P,P) = 353.1 P_1
^{1}H NMR		
IrH	-13.64; br	
	-8.26; br	
^{t}Bu	1.0 – 1.5; br	1.34; dd, $^{3}J(P_1,H)$ = 12.40, $^{5}J(P_2,H)$ = 1.41
		1.49; dd, $^{3}J(P_2,H)$ = 14.29, $^{5}J(P_1,H)$ =2.04
		1.56; dd, $^{3}J(P_1,H)$ = 12.56, $^{5}J(P_2,H)$ = 1.57
$C(CH_3)_2$	0.72; d, $^{3}J(P_2,H)$ = 16.45	1.24; d, $^{3}J(P_2,H)$ = 9.73 Hz
	1.63; d, ^{3}J (P_2,H) =13.70	2.29; d, $^{3}J(P_2,H)$ = 1.93 Hz
PCH_2	2.4 – 4.3; br m	3.08; A part of an ABX pattern, ^{2}J(H,H) = 16.49,
	4.7; br. m	$^{3}J(P_1,H)$ = 8.6, P_1CH_2
		3.18; B part of an ABX pattern, ^{2}J(H,H) = 16.49,
		$^{3}J(P_1,H)$ = 9.26, P_1CH_2
		3.92; dd, ^{2}J (H,H) = 18.45, $^{3}J(P_2,H)$ = 2.35
		5.31; dd, ^{2}J(H,H) = 18.45, $^{3}J(P_2,H)$ = 9.89
IrCH	6.31; br d, ^{2}J(P,H) = 17.82	5.79; dd, ^{2}J(P,H) = 20.41, ^{3}J(P,H) = 7.45
C*H*	6.57; s	7.44; d, ^{4}J(H,H) = 2.20
	6.70; s	7.51; d, ^{4}J(H,H) = 2.20
OCH_3	3,51; s	4.13; s
$^{13}C\{^{1}H\}$ NMR		
CH-Ir		50.39; dd, ^{2}J(P,C) = 13.02, ^{2}J(P,C) = 2.72
^{t}Bu		27.91; br, 30.06; s, 31.14; s
CP		36.02; dd, ^{1}J(P,C) = 7.41, ^{2}J(P,C) = 5.39
		37.08; dd, ^{1}J(P,C) = 16.17, ^{2}J(P,C) = 5.39
		38.98; dd, ^{1}J(P,C) = 14.15, ^{2}J(P,C) = 5.39
		54.69; d, ^{1}J(P,C) = 20.88
CH_3CP_2		23.78; d, ^{2}J(P,C) = 2.4
		28.90; d, ^{2}J(P,C) = 2.4

CH_2P		29.40; d, ^1J(P,C) = 21.9, CH_2P_1
		30.40; d, ^1J(P,C) = 20.0, CH_2P_2
CCH_2P		174.68; dd, ^2J(P,C) = 4.38, ^3J(P,C) = 1.68,
		176.38; s
CH		119.48; d, ^3J(P,C) = 11.45
		120.15; d, ^3J(P,C) = 7.41
OCH_3		60.06; s
CH_3OC		154.28; s
C-Ir		124.5; dd, ^2J(P,C) = 24.58

m* see experimental part

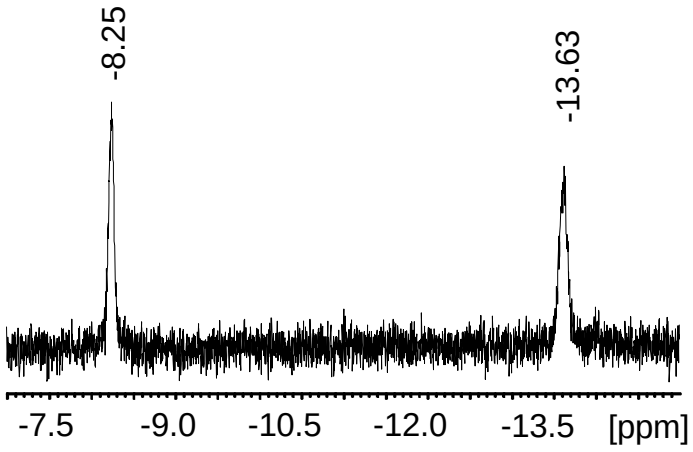

Figure 9 Hydride region of the ^{1}H NMR spectrum of **1o**

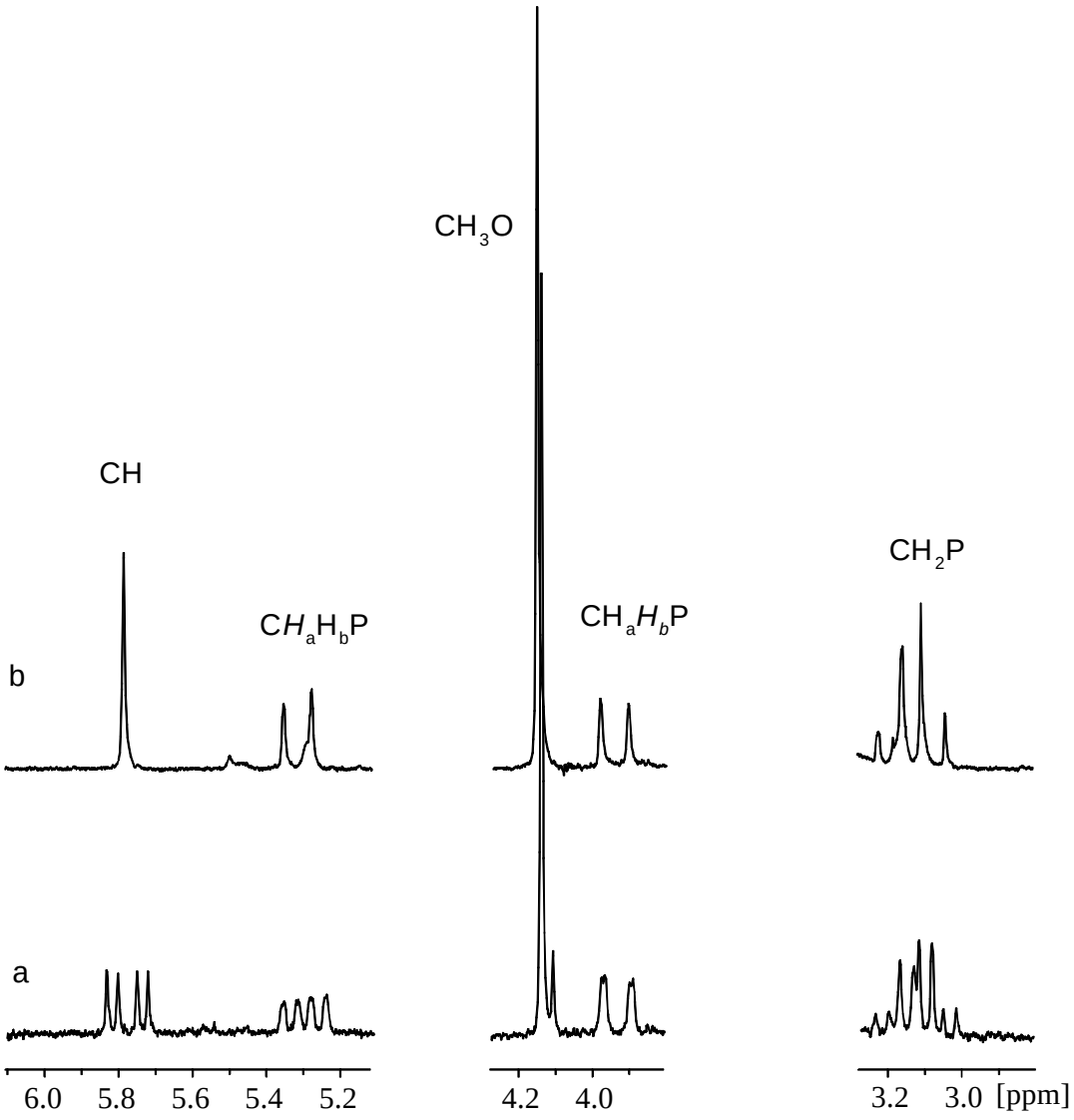

Figure 10 Selected nultipletts of the a) ^{1}H NMR spectrum and b) $^{1}H\{^{31}P\}$ spectrum of **1n**

1.4.8 Discussion

Complex **1b** is the result of two consecutive intramolecular C-H bond activations (Scheme 10 and 13).[50,51] The highly reactive 14-electron intermediate **1k',1k''** is formed after coordination of the two phosphine groups either to $IrCl_3$ followed by reduction or to the $IrCl(COE)_2$ fragment accompanied by loss of COE. Although, according to our calculations, structures **1k',1k''** are not found to be stable, intermediates such as **1k',1k''** have been observed for ruthenium[52-54] and platinum[55] and were proposed for rhodium.[56] Thus, there are two possible pathways from **1k',1k''** to **1b',1b''**. In pathway **A** one of the 36 methyl C-H bonds is oxidatively added to iridium followed by the C-H activation of the aromatic C-H bond, while in pathway **B** the reaction of the aromatic C-H bond is preferred over the methyl C-H bonds. All experimental and theoretical data are in favor of pathway **B**, where the bis-chelate with two thermodynamically stable internal five-membered rings is generated first. The analogy to the Thorpe-Ingold effect, where geminal dialkyl groups enhance ring closure, was emphasized by Shaw.[24,57] Indeed the sterically encumbered *t*-butyl groups at the ligated phosphorus atoms, which mimic the effect of geminal dialkyl groups, kinetically facilitate the intramolecular metalation of the aromatic C-H bond. In contrast to this, we had previously shown that in the case of the PCP pincer complex $\{^tBu_2PCH_2CH_2CHCH_2CH_2P^tBu_2\}IrH_2$ there is an equal ease with which *t*-butyl and the ligand backbone C-H bonds can be activated.[58] Thus, one must consider here kinetic vs thermodynamic selectivity. The formation of the phenyl iridium bond occurs first, inspite of the greater number of methyl C-H bonds, because this bond is stronger than the cyclo alkyl iridium bond from the *t*-butyl group. Jones and Feher consistently pointed out that it is the product M-C bond strength that determines hydrocarbon metalation equilibria.[59]

Bruice and Lightstone have postulated that thermodynamic control of intramolecular cyclization reactions is dominated by enthalpy.[60] They conclude that intramolecular cyclization is driven by an accumulation of NAC (near attack conformations) molecules, which define the required conformations for juxtaposed reactants in the ground state leading to exact conformations in the transition state and to a kinetic selectivity for cyclometalation. In the case of pincer ligands, this most likely involves an η^2 arene intermediate, so there is no direct insertion into the aromatic C-H bond.[61-63] Since **1a** is stable to reductive elimination under the conditions of the reaction, the lowest energy pathway for reductive elimination must be the lowest energy pathway for oxidative addition. Thus, calculations sustain the

observation that **1a'**,**1a''** are thermodynamically the most stable complexes and that structures **1k',1k''** and **1l',1l''** are not observed.

Interestingly enough, although numerous complexes of type **1a** have been synthesized and a broad chemistry with these complexes has been developed, the oxidative addition of a C-H bond of one of the *t*-butyl groups to the metal center to form an isolable complex has not been reported before. For this reason, it is more difficult to explain, why **1b**, with two cyclometalated bonds and easily melting at 200 ^{o}C, forms at all, since the calculations show that it is thermodynamically less stable than **1a** and **1m',1m''**. The most likely attack of a *t*-butyl methyl C-H bond is at the free coordination site opposite to the hydride ligand in **1a.** This will generate a seven coordinate Ir^{V} dihydride chloride complex, which rearranges to give the Ir^{III} dihydrogen complexes **1m',1m''**. Although **1m',1m''** were not observed spectroscopically, their theoretical existence was demonstrated by quantum chemical calculations (appendix C). Comparable η^2-H_2 complexes are well established.[64] As demonstrated by the electrochemical studies, complex **1b** + H_2 is in fast equilibrium with **1a,** the equilibrium being on the side of the chlorohydrido complex **1a**. This explains why there was no indication of an η^2-H_2 complex in the ^{1}H NMR spectra. The loss of H_2 from **1m',1m''** leads to the thermodynamically least stable product **1b**. This is only achieved if H_2 is allowed to escape from the reaction mixture, which renders the overall process irreversible. Moreover, this is consistent with the observation that the presence or absence of hydrogen in the reaction mixture regulates the amounts of **1a** and **1b** regardless of different solvents and temperatures during the reaction. Thus, if H_2 is added to pure **1b**, the hydrochloride complex **1a** is formed exclusively. In this case the attack of hydrogen will occur at the empty coordination site, which is *trans* to the iridium bound CH_2 group, and the η^2-H_2 complex **1m',1m''** will be formed. In order to reductively eliminate the *t*-butyl C-H bond, the dihydrogen complex has to rearrange to give a Ir^{V} dihydride intermediate with at least one hydride ligand *cis* to the CH_2 group bound to iridium. This is the microscopic reverse of the *t*-butyl C-H activation (*vide infra*). That the empty coordination site *trans* to the CH_2 group is easily accessible to donor ligands was demonstrated by the reaction of **1b** with CO which gave the carbonyl complex **1f**.

It is finally interesting to note that evidence from the electrochemical experiments shows that the stability of **1a** and **1b** in their respective oxidized Ir^{IV} states is reversed as compared to the Ir^{III} states (Scheme 12). The redox process appears to be facile and both **3** as well as **1b** are easily oxidizable compounds. Consequently, redox processes should certainly be taken into account when considering both the transformation of **1a** to **1b** and the catalytic

activity of pincer complexes of the type discussed here. Indeed, one-electron oxidation has been shown to favour the reductive elimination of hydrocarbons from hydridoalkyl Ir species[65], which is the reverse reaction of a C-H bond activation process.

The possibility of electron-transfer catalysis (ETC) in the C-H activation reaction of the (PCP)Ir complexes can be revealed by comparison of their electrochemical behaviour with the electrochemistry[66] of Cp*Ir(L)Me_2 (L = phosphine).[67] The oxidized form of Cp*Ir(L)Me_2 irreversibly eliminates CH_4, and subsequently adds an aromatic hydrocarbon. The resulting 17-electron species Cp*Ir(L)MeAr$^{\bullet}$ is able to oxidize the starting material and is itself reduced to the closed shell product Cp*Ir(L)MeAr. This is only possible if the formal potentials of the two redox couples account for favourable thermodynamics of the cross redox reaction. In the case of our pincer complexes, the Diversi et al. mechanism would require that the equilibrium **1a** + **1b**$^+$ $\rightleftharpoons$ **1a**$^+$ + **1b** is shifted to the right hand side. An inspection of the redox potentials E° (**1a**/**1a**$^+$) and E° (**1b**/**1b**$^+$) as estimated in the present work, however, shows that the equilibrium constant of this reaction is smaller than unity and that this homogeneous redox process is not in favour of ETC, i. e. **1b**$^+$ is not able to oxidize **1a** to a large extent. Indeed, simulation shows that the redox equilibrium cannot be detected in the cyclic voltammograms.[35]

1.4.9 Summary

The isolation and X-ray crystal structure of **1b** shows that pincer complexes with pendant P-^{t}Bu_2 groups can form thermally stable multiple C-H insertion reactions by consecutive cyclometalations. The experimental data reveal that in solution there is an equilibrium between **1a** and **1b** + H_2 which implies C-H oxidative addition via an Ir^V oxidation state. Loss of hydrogen is the thermodynamic driving force for the isolation of **1b**. Electrochemical oxidation accelerates the C-H activation via an Ir^{IV} state. Moreover, the isolation of **1b** including its air and temperature stability suggests that it will be an excellent immobilization candidate for catalytic preparations.

2. Experimental Part

2.1 General remarks

All experiments were carried out under an atmosphere of argon by use of standard Schlenk techniques. Solvents were dried with appropriate reagents, distilled, degassed, and stored under argon.

5-Hydroxy-1,3-benzenedicarboxylic acid, 5-Aminoisophthalic acid dimethylester, PBr_3, BBr_3, Me_3SiOT_f were purchased from Aldrich. 3-(triethoxysilyl)chloropropane, 3-(triethoxysilyl)propylisocyanate were purchased from Fluka. Di-*t*-butylphosphine[68],[69] $[Ir(COE)_2Cl]_2$[70] and 3-(triisopropoxysilyl)chloropropane, 3,5-(di-*t*-butylphosphino-methyl)phenol[21] were prepared according to literature procedures. $IrCl_3\ nH_2O$ was a gift from DEGUSSA AG.

Elemental analyses were performed with an Elemental Vario EL analyzer. FAB/FD mass spectra were taken on a Finnigan MAT 711 A instrument, modified by AMD and reported as mass/charge (*m*/*z*). The high resolution $^{31}P\{^1H\}$ and $^{13}C\{^1H\}$ NMR spectra were recorded with a Bruker DRX 250 spectrometer at 298 K. Frequencies and standards were as follows: $^{31}P\{^1H\}$ NMR 101.25 MHz, $^{13}C\{^1H\}$ 62.90 MHz. The ^1H and ^{13}C chemical shifts were calibrated to deuterated solvent peaks, which were reported relative to TMS. All assignments were supported by $^1H\{^{31}P\}$ decoupling and ^{13}C 135DEPT experiments. ^{31}P chemical shifts were measured relative to 85% H_3PO_4 ($\delta = 0$). In all cases the number of the hydrogen atoms bound to iridium was obtained by the multiplicity of selectively decoupled ^{31}P NMR spectra (only the alkane region was decoupled).

Cyclic voltammetric studies. Dichloromethane was used as a solvent with tetra *n*-butylammonium hexafluorophosphate (TBAHFP) as supporting electrolyte (*c* = 0.1 M). Dichloromethane (Fluka) was distilled first and then dried by standing for 10-12 h over activated Al_2O_3. TBAHFP was prepared by a procedure as described before.[71] The electrolyte (dichloromethane + TBAHFP) was degassed by three freeze-pump-thaw cycles before transferring it into the electrochemical cell under argon. Concentrations of the complexes **1a** and **1b** were in the range of $1.10^{-4} - 6.10^{-4}$ M.

Cyclic voltammograms were recorded with a BAS 100 B/W electrochemical workstation (Bioanalytical Systems, West Lafayette, IN, USA) controlled by a standard 80486 personal computer (BAS control program version 2.0). All electrochemical experiments were carried out at room temperature under argon with a gas-tight full-glass three electrode-cell. The working electrode was a Pt-disk electrode (Metrohm, A = 0.064 cm^2). The Pt-disk was polished before each experiment with α-Al_2O_3 (Buehler, 0.05 µm). The counter electrode was a platinum wire (∅ 1 mm) spiral with diameter 7 mm. As the reference electrode, a Haber-Luggin double reference electrode[72] was used. The resulting potentials refer to the Ag/Ag^+ redox system (0.01 M in CH_3CN with 0.1 M TBAHFP). All potentials in this paper are reported to an external fc/fc^+ standard[36] and were rescaled to E^0 (fc/fc^+) = 0.218 V vs Ag/Ag^+.

2.2 Syntheses

2.2.1 3,5-(di-*t*-butylphosphinomethyl)anisole (1)

Di-*t*-butylphosphine (4.75 g, 32.4 mmol) was added to a solution of 3,5-di(bromomethyl)anisole (4.75 g, 16.2 mmol) in 30 mL of acetone. The mixture was stirred for a few minutes and then refluxed for 45 minutes, whereupon a white precipitate is formed. The suspension was allowed to cool to room temperature, and the precipitate was collected on a sintered glass frit, washed once with 5 ml of dry acetone and dried under vacuum. Yield (6.10 g, 88%). A solution of sodium acetate (2.7 g, 32.9 mmol) in 10 mL of water was added to a solution of the phosphonium salt (2.0 g, 4.7 mmol) in 20 mL of water. After stirring for 30 minutes, the aqueous phase was extracted with 20 mL of ether (3-5 times). The diethyl ether was removed from the combined organic layers, and the white gel residue obtained was vacuum dried. Yield (0.97g, 50%). Elemental analysis (%) calcd for $C_{25}H_{46}OP_2$ (424.3): C 70.72, H 10.92; found: C 70.27, H 10.52; MS (EI): *m/z* (%): 424.3 (80) $[M]^+$, 368.3 (100) $[M-{}^t\!Bu]^+$, 311.2 (50) $[M-2{}^t\!Bu]^+$, 255.1 (30) $[M-3{}^t\!Bu]^+$, 199.1 (10) $[M-4{}^t\!Bu]^+$; $^{31}P\{^1H\}$ NMR ($CDCl_3$, 25°C, TMS): δ = 33.9 (s); ^1H NMR ($CDCl_3$, 25°C, TMS): δ = 6.80 (s, 1H; CH), 6.62 (s, 2H; CH), 3.65 (s, 3H; OCH_3), 2.69 (s, 4H; CH_2), 1.02 (d, ^3J(P,H) = 11.06 Hz, 36H; CH_3); $^{13}C\{^1H\}$ NMR ($CDCl_3$, 25°C, TMS): δ = 159.2 (s, $\underline{C}OCH_3$), 142.2 (d, ^2J(P,C) = 12.58 Hz, $\underline{C}CH_2$), 123.1 (t, ^3J(P,C) = 9.43 Hz, $CH_2C\underline{C}H$), 112.0 (d, ^3J(P,C) = 12.58 Hz, $CH_3OC\underline{C}H$), 54.8 (s, OCH_3), 31.4 (d, ^1J(P,C) = 25.16 Hz, $\underline{C}CH_3$), 29.6 (d, ^2J(P,C) = 18.87 Hz, $C\underline{C}H_3$), 28.3 (d, ^1J(P,C) = 25.16 Hz, CH_2).

2.2.2 Sodium 3,5-(di-*t*-butylphosphinomethyl)phenoxide (3)

1.0 g (2.44 mmol) of **2** were dissolved in 50 ml of THF in a Schlenk tube and the solution was transfered to another schlenk tube containing an excess amount of NaH along with a magnetic stirrer. The reaction took place immediately and H_2 gas evolved. The solution was stirred for 10 minutes after which it was let to stand for 16 h so that NaH settels down. The supernatant solution was succed by a pipet into another schlenk tube and used in the reactions as it is. $^{31}P\{^1H\}$ NMR (Acetone, 25 °C, TMS) : $\delta = 30.6$

2.2.3 [N-Acetyl-3,5-di(di-t-butylphosphinomethyl)aniline] (4)

Di-t-butylphosphine (0.8 g, 5.5 mmol) was added to a solution of N-acetyl-3,5-di(chloromethyl)aniline (0.64 g, 2.76 mmol) and potassium carbonate (0.97 g, 7.0 mmol) in 15 ml DMF. Few milliliters of water are added just to dissolve the carbonate and to get homogeneous solution. The reaction mixture was heated at 70 °C for 16 h, then it was poured into 150 ml of water and chilled in ice for 24 h to induce precipitation of the product as an off-white solid material. The product was collected by filtration and washed with saturated Na_2CO_3 (2*20 ml), 1N HCl (1*10 ml), and water (2*20 ml). The solid was then dried under vacuum, yielding 0.1 g (12%) of the product. $^{31}P\{^1H\}$ NMR (Acetone, 25 °C, TMS): $\delta = 34.4$ (s); ^1H NMR (Acetone, 25 °C, TMS): $\delta = 9.04$ (br s, 1H; NH), 7.5 (s, 2H, CH), 7.1 (s, 1H; CH), 2.13 (s, 3H; $COCH_3$), 2.8 (d, ^2J(P,H) = 2.5 Hz, 4H; CH_2), 1.11 (d, ^3J(P,H) = 10.4 Hz, 36H; CH_3).

2.2.4 Reaction of the ligand [N-Acetyl-3,5-di(di-t-butylphosphinomethyl)aniline] (4) with $IrCl_3.nH_2O$

(10 mg, $2.1*10^{-2}$ mmol) of **4** and (0.33 g, $1.05*10^{-2}$) mmol of $IrCl_3.nH_2O$ are suspended in 10 ml isopropanol/H_2O in a ratio of 7:1. The mixture was heated at 85 °C for 24 h. $^{31}P\{1H\}$ NMR of the reaction mixture gave a singlet at 68.8. ^1H NMR showed a hydride peak (triplet) at –44.9, indicating the formation of the product. No product could be seperated.

2.2.5 Reaction of 3,5-dibromophenol (10) with 3-(triethoxysilyl)propylisocyanate

A mixture of **10** (0.5 g, 1.8 mmol), and 3-(triethoxysilyl)propylisocyanate (0.45 g, 1.8 mmol) were placed in a dry schlenk tube. The tube was sealed and heated in an oil bath between 65 °C and 95 °C over a period of 24h. The reaction was followed by IR spectroscopy until the complete disappearance of the isocyanate peak at 2273 cm^{-1}. The final product was analysed by NMR (not clean) and Mass spectra which shows the presence of more than one product. The products were decomposed when trying to seperate them by TLC.

2.2.6 Reaction of 2 with 3-(triethoxysilyl)propylisocyanate

(0.13 g, 0.5 mmol) of 3-(triethoxysilyl)propylisocyanate were added to (0.20 g, 0.5 mmol) of **2** in 20 ml of CH_2Cl_2. The mixture was heated at 35 °C for 4h, and stirred at room temperature for 5h. The solvent was distilled and the residue was dried. ^{31}P and ^{1}H NMR are recorded in acetone. reaction was not successful.

2.2.7 Reaction of 3 with 3-(triethoxysilyl)chloropropane

0.13 g (0.5 mmol) of 3-(triethoxysilyl)chloropropane were added to 0.20 g (0.5 mmol) of **3** in 20 ml of THF. The mixture was heated at 60 °C for 10h, and stirred at room temperature for 2h. The solvent was distilled and the residue was dried. ^{31}P and ^{1}H NMR spectra were recorded in acetone. Reaction was not successful and NMR data were not so indicative.

2.2.8 Reaction of 3 with 3-(tripropoxyoxysilyl)chloropropane.

0.14 g (0.5 mmol) of 3-(tripropoxyoxysilyl)chloropropane were added to 0.20 g (0.5 mmol) of **3** in 20 ml of THF. The mixture was heated at 60 °C for 12h. The solvent was distilled and the residue was dried. ^{31}P and ^{1}H NMR spectra were recorded in acetone. ^{31}P spectrum showed a peak at 30.7 ppm for **23**. The product **23** was then reacted with a stoichiometric amount of $[IrCl(COE)_2]_2$ in C_6D_6 and heated at 60 °C for 12h. ^{31}P NMR spectrum of the reaction mixture showed a peak at 69.2 ppm among other peaks, and ^{1}H NMR spectrum gave a triplet for the hydride at –43.3.

2.2.9 General procedure for the synthesis of 1a and 1b

A suspension of **1** (2.53 g, 5.96 mmol) and $IrCl_3 \cdot nH_2O$ (1.00 g, 3.01 mmol) in 24 mL of *iso*-propanol/water (7:1) was stirred at room temperature for 12 h and then heated at 85°C for 24 h. The reaction mixture was allowed to cool slowly to room temperature with continuous stirring, and then cooled in ice/salt for 24 h. Supernatant solution was withdrawn by pipette, and the precipitate was washed two times with *iso*-propanol/water (7:3) with stirring, and dried under vacuum. A mixture of **1a** and **1b** is always observed.

1a: m.p >200°C (dec.); elemental analysis (%) calcd for $C_{25}H_{46}OP_2IrCl$ (652.0): C 46.04, H 7.10, Cl 5.44; found C 45.92, H 6.92, Cl 5.22; MS (FD): *m/z* (%): 652.0 (100) $[M]^+$; IR (KBr,cm^{-1}): ν = 2866, 2899, 2940 (m, C-H), 2004 (w, Ir-H), 1585 (s, C=C); $^{31}P\{^1H\}$ NMR ([D_8]toluene, 25°C, TMS): δ = 69.1 (s); ^1H NMR ([D_8]toluene, 25°C, TMS): δ = -43.21 (t, ^2J(P,H) = 12.8 Hz, 1H; Ir-H), 1.23 (m,[73] N = 12.80 Hz, 18H; CCH_3), 1.28 (m,[73] N = 12.80 Hz, 18H; CCH_3), 2.99 (m,[73] 2H; CH_aH_bP), 3.03 (m,[73] 2H; CH_aH_bP), 3.56 (s, 3H; OCH_3), 6.70 (s, 2H; CH); $^{13}C\{^1H\}$ NMR ([D_8]toluene, 25°C, TMS): δ = 29.21 (m,[74] N = 4.7 Hz, $C(\underline{C}H_3)_3$), 29.97 (m,[74] N = 4.7 Hz, $C(\underline{C}H_3)_3$), 34.74 (m,[74] N = 22.20 Hz, CP), 35.93 (m,[74] N = 27.80 Hz, CH_2P), 37.54 (m,[74] N = 19.60 Hz, CP), 54.65 (s, OCH_3), 107.83 (m,[74] N = 16.17 Hz, $\underline{C}HCCH_2P$), 135.33 (s, $\underline{C}OCH_3$), 152.18 (t, ^2J(P,C) = 8.4 Hz CIr), 157.34 (m,[74] N = 3.4 Hz, $CH_2\underline{C}CH$).

1b: m.p. 200°C; elemental analysis (%) calcd for $C_{25}H_{44}P_2OIrCl$ (650.4): C 46.18, H 6.82, Cl 5.45; found: C 45.81, H 6.25, Cl 6.23; MS (FAB, 3-NBA): *m/z* (%): 650 (30) $[M]^+$, 615 (100) $[M\text{-}Cl]^+$, 557 (40) $[M\text{-}Cl\text{-}^tBu]^+$, 501 (55) $[M\text{-}Cl\text{-}2^tBu]^+$; IR (KBr, cm^{-1}): ν = 2939, 2864, 2907 (m, C-H), 1584 (C=C); $^{31}P\{^1H\}$ NMR (C_6D_6, 25°C, H_3PO_4): δ = 9.8 (d, ^2J(P,P) = 351.06 Hz; P_2), 50.8 (d, ^2J(P,P) = 351.06 Hz; P_1); ^1H NMR (C_6D_6, 25°C, TMS): δ = 0.72 (d, $^3J(P_2,H)$ = 12.79 Hz, 3H; $C(CH_3)_2$), 1.11 (d, $^3J(P_1,H)$ = 12.79 Hz, 9H; $C(CH_3)_3$), 1.27 (d, $^3J(P_1,H)$ = 12.79 Hz, 9H; $C(CH_3)_3$), 1.35 (d, $^3J(P_2,H)$ = 13.71 Hz, 9H; $C(CH_3)_3$), 1.50 (d, $^3J(P_2,H)$ = 13.71 Hz, 3H; $C(CH_3)_2$), 2.19 (ddd, ^2J(H,H) = 4.68 Hz, $^3J(P_2,H)$ = 5.37 Hz, $^3J(P_1,H)$ = 2.40 Hz, 1H; CH_aH_bIr), 3.08 (m, 4H; PCH_2), 3.55 (ddd, ^2J(H,H) = 4.68 Hz, $^3J(P_2,H)$ = 9.25 Hz, $^3J(P_1,H)$ = 2.17 Hz, 1H; CH_aH_bIr), 3.61 (s, 3H; OCH_3), 6.88 (d, ^4J(H,H) = 2.28 Hz, 1H; CH), 6.94 (d, ^4J(H,H) = 2.28 Hz, 1H; CH); $^{13}C\{^1H\}$ NMR (C_6D_6, 25°C, TMS): δ = -6.71 (dd, ^2J(P,C) = 23.9 Hz, ^2J(P,C) = 1.0 Hz, CH_2Ir), 26.23 (s, $\underline{C}H_3CP_2$), 27.34 (d, ^2J(P,C) = 4.0 Hz, $\underline{C}H_3CP_2$), 29.23, 29.38, 30.70 (dd, ^2J(P,C) = ^4J(P,C) = 1.3 Hz, $\underline{C}H_3CP$),

34.52 (d, ^{1}J(P,C) = 3.4 Hz, CH_2P), 34.92 (s, CH_2P), 35.19 (dd, ^{1}J(P,C) = 14.5 Hz, ^{3}J(P,C) = 5.1 Hz, CP), 36.86 (dd, ^{1}J(P,C) = ^{3}J(P,C) = 8.1 Hz, CP), 41.16 (dd, ^{1}J(P,C) = 16.5 Hz , ^{3}J(P,C) = 3.0 Hz, CP), 55.14 (s, OCH_3), 59.67 (dd, ^{1}J(P,C) = 20.6 Hz, ^{3}J(P,C) = 2.4 Hz, CP), 108.37 (d, ^{3}J(P,C) = 16.8 Hz, CH), 109.33 (d, ^{3}J(P,C) = 16.8 Hz, CH); 140.76 (s, $CH_3O\underline{C}$), 150.00 (dd, ^{2}J(P,C) = 11.1 Hz, ^{3}J(P,C) = 3.7 Hz, $\underline{C}CH_2P$), 153.16 (dd, ^{2}J(P,C) = 14.12 Hz, ^{3}J(P,C) = 5.4 Hz, $\underline{C}CH_2P$), 158.0 (dd, ^{2}J(P,C) = 1.7 Hz, CIr).

2.2.10 Reaction of 1a and 1b with NaH in the presence of H_2

Complexes **1a** and **1b** (10 mg, 0.015 mmol) were treated in THF (3 ml) with a 100% excess of NaH. After stirring the reddish mixtures at room temperature for 1 h under a H_2 atmosphere, they were sonicated for another 6 h with intermittent cooling and vigorous stirring. By continued stirring at room temperature for 24 h the mixtures changed color to pale brown. This solutions were filtered, and THF was removed by a stream of H_2. The residue left was dissolved in C_6D_6 and spectra were recorded.

1c: $^{31}P\{^{1}H\}$ NMR (C_6D_6, 25°C, TMS): δ = 74.5 (s); ^{1}H NMR (C_6D_6 , 25°C, TMS): δ = -9.12 (t, ^{2}J(P,H) = 9.66 Hz, 4H; Ir-H), 1.19 (m,[73] N = 12.8 Hz, 36H; ^{t}Bu), 3.25 (m,[73] N = 7.46 Hz, 4H; $2CH_2$), 3.59 (s, 3H; OCH_3), 6.82 (s, 2H; CH); $^{13}C\{^{1}H\}$ NMR (C_6D_6, 25°C, TMS): δ = 25.7 (s, $C(\underline{C}H_3)_3$), 29.7 (d, ^{1}J(P,C) = 2.5 Hz, CP), 30.3 (s, CP), 41.9 (m,[74] N = 30.3 Hz, CH_2), 55.1 (s, OCH_3), 107.3 (m,[74] N = 15.2 Hz, CH), 141.5 (s, C-Ir), 149.3 (m,[74] N = 15.3 Hz, $CH\underline{C}CH_2$).

1d: If in the reaction mixture of **1c** the solvent is removed by a stream of argon, **1d** is formed exclusively. $^{31}P\{^{1}H\}$ NMR (C_6D_6, 25°C, TMS): δ = 87.4 (s); ^{1}H NMR (C_6D_6, 25°C, TMS): δ = -19.75 (t, ^{2}J(P,H) = 9.14 Hz, 2H; Ir-H), 1.35 (m,[73] N = 13.24 Hz, 36H; ^{t}Bu), 3.24 (m, $2CH_2$), 3.58 (s, 3H; OCH_3), 7.02 (s, 2H; CH).

2.2.11 Reaction of 1a with CO

CO gas was bubbled into a solution of **1a** (30 mg, 0.046 mmol) in benzene in a Schlenk tube. The solution becomes colorless immediately. Evaporation of the solvent under vacuum resulted in the colorless solid **7** in quantitative yield. m.p. = 212-214°C; elemental analysis (%) calcd for $C_{26}H_{46}O_2P_2IrCl$ (680): C 45.90, H 6.82, Cl 5.21; found: C 46.15, H

6.90, Cl 4.86; MS (FD): *m/z* (%): 680.1 (100) $[M]^+$, 643.1 (43) $[M\text{-}Cl]^+$; IR (KBr, cm^{-1}): ν = 2946, 2987 (C-H), 2154 (w, Ir-H), 1987, 1976 (s, CO), 1586 (m, C=C); $^{31}P\{^1H\}$ NMR (C_6D_6, 25°C, TMS): δ = 57.0 (s); ^1H NMR (C_6D_6, 25°C, TMS): δ = -7.59 (t, ^2J(P,H) = 15.38 Hz, 1H; Ir-H), 1.27 (m,[73] N = 13.50 Hz, 18H; $C(CH_3)_3$), 1.38 (m,[73] N = 13.81 Hz, 18H; $C(CH_3)_3$), 2.88 (m, 4H; CH_2), 3.51 (s, 3H; OCH_3), 6.61 (s, 2H; CH). $^{13}C\{^1H\}$ NMR (C_6D_6, 25°C, TMS): δ = 29.1 (m,[74] N = 4.1 Hz, $C(\underline{C}H_3)_3$), 29.9 (m,[74] N = 4.1 Hz, $C(\underline{C}H_3)_3$), 36.47 (m,[74] N = 20.2 Hz, CP), 36.81 (m,[74] N = 26.27 Hz, CP), 38.3 (m,[74] N = 28.29 Hz, CH_2P), 54.77 (s, OCH_3), 108.3 (m,[74] N = 15.49 Hz, CH), 147.02 (m,[74] N = 12.13 Hz , $\underline{C}CH_2P$), 127.3 (s, $\underline{C}OCH_3$), 157.70 (t, ^2J(P,C) = 1.4 Hz, CIr), 182.4 (t, ^2J(P,C) = 5.03 Hz, CO).

2.2.12 Reaction of 1b with CO

CO gas was bubbled into a solution of **1b** (30 mg, 0.046 mmol) in benzene in a Schlenk tube. The solution immediately becomes colorless. Evaporation of the solvent under vacuum gave the colorless solid **1f** in quantitative yield. m.p. = 214-216 °C; elemental analysis (%) calcd for $C_{26}H_{44}O_2P_2IrCl$ (678): C 46.04, H 6.54, Cl 5.23; found: C 46.49, H 5.89, Cl 6.01; MS (FAB, 3-NBA): *m/z* (%): 679.2 (3) $[M+1]^+$, 650.2 (30) $[M\text{-}CO]^+$, 643.3 (45) $[M\text{-}Cl]^+$; IR (KBr, cm^{-1}): ν = 2950 (m, C-H), 1990 (s, CO), 1587 (m, C=C); $^{31}P\{^1H\}$ NMR (C_6D_6, 25°C, H_3PO_4): δ = -22.8(d, ^2J(P,P)= 317.2 Hz; P_2), 42.1 (d, ^2J(P,P) = 317.2 Hz; P_1); ^1H NMR (C_6D_6, 25°C, TMS): δ = 0.75 (ddd, ^2J(H,H) = 8.54 Hz, ^3J(P_2,H) = 7.69 Hz, ^3J(P_1,H) = 4.08 Hz, 1H; CH_aH_bIr), 0.94 (d, ^3J(P,H) = 15.38 Hz, 3H; $C(CH_3)_2$), 1.22 (d, ^3J(P,H) = 12.87 Hz, 9H; $C(CH_3)_3$), 1.29 (d, ^3J(P,H) = 13.5 Hz, 9H; $C(CH_3)_3$), 1.32 (d, ^3J(P,H) = 12.56 Hz, 9H; $C(CH_3)_3$), 1.77 (d, ^2J(P,H) = 16.01 Hz, 3H; $C(CH_3)_2$), 2.29 (ddd, ^2J(H,H) = 8.54 Hz, ^3J(P_2,H) = 13.58 Hz, ^3J(P_1,H) = 2.43 Hz, 1H; CH_aH_bIr), 2.89 and 3.01 (AB part of an ABMX spin system, ^2J(H_a,H_b) = 16.64 Hz, ^2J(P,H_a) = 9.73 Hz, ^2J(P,H_b) = 9.42 Hz, ^4J(P,H_b) = 2.0 Hz, 2H; CH_2P), 3.23 (m, 2H; CH_2P_2), 3.63 (s, 3H; OCH_3), 6.80 (s, 2H; CH); $^{13}C\{^1H\}$ NMR (C_6D_6, 25°C, TMS): δ = 14.25 (dd, ^2J(P,C) = 30.65 Hz, ^2J(P,C) = 3.03 Hz, CH_2Ir), 28.35 (s, $C(\underline{C}H_3)_2$), 30.00 (s, $C(\underline{C}H_3)_2$), 30.28 (d, ^2J(P,C) = 2.69 Hz, $C(\underline{C}H_3)_3$), 30.4 (s, $C(\underline{C}H_3)_3$), 33.66 (dd, ^2J(P,C) = 3.37 Hz, ^4J(P,C) = 0.67 Hz, $C(\underline{C}H_3)_3$), 34.35 (dd, ^1J(P,C) = 8.42 Hz, ^3J(P,C) = 8.42 Hz, CP), 35.84 (d, ^1J(P,C) = 28.97 Hz, CH_2P), 36.95 (d, ^1J(P,C) = 26.95 Hz, CH_2P), 37.27 (dd, ^1J(P,C) = 16.17 Hz, ^3J(P,C) = 2.02 Hz, CP), 38.27 (dd, ^1J(P,C) = 15.16 Hz, ^3J(P,C) = 6.40 Hz, CP), 55.22 (s, OCH_3), 55.55 (dd, ^1J(P,C) = 27.96 Hz, ^3J(P,C) = 5.05 Hz, CP), 108.76 (d, ^3J(P,C) = 14.82 Hz, CH), 109.72 (d, ^3J(P,C) = 15.50 Hz, CH), 132.1

(s, $\underline{C}OCH_3$), 146.14 (dd, ^2J(P,C) = 8.08 Hz, ^3J(P,C) = 2.69 Hz, CH$\underline{C}CH_2$P), 148.0 (dd , ^2J(P,C) = 11.45 Hz, ^3J(P,C) = 3.37 Hz, CH$\underline{C}CH_2$P), 158.1 (dd, ^2J(P,C) = 1.01 Hz, ^2J(P,C) = 1.01 Hz, CIr), 177.53 (d, ^2J(P,C) = 6.06 Hz, CO).

2.2.13 Reaction of 1a and 1b with NH_3

Ammonia (aq) has been added dropwise or ammonia (g) has been bubbled into a solution of **1a** or **1b** in a deuterated solvent **(**benzene, dichloromethane, or acetone) until no further change in color was taking place and spectra were recorded.

1i: $^{31}P\{^1H\}$ NMR (Acetone d_6, 25°C, H_3PO_4): δ = 50.36 (s); ^{1}H NMR (Acetone d_6, 25°C, TMS): δ = -20.70 (t, ^2J(P,H) = 15.71 Hz, 1H; Ir-H), 1.27 (m, N = 12.2 Hz, 36H; $C(CH_3)_3$), 2.97 and 3.16 (AB pattern, ^2J(H,H) = 16.8 Hz, 4H; CH_2P), 3.62 (s, 3H; OCH_3), 6.49 (s, 2H; CH).

1j: $^{31}P\{^1H\}$ NMR (Acetone d_6, 25°C, H_3PO_4): δ -18.8 (d, ^2J(P,P)= 366.1 Hz; P_2), 34.4 (d, ^2J(P,P) = 366.1 Hz; P_1); ^{1}H NMR (Acetone d_6, 25°C, TMS): δ 0.84 (d, ^3J(P,H) = 13.2 Hz, 3H; $C(CH_3)_2$), 1.17 (d, ^3J(P,H) = 11.3 Hz, 9H; $C(CH_3)_3$), 1.18 (d, ^3J(P,H) = 12.9 Hz, 9H; $C(CH_3)_3$), 1.28 (d, ^3J(P,H) = 12.5 Hz, 9H; $C(CH_3)_3$), 1.54 (d, ^2J(P,H) = 14.8 Hz, 3H; $C(CH_3)_2$), 2.30 (ddd, ^2J(H,H) = 11.1 Hz, ^3J(P_2,H) = 8.7 Hz, ^3J(P_1,H) = 1.2 Hz, 1H; CH_aH_bIr), 2.60 – 3.00 (m, 4H; CH_2P), 3.61 (s, 3H; OCH_3), 6.54 (d, ^4J(H,H) = 2.3 Hz, 1H; CH), 6.57 (d, ^4J(H,H) = 2.3 Hz, 1H; CH), 9.9 (br, NH_3).

2.2.14 Reaction of 1a and 1b with CH_3CN

Acetonitrile has been added dropwise to a solution of **1a** or **1b** in a deuterated solvent (benzene, dichloromethane, or acetone) until no further change in color was taking place and spectra were recorded.

1h: ^{31}P NMR (CD_2Cl_2, 25°C, H_3PO_4): δ 36.7 (d, ^2J(P,P) = 366.6 Hz; P_1); -19.50 (d, ^2J(P,P) = 366.6 Hz; P_2). ^{1}H NMR (CD_2Cl_2, 25°C, TMS): δ 0.66 (m, 1H, CH_aH_bIr) 0.79 (d, ^3J(P,H) = 13.8 Hz, 3H; $C(CH_3)_2$), 1.22 (d, ^3J(P,H) = 12.2 Hz, 9H; $C(CH_3)_3$), 1.32 (d, ^3J(P,H) = 11.6 Hz, 9H; $C(CH_3)_3$), 1.45 (d, ^3J(P,H) = 13.2 Hz, 9H; $C(CH_3)_3$), 1.45 (d, ^3J(P,H) = 13.2 Hz, 3H; $C(CH_3)_2$), 1.97 (s, 3H, CH_3CN), 2.96 (m, 2H; CH_2P), 3.33 (m, 2H; CH_2P), 3.69 (s, 3H; OCH_3), 3.96 (m, 1H; CH_aH_bIr), 6.59 (br, 2H; CH).

1g: $^{31}P\{^{1}H\}$ NMR (CD_2Cl_2, 25°C, H_3PO_4): δ = 55.12 (s); ^{1}H NMR (CD_2Cl_2, 25°C, TMS): δ = -22.92 (br, Ir-H), 1.15 (m*, N = 13.2 Hz, 18H; $C(CH_3)_3$), 1.28 (m, N = 12.6 Hz, 18H; $C(CH_3)_3$), 1.94 (s, 3H; CH_3CN), 2.93 ($[ABX]_2$, ^{2}J(H,H) = 16.8 Hz, N = 8.16 Hz, 2H; CH_2P), 3.06 ($[ABX]_2$, ^{2}J(H,H) = 16.8 Hz, N = 6.4 Hz**,** 2H; CH_2P), 3.65 (s, 3H; OCH_3), 6.49 (s, 2H; CH).

2.2.15 Synthesis of 1n

A solution of **1b** (20 mg, 0.03 mmol) in benzene was treated with (68 mg, 0.03 mmol) of Me_3SiOT_f. The solution changed color instantly from red to blue. Pentane was added dropwise until complete precipitation of the cation. The supernatant solution was succed by a dropper and the precipitate was dried under vacuum. NMR spectra were recorded in acetone d_6. MS (calcd): 798, MS (FD): *m/z* (%): 762.5 (40)$[M - Cl]^+$, 648.3 (80) $[M - CF_3SO_2O]^+$, 613.3 (50) $[M - CF_3SO_2O - Cl]^+$; $^{31}P\{^{1}H\}$ NMR ($[D_6]$ acetone, 25°C, H_3PO_4): δ = 10.4 (d, ^{2}J(P,P) = 353.1 Hz, P_2), 16.10 (d, ^{2}J(P,P) = 353.1 Hz, P_1)**;** ^{1}H NMR ($[D_6]$ acetone, 25°C, TMS): δ = 1.24 (d, $^{3}J(P_2,H)$ = 9.73 Hz, 3H; $C(CH_3)_2$), 1.34 (dd, $^{3}J(P_1,H)$ = 12.40 Hz, $^{5}J(P_2,H)$ = 1.41 Hz, 9H; $C(CH_3)_3$), 1.49 (dd, $^{3}J(P_2,H)$ = 14.29 Hz,$^{5}J(P_1,H)$ = 2.04 Hz, 9H; $C(CH_3)_3$), 1.56 (dd, $^{3}J(P_1,H)$ = 12.56 Hz, $^{5}J(P_2,H)$ = 1.57 Hz, 9H; $C(CH_3)_3$), 2.29 (d, ^{3}J (P_2,H) = 11.93 Hz, 3H; $C(CH_3)_2$), 3.08 (A part of an ABX pattern, ^{2}J(H,H) = 16.49 Hz, $^{3}J(P_1,H)$ = 8.6 Hz, 1H; P_1CH_2), 3.18 (B part of an ABX pattern, ^{2}J(H,H) = 16.49 Hz, $^{3}J(P_1,H)$ = 9.26 Hz, 1H; P_1CH_2), 3.92 (dd, ^{2}J (H,H) = 18.53 Hz, $^{3}J(P_2,H)$ = 2.35 Hz, 1H; P_2CH_2), 4.13 (s, 3H; OCH_3), 5.31 (dd, ^{2}J(H,H) = 19.15 Hz, $^{3}J(P_2,H)$ = 10.67 Hz, 1H; P_2CH_2), 5.79 (dd, ^{2}J(P,H) = 20.40 Hz, ^{3}J(P,H) = 7.45 Hz, 1H; CHIr), 7.44 (d, ^{4}J(H,H) = 2.20 Hz, 1H; CH), 7.51 (d, ^{4}J(H,H) = 2.20 Hz, 1H; CH); ^{13}C NMR (250 MHz, $[D_6]$ acetone, 25°C, TMS): δ = 23.78 (d, ^{2}J(P,C) = 2.4 Hz, $C(CH_3)_2$), 27.91 (br, $C(CH_3)_3$), 28.9 (d, ^{2}J(P,C) = 2.4 Hz, $C(CH_3)_2$), 29.40 (d, ^{1}J(P,C) = 21.9 Hz, CH_2P_1), 30.06 (s, $C(CH_3)_3$), 30.4 (d, ^{1}J(P,C) = 20.0 Hz, CH_2P_2), 31.14 (s, $C(CH_3)_3$), 36.02 (dd, ^{1}J(P,C) = 7.41 Hz, ^{2}J(P,C) = 5.39 Hz, CP), 37.08 (dd, ^{1}J(P,C) = 16.17 Hz, ^{2}J(P,C) = 5.39 Hz, CP), 38.98 (dd, ^{1}J(P,C) = 14.15 Hz, ^{2}J(P,C) = 5.39 Hz, CP), 50.39 (dd, ^{2}J(P,C) = 13.02 Hz, ^{2}J(P,C) = 2.72 Hz, CHIr), 54.69(d, ^{1}J(P,C) = 20.88 Hz, CP), 60.06 (s, OCH_3), 119.48 (d, ^{3}J(P,C) = 11.45 Hz, CH), 120.15 (d, ^{3}J(P,C) =7.41 Hz, CH), 124.5 (dd, ^{2}J(P,C) = 24.58 Hz, C-Ir), 154.28 (s,CH_3OC), 174.68 (dd, ^{2}J(P,C) = 4.38 Hz, ^{3}J(P,C) = 1.68 Hz, $\underline{C}CH_2P$), 176.38 (s, $\underline{C}CH_2P$).

2.2.16 Synthesis of 1o

A freshly prepared sample of **1n** was suspended and stirred in toluene d_8 in a small schlenk tube under argon to give a blue colored solution. The sample was transferred to an NMR tube and the tube was sealed. The sample was frozen in N_2 and pumped three times and the argon was substituted by H_2. The sample was allowed to warm up slowly until color changed to red where the tube was shaken and brought to -40°C. The NMR spectra were recorded at -40 °C, -30 °C, -10 °C and finally at room temperature where the intermediate was finally transformed into **1a**.

1o: $^{31}P\{^1H\}$ NMR ([D_6] acetone, -40°C, H_3PO_4): δ = -10.70 (d, ^2J(P,P) = 321.5 Hz, P_2), 6.2 (d, ^2J(P,P) = 321.5 Hz, P_1**)**; ^1H NMR ([D_6] acetone, 25°C, TMS): δ = -13.64 (br, 1H; Ir-H), -8.26 (br, 1H; Ir-H), 0.72 (d, $^3J(P_2,H)$ = 16.45 Hz, 3H; $C(CH_3)_2$), 1.0-1.5 (br, 27H; $C(CH_3)_3$), 1.63 (d, ^3J (P_2,H) = 13.70 Hz, 3H; $C(CH_3)_2$), 2.4-4.3 (br m, 2H; P_1CH_2), 3.52 (s, 3H; OCH_3), 4.7 (br m, 1H; P_2CH_2), 6.13 (br d, ^2J(P,H) = 17.82 Hz, 1H; CHIr), 6.57 (s, 1H; CH), 6.70 (s, 1H; CH).

3. Appendices

Appendix A1. Crystal data and collection parameters of **1b**

Formula	$C_{25}H_{44}ClIrOP_2$
M [g mol^{-1}]	650.19
Space group	$P2_1/n$
a [Å]	8.344(2)
b [Å]	22.033(5)
c [Å]	15.031(3)
β [°]	104.04(2)
Volume [Å^{-3}]	2680.8(11)
Z	4
ρ_{calcd} [g cm^{-3}]	1.611
Radiation	$Mo_{K\alpha}$ (λ = 0.71073 Å)
μ [mm^{-1}]	5.214
θ_{max} [°]	27.5
Index ranges	$-1 \le h \le 10$; $-28 \le k \le 1$; $-19 \le l \le 19$
Measured reflns	7764
Unique reflns	6141
Observed reflns	5559 [$I \ge 2\sigma(I)$]
Parameters	284
Refinement method	full-matrix least-squares on F^2
GoF	1.087
$wR2$[a]	0.0805 (observed data), 0.0827 (all data)
$R1$[b]	0.0328 (observed data), 0.0373 (all data)
Final diff Four. map [e Å^{-3}]	min: -1.685, max: 2.361

[a] $wR2 = [\Sigma[w(F_o^2-F_c^2)^2] / \Sigma[w(F_o^2)^2]]^{0.5}$; $w = [\exp(5 \sin\theta)^2]/ [\sigma^2(F_o^2) + 6.3966P + (0.039P)^2]$; $P = [F_o^2 + 2F_c^2]/3$. [b] $R1 = \Sigma(||F_o|-|F_c||) / \Sigma|F_o|$.

Appendix A2. Atomic coordinates (x 10^4) and equivalent isotropic displacement parameters (A^2 x 10^3) for **1b**. U(eq) is defined as one third of the trace of the orthogonalized Uij tensor.

Atom	x	y	z	U(eq)
Ir(1)	6087(1)	8170(1)	7545(1)	19(1)
Cl	5056(2)	7639(1)	8739(1)	37(1)
P(1)	7573(1)	7360(1)	7164(1)	22(1)
P(2)	5031(1)	9100(1)	7713(1)	19(1)
O	8453(4)	9524(2)	4437(2)	34(1)
C(1)	9203(6)	6918(2)	7995(4)	32(1)
C(2)	10469(7)	7384(3)	8491(5)	53(2)
C(3)	8486(7)	6600(3)	8719(4)	51(2)
C(4)	10048(8)	6447(3)	7518(4)	52(2)
C(5)	5918(6)	6868(2)	6430(3)	31(1)
C(6)	5203(7)	6429(2)	7007(4)	43(1)
C(7)	6473(7)	6524(3)	5667(4)	44(1)
C(8)	4531(6)	7323(3)	5994(4)	42(1)
C(9)	6952(5)	9273(2)	8618(3)	31(1)
C(10)	7821(5)	8668(2)	8472(3)	28(1)
C(11)	7904(7)	9825(2)	8426(5)	53(2)
C(12)	6724(7)	9299(3)	9587(4)	51(2)
C(13)	3018(5)	9339(2)	7936(3)	23(1)
C(14)	2739(6)	9042(2)	8809(3)	37(1)
C(15)	2936(6)	10036(2)	8006(4)	35(1)
C(16)	1675(5)	9108(3)	7124(3)	36(1)
C(17)	5162(5)	9526(2)	6684(3)	28(1)

Appendix A2. continued

Atom	x	y	z	U(eq)
C(18)	6353(5)	9190(2)	6231(3)	24(1)
C(19)	6847(5)	8596(2)	6513(3)	21(1)
C(20)	7959(5)	8319(2)	6062(3)	22(1)
C(21)	8670(6)	7701(2)	6367(3)	32(1)
C(22)	6917(5)	9490(2)	5549(3)	25(1)
C(23)	7979(5)	9196(2)	5108(3)	24(1)
C(24)	8481(5)	8609(2)	5352(3)	26(1)
C(40)	9806(6)	9292(2)	4127(4)	38(1)

Appendix B1 Crystal data and structure refinement for **1e**

Identification code	h
Empirical formula	C26 H45 Cl Ir O2 P2
Formula weight	679.21
Temperature	173(2) K
Wavelength	0.71073 A
Crystal system, space group	Monoclinic, P2(1)/n
Unit cell dimensions	a = 17.607(3) A alpha = 90 deg. b = 11.3806(17) A beta = 96.937(13) deg. c = 28.679(4) A gamma = 90 deg.
Volume	5704.5(15) A^3
Z, Calculated density	8, 1.582 Mg/m^3
Absorption coefficient	4.907 mm^-1
F(000)	2728
Crystal size	0.4 x 0.3 x 0.1 mm
Theta range for data collection	2.14 to 27.51 deg.
Limiting indices	-22<=h<=1, -14<=k<=1, -37<=l<=37
Reflections collected / unique	15659 / 13005 [R(int) = 0.0350]
Completeness to theta	= 27.51 99.2 %
Absorption correction	Empirical
Max. and min. transmission	0.6143 and 0.3445
Refinement method	Full-matrix least-squares on F^2
Data / restraints / parameters	13005 / 0 / 604
Goodness-of-fit on F^2	1.016
Final R indices [I>2sigma(I)]	R1 = 0.0555, wR2 = 0.1241
R indices (all data)	R1 = 0.0834, wR2 = 0.1389
Extinction coefficient	0.00008(3)
Largest diff. peak and hole	6.314 and -3.664 e.A^-3

Appendix B2. Atomic coordinates (x 10^4) and equivalent isotropic displacement parameters (A^2 x 10^3) for **1e**. U(eq) is defined as one third of the trace of the orthogonalized Uij tensor.

Atom	x	y	z	U(eq)
Ir(1)	4399(1)	4582(1)	1983(1)	29(1)
Cl(1)	5720(1)	4288(2)	2373(1)	38(1)
P(1)	3997(1)	5923(2)	2519(1)	26(1)
P(2)	4408(1)	2976(2)	1468(1)	29(1)
O(1)	1019(4)	5137(7)	1088(3)	48(2)
O(2)	4771(5)	6525(8)	1312(3)	62(2)
C(1)	3570(5)	5223(9)	3019(3)	41(2)
C(3)	2867(6)	4520(10)	2823(4)	54(3)
C(4)	4161(7)	4385(11)	3300(4)	58(3)
C(5)	4629(5)	7202(8)	2738(3)	35(2)
C(6)	5116(6)	7571(9)	2360(4)	49(3)
C(7)	5171(6)	6843(10)	3174(3)	47(2)
C(8)	4146(6)	8293(9)	2851(4)	54(3)
C(9)	3182(5)	6595(8)	2146(3)	33(2)
C(10)	2829(5)	5684(8)	1803(3)	31(2)
C(11)	2080(5)	5784(8)	1598(3)	35(2)
C(12)	1764(5)	4936(8)	1283(3)	34(2)
C(13)	2187(5)	3962(9)	1181(3)	36(2)
C(14)	2947(5)	3840(8)	1400(3)	33(2)
C(15)	3279(4)	4711(8)	1697(3)	29(2)
C(16)	3383(5)	2709(8)	1338(3)	38(2)
C(17)	4829(7)	1550(9)	1718(4)	52(3)
C(18)	4647(9)	1474(12)	2240(4)	75(4)

Appendix B2 continued

Atom	x	y	z	U(eq)
C(19)	4452(8)	486(9)	1447(5)	72(4)
C(20)	5701(6)	1501(10)	1713(5)	65(3)
C(21)	4746(5)	3285(9)	877(3)	37(2)
C(22)	4172(6)	4146(9)	619(3)	45(2)
C(23)	4729(6)	2193(10)	562(4)	51(3)
C(24)	5535(6)	3801(10)	942(4)	51(3)
C(25)	679(7)	4302(12)	769(5)	73(4)
C(26)	4681(4)	5851(7)	1553(3)	22(2)

Appendix C. Relative thermodynamical stabilities [kcal/mol] of the complexes given in Scheme 13 as obtained by the various computational procedures

(a) X = OCH_3:

	B3LYP/SDD(f)	SVWN/SDD(f)	B3LYP/LACVP*	SVWN/LACVP*
1a'	0.0	0.0	0.0	0.0
1m'	+28.5	+16.3	+30.1	19.7
1b'+ H_2	+34.6	+38.4	+31.9	36.8
1k'[a]	-	-	-	-
1l'[a]	-	-	-	-

a: **1k'**and **1l'**represent no stable structures (see text)

(b) X = NO_2:

	B3LYP/SDD(f)	SVWN/SDD(f)	B3LYP/LACVP*	SVWN/LACVP*
1a''	0.0	0.0	0.0	0.0
1m''	+29.1	+16.7	+30.1	21.4
1b''+ H_2	+34.9	+38.5	+33.7	37.9
1k''[a]	-	-	-	-
1l''[a]	-	-	-	-

a: **1k''**and **1l''**represent no stable structures (see text)

Appendix D. Calculated bond distances [Å] in the Ir moiety for the model complexes **1a'**, **1a''**, **1m'**, **1m''**, **1b'** and **1b''** (same atom numbering as in Figure 4)

(a) X = OCH_3:

	B3LYP/SDD(f)	SVWN/SDD(f)	B3LYP/LACVP*	SVWN/LACVP*
1a'				
Ir-H	1.555	1.566	1.558	1.582
Ir-Cl	2.477	2.403	2.432	2.363
Ir-P(1)	2.349	2.300	2.292	2.243
Ir-P(2)	2.356	2.307	2.324	2.288
Ir-C(19)	2.041	2.003	2.062	2.017
1m'				
H-H	0.799	0.902	0.789	0.897
Ir…$H_{av.}$	1.905	1.769	1.927	1.796
Ir-Cl	2.540	2.480	2.513	2.439
Ir-P(1)	2.349	2.292	2.316	2.257
Ir-P(2)	2.341	2.307	2.294	2.257
Ir-C(19)	2.076	2.045	2.080	2.055
Ir-C(10)	2.105	2.084	2.110	2.087
1b'				
Ir-Cl	2.493	2.425	2.454	2.379
Ir-P(1)	2.345	2.287	2.301	2.246
Ir-P(2)	2.330	2.290	2.288	2.251
Ir-C(19)	2.056	2.105	2.071	2.012
Ir-C(10)	2.087	2.051	2.098	2.059

(b) X = NO_2:

	B3LYP/SDD(f)	SVWN/SDD(f)	B3LYP/LACVP*	SVWN/LACVP*
1a''				
Ir-H	1.557	1.569	1.579	1.587
Ir-Cl	2.461	2.394	2.419	2.351
Ir-P(1)	2.356	2.305	2.312	2.264
Ir-P(2)	2.364	2.314	2.328	2.278
Ir-C(19)	2.021	1.980	2.029	1.991
1m''				
H-H	0.795	0.894	0.797	0.883
Ir…$H_{av.}$	1.921	1.783	1.930	1.807
Ir-Cl	2.527	2.458	2.484	2.428
Ir-P(1)	2.354	2.309	2.315	2.225
Ir-P(2)	2.343	2.306	2.298	2.261
Ir-C(19)	2.058	2.011	2.066	2.023
Ir-C(10)	2.107	2.089	2.114	2.075
1b''				
Ir-Cl	2.475	2.411	2.441	2.370
Ir-P(1)	2.352	2.296	2.300	2.253
Ir-P(2)	2.333	2.294	2.290	2.255
Ir-C(19)	2.038	1.995	2.058	2.015
Ir-C(10)	2.093	2.056	2.102	2.064

4. References

[1] P. W. Atkins, *Physical Chemistry*, Oxford University Press, New York **1992**.

[2] M. J. Burk, R. H. Crabtree, M. P. McGrath, *J. Chem. Soc. ,Chem. Commun.* **1985,** 1829-1830.

[3] R. H. Crabtree, J. M. Mihelcic, J. M. Quirk, *J. Am. Chem. Soc.* **1979,** *101,* 7738-7740.

[4] D. Baudry, M. Ephritikhine, H. Felkin, R. Holmes-Smith, *J. Chem. Soc. ,Chem. Commun.* **1983,** 788.

[5] H. Felkin, T. Fillebeen-Kahn, R. Holmes-Smith, J. Zakrezwski, *Tetrahedron Lett.* **1984,** *25,* 1279.

[6] H. Felkin, T. Fillebeen-Kahn, R. Holmes-Smith, J. Zakrezwski, *Tetrahedron Lett.* **1985,** *26,* 1999.

[7] *Transition Metal Hydrides*, (Ed.: A. Dedieu) VCH Publishers, Weinheim **1992**.

[8] S. A. Cotton, *Chemistry of Precious Metals*, Chapman and Hall, London **1997,** p. 78.

[9] R. S. Dickson, *Organometallic Chemistry of Rhodium and Iridium*, Academic Press, New York, **1983**.

[10] M. J. Burk, R. H. Crabtree, *J. Am. Chem. Soc.* **1987,** *109,* 8025-8032.

[11] M. Gupta, C. Hagen, W. C. Kaska, R. E. Cramer, C. M. Jensen, *J. Am. Chem. Soc.* **1997,** *119,* 840-841.

[12] C. M. Jensen, *Chem. Commun.* **1999,** 2443-2449.

[13] W.-W. Xu, G. P. Rosini, M. Gupta, C. M. Jensen, W. C. Kaska, K. Krogh-Jespersen, A. S. Goldman, *J. Chem. Soc. ,Chem. Commun.* **1997,** 2273-2274.

[14] F. C. Liu, A. S. Goldman, *Chem. Commun.* **1999,** 655-656.

[15] M. Albrecht, G. van Koten, *Angew. Chem. Int. Ed.* **2001,** *40,* 3750-3781.

[16] P. Bolt, D. Bruhnke, *J. Prakt. Chem. /Chem. -Ztg.* **1994,** 110-114.

[17] D. E. Bergbreiter, P. L. Osburn, Y. S. Liu, *J. Am. Chem. Soc.* **1999,** *121,* 9531-9538.

[18] V. Boekelheide, R. W. Griffin, *J. Org. Chem.* **1969,** *34,* 1960-1961.

[19] H. E. Zimmerman, G. Jones, *J. Am. Chem. Soc.* **1970,** *92,* 2753-2761.

[20] J. C. Grimm, C. Nachtigal, H.-G. Mack, W. C. Kaska, H. A. Mayer, *Inorg. Chem. Commun.* **2000,** *3,* 511-514.

[21] N. Ashkenazi, A. Vigalok, S. Parthiban, Y. Ben-David, L. J. W. Shimon, J. M. L. Martin, D. Milstein, *J. Am. Chem. Soc.* **2000,** *122,* 8797-8798.

[22] H. K. Kim, S. J. Kang, S. K. Choi, Y. H. Min, C. S. Yoon, *Chem. Mater.* **1999,** *11,* 779-788.

[23] C. J. Moulton, B. L. Shaw, *J. Chem. Soc. ,Dalton Trans.* **1976,** 1020-1024.

[24] B. L. Shaw, *J. Organomet. Chem.* **1980,** *200,* 307-318.

[25] B. Rybtchinski, Y. Ben-David, D. Milstein, *Organometallics* **1997,** *16,* 3786-3793.

[26] S. R. Klei, T. D. Tilley, R. G. Bergman, *J. Am. Chem. Soc.* **2000,** *122,* 1816-1817.

[27] S. Q. Niu, M. B. Hall, *J. Am. Chem. Soc.* **1999,** *121,* 3992-3999.

[28] E. Lindner, R. Fawzi, H. A. Mayer, K. Eichele, W. Hiller, *Organometallics* **1992,** *11,* 1033-1043.

[29] D. W. Lee, W. C. Kaska, C. M. Jensen, *Organometallics* **1998,** *17,* 1-3.

[30] D. Morales-Morales, D. W. Lee, Z. H. Wang, C. M. Jensen, *Organometallics* **2001,** *20,* 1144-1147.

[31] M. Brookhart, M. L. H. Green, *J. Organomet. Chem.* **1983,** *250,* 395-408.

[32] A. C. Albeniz, G. Schulte, R. H. Crabtree, *Organometallics* **1992,** *11,* 242-249.

[33] R. H. Crabtree, E. M. Holt, M. Lavin, S. M. Morehouse, *Inorg. Chem.* **1985,** *24,* 1986-1992.

[34] S. Nemeh, C. Jensen, E. Binamira-Soriaga, W. C. Kaska, *Organometallics* **1983,** *2,* 1442-1447.

[35] F. Novak, H. A. Mayer, and B. Speiser

[36] G. Gritzner, J. Kuta, *PureAppl. Chem.* **1984,** *56,* 461-466.

[37] D. H. Evans, *Chem. Rev.* **1990,** *90,* 739-751.

[38] A. Valat, M. Person, L. Roullier, E. Laviron, *Inorg. Chem.* **1987,** *26,* 332-335.

[39] S. H. Vosko, L. Wilk, M. Nusair, *Canadian J. Phys.* **1980,** *58,* 1200.

[40] A. D. Becke, *J. Chem. Phys.* **1993,** *98,* 5648.

[41] U. Wedig, M. Dolg, H. Stoll, H. Preuss, *Quantum Chemistry: The Challenge of Transition Metals and Coordination Chemistry*, (Ed.: A. Veillard) Reidel, Dordrecht, **1968,** p. 79.

[42] A. W. Ehlers, M. Böhme, S. Dapprich, A. Gobbi, A. Höllwarth, V. Jonas, K. F. Köhler, R. Stegmann, A. Veldkamp, G. Frenking, *Chem. Phys. Lett.* **1993,** *208,* 111.

[43] P. J. Hay, W. R. Wadt, *J. Chem. Phys.* **1985,** *82,* 299.

[44] Gaussian 98, Revision A.7, Gaussian, Inc., Pittsburgh, PA (USA), **1998**.

[45] Jaguar 3.5, Schrödinger, Inc., Portland, OR (USA), **1998**.

[46] *Titan 1.0.5*, Wavefunction, Inc., Irvine, CA, and Schrödinger, Inc., Portland, OR, (USA), **2000**.

[47] M. Aizenberg, D. Milstein, *J. Chem. Soc. ,Chem. Commun.* **1994,** 411-422.

[48] B. E. Mann, C. Masters, B. L. Shaw, *J. Chem. Soc. (A)* **1971,** 1104-1106.

[49] P. J. Alaimo, R. G. Bergman, *Organometallics* **1999,** *18,* 2707-2717.

[50] M. E. van der Boom, S. Y. Liou, L. J. W. Shimon, Y. Ben-David, D. Milstein, *Organometallics* **1996,** *15,* 2562-2568.

[51] A. D. Ryabov, *Chem. Rev.* **1990,** *90,* 403.

[52] P. Dani, M. A. M. Toorneman, G. P. M. van Klink, G. van Koten, *Organometallics* **2000,** *19,* 5287-5296.

[53] P. Dani, T. Karlen, R. A. Gossage, W. J. J. Smeets, A. L. Spek, G. van Koten, *J. Am. Chem. Soc.* **1997,** *119,* 11317-11318.

[54] P. Dani, M. Albrecht, G. P. M. van Klink, G. van Koten, *Organometallics* **2000,** *19,* 4468-4476.

[55] M. E. van der Boom, M. Gozin, Y. Ben-David, L. J. W. Shimon, F. Frolow, H.-B. Kraatz, D. Milstein, *Inorg. Chem.* **1996,** *35,* 7068-7073.

[56] S.-Y. Liou, E. Milko, D. Milstein, *Chem. Commun.* **1998,** 687-688.

[57] B. L. Shaw, *J. Am. Chem. Soc.* **1975,** *97,* 3856-3857.

[58] M. A. McLoughlin, R. J. Flesher, W. C. Kaska, H. A. Mayer, *Organometallics* **1994,** *13,* 3816-3822.

[59] W. D. Jones, F. J. Feher, *Acc. Chem. Res.* **1989,** *22,* 91-100.

[60] T. C. Bruice, F. C. Lightstone, *Acc. Chem. Res.* **1999,** *32,* 127-136.

[61] A. Vigalok, O. Uzan, L. J. W. Shimon, Y. Ben-David, J. M. L. Martin, D. Milstein, *J. Am. Chem. Soc.* **1998,** *120,* 12539-12544.

[62] A. Vigalok, B. Rybtchinski, L. J. W. Shimon, Y. Ben-David, D. Milstein, *Organometallics* **1999,** *18,* 895-905.

[63] M. Albrecht, A. L. Spek, G. van Koten, *J. Am. Chem. Soc.* **2001,** *123,* 7233-7246.

[64] P. G. Jessop, R. H. Morris, *Coord. Chem. Rev.* **1992,** *121,* 155-284.

[65] A. Pedersen, M. Tilset, *Organometallics* **1994,** *13,* 4887-4894.

[66] P. Diversi, S. Iacoponi, G. Ingrosso, F. Laschi, A. Lucherini, P. Zanello, *J. Chem. Soc. ,Dalton Trans.* **1993,** 351-352.

[67] P. Diversi, S. Iacoponi, G. Ingrosso, F. Laschi, A. Lucherini, G. Pinzino, G. Uccello-Barretta, P. Zanello, *Organometallics* **1995,** *14,* 3275-3287.

[68] K. Timmer, D. H. M. W. Thewissen, J. W. Marsmann, *Recl. Trav. Chim. Pays-Bas* **1988,** *107,* 248-255.

[69] W. Voskuil, J. F. Arens, *Recl. Trav. Chim. Pays-Bas* **1963,** *82,* 302-304.

[70] J. L. Herde, J. C. Lambert, C. V. Senoff, *Inorganic Synthesis* **1974,** *73,* 18-20.

[71] S. Dümmling, E. Eichhorn, S. Schneider, B. Speiser, M. Würde, *Curr. Sep.* **1996,** *15,* 53-56.

[72] B. Gollas, B. Krauß, B. Speiser, H. Stahl, *Curr. Sep.* **1994,** *13,* 42-44.

[73] a) m: $[A_9X]_2$ pattern $N = |^3J_{PH} + {}^5J_{PH}|$; b) m: $[ABX]_2$ pattern, $N = |^2J_{PH} + {}^4J_{PH}|$.

[74] a) m: AXX' pattern $N = |^2J_{PC} + {}^4J_{PC}|$; b) m: AXX' pattern, $N = |^1J_{PC} + {}^3J_{PC}|$; c) m: AXX' pattern, $N = |^3J_{PC} + {}^5J_{PC}|$.

Summary

Homogeneous catalytic dehydrogenation of saturated hydrocarbons is just one part of a concerted effort to develop and broaden the scope of transition metal catalyzed C-H bond reactivity. Several studies of alkane activation by rhodium and iridium complexes have shown that oxidative addition of C-H bonds is kinetically preferred despite their greater bond strength. The PCP pincer complexes of iridium may have presented the opportunity of a breakthrough in this area because they can interact with alkanes via dehydrogenation pathways to give olefins at 200°C and above.

PCP pincer ligands X-C_6H_3-3,5-$(CH_2P^tBu_2)_2$ with X = OCH_3 (**1**), OH (**2**), O^- (**3**), $NHCOCH_3$ (**4**) have been prepared in a series of steps which have been described in the literature (schemes 2, 3a, 3b, 4). The ligands have been characterised by NMR spectroscopy as well as by mass spectroscopy and elemental analysis for **1**. Treatment of **1** with $IrCl_3$ in *i*-PrOH/H_2O gives the cyclometalated pincer clorohydrido iridium complex [CH_3O-C_6H_3-3,5-$(CH_2P^tBu_2)_2$]IrHCl (**1a)**. A second intramolecular oxidative addition reaction of one of the *t*-butyl C-H bonds to the Ir^{III} center followed by the reductive elimination of H_2 gives the novel doubly metalated compound **1b** which is stable to air and water. The same results were obtained when ligand **1** was reacted with $[Ir(COE)_2Cl]_2$ in toluene. When **1b** is treated with hydrogen, **1a** is formed exclusively. Both complexes **1a** and **1b** have been completely characterised by elemental analysis and by their NMR spectra.

X-ray crystallographic analysis of **1b** revealed a chelated square pyramidal iridium compound with two cyclometalated five-membered rings in the plane and the iridium bound methylene group of the four-membered ring in the apical position. The free coordination site is protected by an agostic C-H-bond. While a phosphorus-phosphorus coupling constant of 351.1 Hz establishes the *trans*-position of the phosphorus groups there is no indication of a hydridic or weakly bound hydrogen.

The broad temperature range of stability and interaction suggests that functionalization of the PCP pincer complexes for immobilization to enable easy separation of the catalyst from the products is promising. Experiments were carried to attach hydrolysable groups to these ligand complexes for the purpose of stationary phase synthesis. Reaction of ligands **2**, **3** with 3-(triethoxysilyl)propylisocyanate or 3-(triethoxysilyl)chloropropane were not successful. It is likely that the –OH group in the phenol or the $–O^-$ group in the phenoxide may attack the

$(EtO)_3Si$- group. Positive results can be obtained using the 3-(triisopropoxysilyl)chloropropane where the isopropyl group is bulky enough to protect the silicon center.

Both complexes **1a** and **1b** are found to react with NaH/H_2 to give the same tetrahydride $\{CH_3O\text{-}C_6H_3\text{-}2,6\text{-}(CH_2P^tBu_2)_2\}IrH_4$ **1c** or the dihydride $\{CH_3O\text{-}C_6H_3\text{-}2,6\text{-}(CH_2P^tBu_2)_2\}IrH_2$ **1d.** They also react instantly with carbon monoxide to give the corresponding carbonyl products **1e** and **1f**, both are completely identified by their IR, Mass, and NMR spectra. The structure of the carbonyl complex **1e** $[CH_3O\text{-}C_6H_3\text{-}3,5\text{-}(CH_2P^tBu_2)_2]IrCOHCl$ was confirmed also by X-ray crystallographic analysis. The x-ray data are comparable with that of related compounds like the dihydrido complex $\{C_6H_3\text{-}2,6\text{-}(CH_2P^tBu_2)_2\}IrH_2$, the dinitrogen compound $[\{C_6H_3\text{-}2,6\text{-}(CH_2P^tBu_2)_2\}Ir]_2(\mu\text{-}N_2)$, the hydrido hydroxy complex $\{C_6H_3\text{-}2,6\text{-}(CH_2P^tBu_2)_2\}IrH(OH)$, and the nitro functionalised hydrochloro compound $\{4\text{-}NO_2\text{-}C_6H_2\text{-}2,6\text{-}(CH_2P^tBu_2)_2\}Ir(H)Cl$ with the CO group aquiring a perpendicular position to the aromatic ring. Complexes **1a** and **1b** react also immediately with NH_3 and CH_3CN where the products are identified also by their $^{31}P\{^1H\}$ NMR and ^1H NMR spectra.

The redox properties of **1a** and **1b** were investigated by cyclic voltammetric experiments in a dichloromethane/tetra-*n*-butylammonium hexafluorophosphate electrolyte at a Pt electrode. Both compounds are oxidized at potentials only a few hundred mV positive of the ferrocene standard potential . The results establish an equilibrium between the pincer chlorohydrido compound and the doubly metalated complex and H_2. The voltammetric behaviour indicates a "square scheme" electrode reaction mechanism with solution equilibria between two redox active complexes on both, the Ir^{III} and the Ir^{IV} oxidation states . Both complexes were found to be oxidized to the d^5 Ir^{IV} oxidation state by losing one electron .

The unusual stability of the doubly metalated complex was supported by density functional calculations at various levels of theory for the model compounds. ($X = OCH_3$ and NO_2) as well as for complex **1b.** The nitro functionalized complex was taken into consideration, since an X-ray structure of the square-pyramidal $\{4\text{-}NO_2\text{-}C_6H_2\text{-}2,6\text{-}(CH_2P^tBu_2)_2\}Ir(H)Cl$ together with DFT calculations on $\{4\text{-}NO_2\text{-}C_6H_2\text{-}2,6\text{-}(CH_2PH_2)_2\}Ir(H)Cl$ was reported. Thus, experimental and theoretical data for the two types of structures represented by **1a** and **1b** can be compared. Almost parallel trends in the theoretical energy differences are obtained for the methoxy and the nitro compounds. All computational procedures predict the square-pyramidal chlorohydrido complexes **1a`**, **1a``** to be most stable.

The structures **1m`**, **1m``** are higher in energy by ca. 16 to 30 kcal/mol, depending on whether the SVWN or the B3LYP approach is applied. The results show the coordination of two hydrogen atoms best described as η^2-coordinated dihydrogen and suggest an Ir(V) oxidation state as intermediate. To verify the Ir(V) intermediate hypothesis, the cyclic complex **1b** was treated with Me_3SiOT_f. The reaction takes place immediately at room temperature to get a cation **1n** which is slightly soluble in benzene and toluene and completely dissolves in acetone. The structure of **1n** was elucidated by $^{31}P\{^1H\}$ NMR, ^1H NMR and $^{13}C\{^1H\}$ NMR spectroscopy and mass spectroscopy. $^1H\{^{31}P\}$ NMR and 2D C-H correlation experiments were done to confirm the CHIr group and to show that the structural identity of the molecule did not change compared to **1b**.

Hydrogen was added to the cation at –40°C where the ^1H NMR spectrum of the intermediate showed two hydride absorptions at –8.3 and –13.7 ppm. which suggests an intermediate with Ir(V) oxidation state.

Meine akademische Ausbildung verdanke ich:

I. Al-najjar, R. Al-Zaro, M. El-Abadeleh, S. Haddad, H. Hodali, A. Jaber, A. Jarrar, F. Jumean, M. R. Kamal, A. Kasim, E. Lindner, H. A. Mayer, M. Nazer, N. Qassis, S. S. Sabri, A. Seyam, B. Speiser, J. Strähle, J. Zahr, K. P. Zellar, M. Zughul,W. Voelter, M. Zughul.